Evaluation of Laboratory and Field Produced
Cold Recycled and Full Depth Reclaimed Asphalt Pavement Materials

by

David E. Allain

A thesis submitted to the Graduate Faculty of
Auburn University
in partial fulfillment of the
requirements for the Degree of
Master of Science

Auburn, Alabama
May 1st, 2021

Keywords: Pavement, Asphalt, RAP,
Cold Recycling, Reclamation

Approved by

Dr. Benjamin F. Bowers, Chair, Assistant Professor, Civil and Environmental Engineering
Dr. David Timm, Brasfield & Gorrie Professor, Civil and Environmental Engineering
Dr. Adriana Vargas, Assistant Research Professor, National Center for Asphalt Technology

ABSTRACT

Cold recycling (CR) and full depth reclamation (FDR) are sustainable processes of recycling existing pavement materials to construct stronger stabilized base layers. The recycled asphalt pavement's materials vary in composition, and research is necessary to study performance differences with respect to cracking resistance, rutting, stability, and indirect tensile strength considering the material's physical and chemical properties. Hot mix asphalt (HMA) has had decades of research into national and worldwide standards for designing a mixture for all types of pavement performance requirements. The performance tests designed for HMA can identify potential deficiencies in the mixture during the design phase, sparing time and resources in constructing a pavement that would fail before its design life is achieved. Cold recycling and FDR currently do not have widely implemented national standards for mixture designs, and there are many agencies and associations that have their own recommend practices. Additionally, performance testing of CR and FDR mixtures in a laboratory setting are not as widely researched and developed as they are for HMA mixtures. Many CR and FDR field projects are constructed to find empirical evidence from field performance as it relates to different variables and outcomes recorded. A mechanistic-empirical approach is needed to describe the physical performance with empirically derived equations from laboratory performance tests.

In 2019, the Minnesota Department of Transportation (DOT) Road Research Project (MnROAD) constructed 16 test sections comprised of various CR and FDR mixtures, as well as with multiple HMA mill-and-fill control sections. Two CR mixture processes, Cold in-place recycling (CIR) and cold central plant recycling (CCPR), as well as FDR were recycled and stabilized using foamed or emulsified asphalt. The new mixture was then paved as a strengthened

recycled or stabilized base layer and overlaid with an HMA surface. The intention of the MnROAD project is to quantify the benefits of these pavement preservation techniques.

The sections' recycled and reclaimed mixtures were sampled during the construction phase. Some samples were compacted in a mobile laboratory using equipment from the National Center for Asphalt Technology (NCAT), to be tested for dynamic modulus. Multiple specimens were mixed and compacted at the main NCAT laboratory for the testing of indirect tensile strength, Marshall stability, cracking resistance, and rutting potential. Additional samples were mixed and compacted at NCAT and cut to large and small specimen sizes for additional dynamic modulus testing. Field cores were also recovered from the 70th Street CR and FDR test sections used to determine their dynamic modulus. Investigating the types of specimens used and their dynamic moduli allows for validation into whether difference in mixing and compaction methods affect the validity the test section laboratory results as compared to the field. A statistical analysis on the similarities of the mixing and compacting methods was performed. From the results it was found that some of the 70th Street CR test sections' dynamic moduli correlated well to laboratory mixed and compacted sample's types. At certain temperatures, typically ambient to high temperatures, the dynamic moduli were similar for all mixing and compacting methods. The small-scale laboratory mixed and compacted specimen did not equate to the field core dynamic moduli for most CR and FDR sections. It was found that at cold pavement temperatures, the dry density may be a good predictor for the dynamic modulus of CR mixtures.

ACKNOWLEDGEMENTS

First and foremost, I would like to thank my advising professor, Dr. Benjamin Bowers, for his encouraging and inspiring attitude towards my research and career path. His advice, guidance, mentorship has been unyielding, and I am grateful for the opportunity to complete my master's under him. I would also like to thank my committee, Dr. Adriana Vargas, and Dr. David Timm, for taking their time in reviewing my thesis and contributing to my completion of the master's program at Auburn University. They both have been an integral part of my success at Auburn University.

There have been many people during my time in Auburn that have contributed to my successes and continue to push me to do my best. I first want to thank my wife, Katie, for her love, support, and encouragement in all my graduate studies. Thank you for supporting me when my research pulled me away from home for many weekends and holidays. Also, I would like to express gratitude towards my parents, Michael and Donna Allain, and my in-laws, Steve and Sarah Jenkins, for their love and guidance through this period of life.

This thesis would not be possible without the support of my friends in Auburn and colleagues at NCAT. Specifically, I would like to recognize Adam Taylor, Nathan Moore, Tina Taylor, and Jason Moore for their guidance during my time in the laboratory at NCAT. I have learned so many different skills from each of you, and I thank you for allowing me time to ask so much from you. I also want to thank my graduate research friends at NCAT: Surendra Gatiganti, Danny Martinez, Towhid Rahman, Mostafa Nakhaei, Mawazo Fortunatas, David Vivanco, Anurag Anand, Tiana Lynn, and Megan Foshee who have encouraged me to pursue excellence in what I do. My sisters Rachel and Hannah and my brother Jonathan have been so supportive of my studies as well and I thank them for that. Finally, I want to show gratitude towards my dearest friends who

have supported me in prayer and fellowship over everything I have accomplished while in graduate school: Kolby and Katlyn Baas, Robbie and Janet Claybrook, Kade and Kayla Simmons, Tristan Luther, and Jake Jenkins.

TABLE OF CONTENTS

ABSTRACT ..... **II**

ACKNOWLEDGEMENTS ..... **IV**

TABLE OF CONTENTS ..... **VI**

LIST OF TABLES ..... **IX**

LIST OF FIGURES ..... **XI**

LIST OF ABBREVIATIONS ..... **XV**

CHAPTER 1 – INTRODUCTION **1**

1.1 Background **1**

1.2 Objectives **4**

1.3 Scope **4**

1.4 Organization of Thesis **6**

CHAPTER 2 – LITERATURE REVIEW **8**

2.1 Cold Recycling and Full Depth Reclamation **9**

2.2 Recycling/Stabilizing Agents **11**

2.2.1 Emulsified Asphalt 11

2.2.2 Foamed Asphalt 12

2.3 Mixture Design Process **14**

2.3.1 RAP Sampling 15

2.3.2 Establishing a Water/Density Relationship 16

2.3.3 Selection of Recycling/Stabilizing Agents 16

2.3.4 Active Fillers 17

2.3.5 Preparing and Testing Specimen 17

2.4 Performance Testing **20**

2.4.1 IDEAL-CT 20

2.4.2 Hamburg Wheel Track 21

2.4.3 Dynamic Modulus 23

2.4.4 Recycled Pavement Performance 23

2.5 Summary of the Literature Review 27

CHAPTER 3 – METHODOLOGY 28

3.1 Mixture Design 28

3.1.1 Obtaining Materials 29

3.1.2 Processing and Preparation of Materials 30

3.1.3 Mixing and Compacting 34

3.1.4 Indirect Tensile Strength Verification 39

3.2 As-Built Mixture Specimen Production and Testing 42

3.2.1 Obtaining RAP Samples 43

3.2.2 Processing and Preparation of Materials 44

3.2.3 Mixing and Compacting 44

3.2.4 Curing 45

3.2.5 Performance Testing 46

3.3 Plant-Mixed Lab-Compacted Specimen 54

3.4 Plant-Mixed Field-Compacted Specimen 55

3.5 Summary of the Methodology 61

CHAPTER 4 – RESULTS 62

4.1 Mixture Design 62

4.1.1 Foamed Binder Properties 62

4.1.2 Gradations 64

4.1.3 Moisture-Density Relationship 66

4.1.4 Indirect Tensile Strength Testing 67

4.1.5 Marshall Stability Testing 69

4.2 As-Built Mixtures 70

4.2.1 Comparison of CR and FDR Mixtures 72

4.3 Comparison of the Mixture Designs and As-Built Mixtures 91

4.3.1 Foamed Mixtures 91

4.3.2 Emulsified Mixtures 96

4.4 Impact of Mixing and Compaction Methods on Specimen Performance 97

4.4.1 Specimen Density Comparison 97

4.4.2 Dynamic Modulus Comparisons..... 100
4.5 Summary of the Results 109
CHAPTER 5 – CONCLUSIONS AND RECOMMENDATIONS 111
5.1 Conclusions..... 111
5.2 Recommendations..... 112
REFERENCES..... 114
APPENDIX A: DYNAMIC MODULUS RESULTS A-1

LIST OF TABLES

Table 1: Emulsion/aggregate type compatibility (Wirtgen 2012). 11

Table 2: Emulsion mixture design and as-built mixture properties. 42

Table 3: Foam mixture design and as-built mixture properties. 42

Table 4: Testing regime for each stabilizing agent used. 43

Table 5: Performance test specimen dimension requirements. 45

Table 6: Data quality characteristics (AASHTO T378). 53

Table 7: OFWC summarized results. 64

Table 8: ITS mixture design results summarized. 69

Table 9: Marshall stability mixture design results. 70

Table 10: As-built constructed mixture properties. 70

Table 11: Mixture moisture contents and target densities as recorded from construction. 78

Table 12: As-built mixture's ITS test results summarized. 80

Table 13: As-built mixture's MS test results summarized. 81

Table 14: Summarized IDEAL-CT mixture results. 84

Table 15: HWT mixture result trendline values 90

Table 16: Foamed CR ITS result comparison between mixture design and as-built mixtures 95

Table 17: Two sample t-test p-values comparing the means of ITS mixture design and as-built mixtures 96

Table 18: Emulsion CR and FDR MS result comparison between mixture design and as-built mixtures 97

Table 19: Two sample *t*-test p-values comparing the dry densities of the LMLC and PMLC samples prior to coring 98

Table 20: One-way ANOVA Tukey multiple comparison p-values comparing the dry densities of the four dynamic modulus specimen types..... 100

Table 21: One-way ANOVA test omnibus p-values comparing the dynamic modulus results for all four specimen types. 102

Table 22: One-way ANOVA Tukey multiple comparison p-values comparing the dynamic modulus between the four specimen types, CIR..... 102

Table 23: One-way ANOVA Tukey multiple comparison p-values comparing the dynamic modulus between the four specimen types, CCPR. 102

LIST OF FIGURES

Figure 1: MnROAD test site on 70th Street (Vargas 2019). 5

Figure 2: CIR multi-unit recycling train (Sebaaly et al. 2018). 9

Figure 3: CCPR mobile recycling plant (Diefenderfer & Apeagyei 2014). 9

Figure 4: Foamed asphalt binder creation (Wirtgen 2012). 12

Figure 5: Foamed binder mastic (Wirtgen 2012)..... 13

Figure 6: OFWC determination (Wirtgen 2012). 14

Figure 7: Indirect tensile strength breaking head..... 19

Figure 8: Hamburg curve with test parameters (AASHTO T324-19 2020). 22

Figure 9: Hamburg HMA specimen example after 20,000 passes with good rutting resistance. 22

Figure 10: NCAT Test Track Phase V, VDOT experiment average as-built thicknesses and depth of instrumentation (West et al. 2018)..... 24

Figure 11: VDOT I-81 cross sections for left and right lanes (Diefenderfer and Apeagyei 2014). 25

Figure 12: NCAT pavement preservation CIR test sections' cross sections (Martinez 2020). ... 26

Figure 13: NCAT pavement preservation CCPR test sections' cross sections (Martinez 2020). 26

Figure 14: Wirtgen WLB-10S laboratory foamer and WLM-30 laboratory pugmill..... 29

Figure 15: Mini-stockpile of RAP split into quadrants during the homogenization process. 31

Figure 16: Modified Proctor test, seeping excess moisture. 34

Figure 17: Raw RAP in the WLM-30 pugmill for laboratory foamed asphalt recycling. 35

Figure 18: RAP-and-cement mixture in the WLM-30 pugmill for laboratory foamed asphalt recycling..... 36

Figure 19: Recycled asphalt mixture in the WLM-30 pugmill before foamed asphalt injected. 37

Figure 20: Completed foamed recycled asphalt mixture in the WLM-30 pugmill. 37

Figure 21: Cohesion check of foamed cold recycled material..... 38

Figure 22: Dispersion of foamed asphalt check by hand..... 38

Figure 23: Water bath for conditioning samples for ITS or MS..... 40

Figure 24: PINE Marshall apparatus used for ITS and MS testing. 41

Figure 25: TestQuip load frame with a CCPR-F specimen..... 47

Figure 26: HWT specimens loaded into the cylindrical specimen mounting systems. 48

Figure 27: James Cox & Sons Hamburg Wheel Tracker (James Cox and Sons 2018). 49

Figure 28: Wet coring drill stand with 50 mm core bit and sample. 50

Figure 29: IPC Global gauge point fixing jig. 51

Figure 30: IPC Global AMPT PRO with a large dynamic modulus specimen in the conditioning chamber..... 53

Figure 31: FDR-E PMLC sample breakage shown after coring..... 55

Figure 32: CIR field core samples, foam (left) and emulsion (right). 56

Figure 33: CCPR field core samples, foam (left) and emulsion (right)..... 56

Figure 34: Cold recycled field core sample showing a thin lift..... 57

Figure 35: Cold recycled field core sample with the milled pavement surface exposed as a result of too thin a lift. 58

Figure 36: Cold recycled field core with milled pavement surface imposed on the specimen. .. 58

Figure 37: CIR-E PMFC-S specimen with crack seal along its longitudinal axis..... 59

Figure 38: FDR-E field core specimen..... 60

Figure 39: FDR-E PMFC-S specimen broken during coring. 60

Figure 40: OFWC at a 165°C binder temperature..... 63

Figure 41: OFWC at a 160°C binder temperature. 63

Figure 42: OFWC at a 150°C binder temperature. 64

Figure 43: Mixture design gradations for CIR-F and CCPR-F. 65

Figure 44: Modified Proctor test results for the foamed CR mixture designs. 67

Figure 45: ITS results for the CIR-F mixture design. 68

Figure 46: ITS results for the CCPR-F mixture design. 68

Figure 47: CIR-E as-built mixture gradations. 73

Figure 48: CCPR-E as-built mixture gradations. 73

Figure 49: CIR-F as-built mixture gradations. 74

Figure 50: CCPR-F as-built mixture gradations. 74

Figure 51: FDR-E as-built mixture gradations. 75

Figure 52: CIR as-built mixture black rock gradations. 76

Figure 53: Comparison of CCPR-E and CCPR-F as-built black rock gradations. 77

Figure 54: As-built mixture laboratory recorded gradations. 78

Figure 55: Laboratory samples dry density comparisons to the mixture target dry density. 79

Figure 56: As-built mixture's ITS test results with the 45 psi dry requirement. 80

Figure 57: As-built mixture's MS test results with the 1,250 lbf dry requirement 81

Figure 58: Engineered Emulsion and water seepage from compacting the 5.4% moisture content as-built CCPR-E mixture. 83

Figure 59: IDEAL-CT mixtures results. 84

Figure 60: Hamburg wheel track test results. 86

Figure 61: CIR-E Hamburg test specimen after failure. 86

Figure 62: CIR-F Hamburg test specimen after failure. 87

Figure 63: CCPR-E Hamburg test specimen after failure. 87

Figure 64: CCPR-F Hamburg test specimen after failure..... 88

Figure 65: FDR-E Hamburg test specimen after failure. 88

Figure 66: Hamburg rutting test data plotted with linear regression line and R^2 value..... 90

Figure 67: Comparison of CIR-F mixture design and as-built mixture black rock gradations. .. 92

Figure 68: Comparison of CCPR-F mixture design and as-built mixture black rock gradations.93

Figure 69: CIR-F ITS comparison between mixture design and as-built mixture..... 94

Figure 70: CCPR-F ITS test result comparison between mixture design and as-built mixture... 94

Figure 71: Pre-cored LMLC and PMLC specimen dry density comparisons to their field recorded target dry densities. 98

Figure 72: Prepared dynamic modulus specimen dry densities by specimen type..... 100

Figure 73: Comparison of dynamic moduli from LMLC-L and LMLC-S specimens for all testing temperatures and frequencies. 101

Figure 74: CIR-E semi-log master curves. 105

Figure 75: CCPR-E semi-log master curves. 106

Figure 76: CIR-F semi-log master curves..... 107

Figure 77: CCPR-F semi-log master curves. 108

Figure 78: CR PMFC-S semi-log master curves. 109

Figure 79: CIR-E dynamic modulus and phase angle data..... A-1

Figure 80: CIR-F dynamic modulus and phase angle data. A-2

Figure 81: CCPR-E dynamic modulus and phase angle data. A-3

Figure 82: CCPR-F dynamic modulus and phase angle data. A-4

Figure 83: FDR-E Dynamic Modulus and Phase Angle Data. A-4

LIST OF ABBREVIATIONS

AASHTO	American Association of State and Highway Transportation Officials
AC	Asphalt Content
AET	American Engineering Testing, Inc.
AMPT	Asphalt Mixture Performance Tester
ARRA	Asphalt Recycling and Reclaiming Association
CIR	Cold In-Place Recycling
CIR-E	Cold In-Place with Emulsion
CIR-F	Cold In-Place with Foam
CCPR	Cold Central Plant Recycling
CCPR-E	Cold Central Plant with Emulsion
CCPR-F	Cold Central Plant with Foam
CR	Cold Recycling
CT_{Index}	Cracking Tolerance Index
DOT	Department of Transportation
EE	Engineered Emulsion
ESALs	Equivalent Single Axle Loads
FDR	Full Depth Reclamation
FDR-E	Full Depth Reclamation with Emulsion
GHG	Greenhouse Gas
HMA	Hot Mix Asphalt
HWT	Hamburg Wheel Track
IDEAL-CT	Indirect Tensile Asphalt Cracking Test

ITS	Indirect Tensile Strength
LMLC	Laboratory-Mixed Laboratory-Compacted
LMLC-L	Laboratory-Mixed Laboratory-Compacted Small
LMLC-S	Laboratory-Mixed Laboratory-Compacted Large
LS	Large-Scale
LVDTs	Linear Variable Differential Transformers
MDD	Maximum Dry Density
MnROAD	Minnesota DOT Road Research Project
MS	Marshall Stability
MSR	Marshall Stability Ratio
NCAT	National Center for Asphalt Technology
NCHRP	National Cooperative Highway Research Program
OFWC	Optimum Foamed Water Content
OMC	Optimum Moisture Content
PG	Performance Grade
PMFC	Plant-Mixed Field-Compacted
PMFC-S	Plant-Mixed Field-Compacted Small
PMLC	Plant-Mixed Laboratory-Compacted
PMLC-L	Plant-Mixed Field-Compacted Large
RAP	Recycled Asphalt Pavement
SGC	Superpave Gyratory Compactor
SSD	Saturated Surface Dry
SS	Small-Scale

S_t	Tensile Strength
TSR	Tensile Strength Ratio
VDOT	Virginia Department of Transportation

CHAPTER 1 – INTRODUCTION

1.1 Background

A common practice for rehabilitating and/or reconstructing a pavement at the end of its design life is to mill the surface layer and replace it with a new hot mix asphalt (HMA) surface lift. This method, known as reactive maintenance, has not proven to eliminate all structural issues such as bottom-up cracking or rutting in the underlying layers. Funding for the reconstruction of roads is limited and processes that save taxpayer dollars are needed. Cold recycling (CR) was implemented as early as the 1900's but gained significant support in the 1970's, using degraded and damaged existing pavements to construct newer and stronger bound base layers for roads. They can also eliminate some structural issues if performed properly. Recycling existing asphalt concrete (AC) pavements decreases the budget needed for projects by eliminating the need for virgin materials and in some instances, haul trucks (Asphalt Recycling and Reclaiming Association [ARRA] 2015).

Cold recycling consists of two subcategories that only manipulate the bound (asphalt) pavement layers, Cold In-place Recycling (CIR) and Cold Central Plant Recycling (CCPR). Cold in-place recycling commonly consists of a cold planning (CP) machine, tanker trucks, screening and sizing units, mixers, pavers, and compaction rollers. The existing AC pavement is milled from the surface using CP and is immediately crushed, screened, re-mixed, and repaved. Cold central plant recycling is different in that it uses a central plant to recycle an existing pavement or stockpile of recycled asphalt pavement (RAP). The RAP from an existing pavement can be hauled to a mobile or stationary plant for crushing, screening, and mixing. The recycled mixture is then hauled to the construction site and paved back down. It is typical to find CR occurring at depths of two to four inches below the surface (ARRA 2015).

Full depth reclamation (FDR) takes recycling a step deeper than CR by incorporating multiple pavement layers, including unbound layers of the base and subgrade. This can eliminate many distresses and structural deficiencies throughout the multiple layer makeup of the existing pavement while also improving strength and durability (Wirtgen 2012).

The most common recycling and stabilizing agents for CR and FDR, respectively, are foamed and emulsified asphalt. For HMA, a mixing temperature is defined as the temperature at which the virgin aggregate will be dry and the asphalt binder viscosity will be reduced to achieve uniform coating of the aggregate. Additionally, the HMA compaction temperature is defined as the temperature at which adequate in-place density can be met (Asphalt Institute 2014). Cold recycling and FDR mix RAP at ambient temperatures. A hot liquid asphalt binder cannot be used because the temperature will decrease significantly in the mixture and complete coating of the RAP particles would not be achieved. Instead, some hot asphalts can be mixed with water and high-pressure air to create a foamed asphalt mixture. This expands the binder many times its original volume. The viscosity is reduced significantly and mixing at lower temperatures without workability issues can be achieved. Asphalt emulsions can also be incorporated into ambient temperature crushed RAP for recycling and reclaiming because the emulsifier separates the asphalt globules from one another, allowing it to be poured similar to water at room temperature. Mixing can also occur at room temperature, and only curing of the mixture is required to evaporate all water from the emulsion, at which point the mixture should have its complete strength.

Hot mix asphalt uses temperature to vary the viscosity of the binder, allowing for more control over the compactive effort. Cold recycling and FDR use additional water to aid in compaction at ambient temperatures, which is similar to compacting soils. The additional water acts as a lubricant between the RAP particles and allows mixtures to achieve a maximum dry

density. The additional water for foamed mixtures is solely used for improving compaction while emulsified mixtures can also use the water to ensure adequate coating of the RAP with emulsion (ARRA 2015). Hot mix asphalts do not require a curing period. Once an HMA pavement is compacted and cooled it can be trafficked immediately. It is recommended to close the lanes of traffic in which recycling or reclamation occurred so that the water can evaporate, and the maximum strength of the layers can be achieved.

The performance of some CR and FDR paved layers have been researched, but there are still questions and concerns over whether the mixture design and construction practices have been optimized for performance. The CR and FDR layers have typically been designed and constructed using methods similar to HMA, although the mixtures differ extensively in material properties. The National Center for Asphalt Technology (NCAT) and the Minnesota Department of Transportation (DOT) Road Research Project (MnROAD) have collaborated to study optimal pavement preservation techniques. These studies involve constructing and monitoring multiple CR, FDR, and HMA layers to inspect field performance of the different mixture types. The NCAT Test Track has some sponsored CR and FDR incorporated sections, as well as sections located on Highway 280 in Opelika, Alabama. The MnROAD CR and FDR sections are located on 70th Street in Otsego and Albertville, Minnesota. An evaluation of differences in laboratory and field produced CR and FDR mixtures has not yet been conducted for the MnROAD 70th Street test sections. This thesis aims to investigate whether properties between mixing and compaction methods, as well as recycling/stabilizing agents are similar, and provide recommendations for future CR and FDR research.

1.2 Objectives

This study focuses on the following objectives to provide a better understanding of the CR and FDR mixture properties:

1. Compare the laboratory mixture design and as-built mixtures using their gradations and indirect tensile strengths (ITS).
2. Provide a comparison of the CR and FDR mixtures with their respective recycling and stabilizing agents through a combination of tests such as: ITS, Marshall stability (MS), Indirect Tensile Asphalt Cracking Test (IDEAL-CT), Hamburg wheel tracking (HWT), and dynamic modulus.
3. Compare the laboratory mixed large-scale (LS) and small-scale (SS) specimens using dynamic modulus to investigate whether they produce equivalent results.
4. Investigate the impact of the mixing and compaction methods on the dynamic modulus.

1.3 Scope

To complete the research objectives, multiple test sections were constructed at the MnROAD test site on 70th Street, seen in Figure 1. Sixteen 500-foot test cells were constructed across two lanes: each lane with eight cells. Of those sixteen constructed cells, seven included CR or FDR. Each of the five CR sections were constructed to be three-inch lifts of recycled material on top of a one-inch existing bound layer and surfaced with a one-inch lift of HMA. The two FDR sections were constructed to be seven-inch lifts on top of a three-inch existing unbound granular base layer and surfaced with the one-inch lift of HMA. The additional sections were used as mill-and-fill control sections and are not discussed further in this thesis.

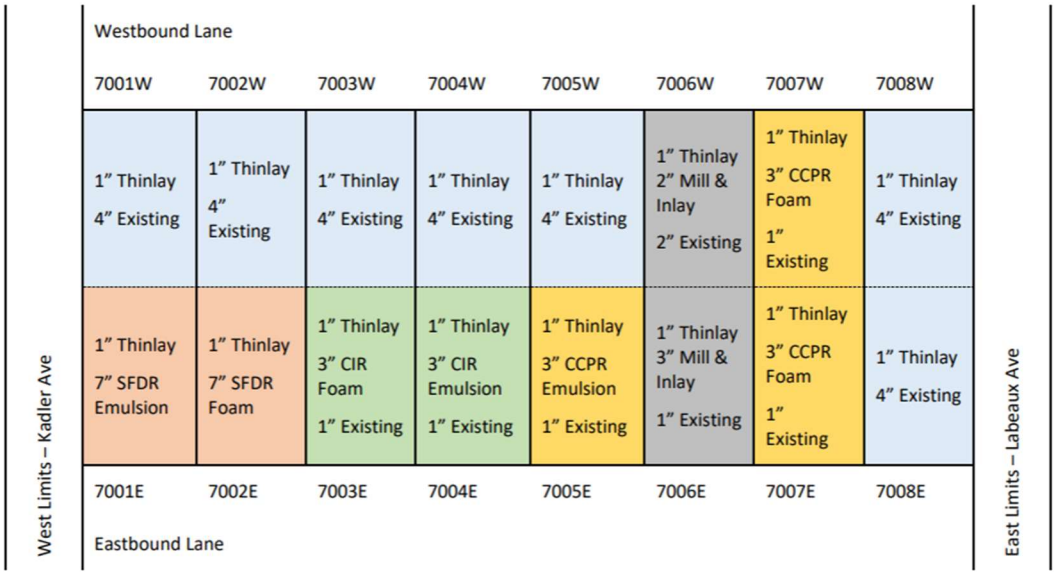

Figure 1: MnROAD test site on 70th Street (Vargas 2019).

NCAT performed the CR foamed mixture designs using crushed field core samples of the existing pavement for the CIR, and stockpiled RAP from a local asphalt plant designated for use during the CCPR construction phase. Ingevity performed the emulsified CIR and CCPR mixture designs, and American Engineering Testing (AET) performed the FDR mixture designs. Foam and emulsion asphalt contents used during construction were recorded along with moisture contents and were supplied to NCAT as the as-built mixture. Adverse weather occurred during the week of construction, and the in-place moisture content was much higher than previously anticipated. Because of this, changes were made to the moisture contents by an experienced person performing the recycling and reclaiming construction work.

A study of each of the recycled and reclaimed mixtures was performed in the laboratory using materials collected at the site during the construction phase. Samples were mixed and compacted in the laboratory to mimic the wet-density values recorded during construction, later referred to as laboratory-mixed laboratory-compacted (LMLC). Additionally, samples were compacted in a mobile laboratory on-site using materials processed and mixed by the construction

equipment, later referred to as plant-mixed laboratory-compacted (PMLC). These samples were collected and shipped to NCAT to be cored and tested for dynamic modulus. Finally, field cores were recovered from the CR and FDR test sections 14 months after construction began and were delivered to NCAT to test for their dynamic modulus, later referred to as plant-mixed field-compacted (PMFC). These samples were used to validate whether plant and laboratory mixing and field and laboratory compacting provided similar dynamic modulus results.

1.4 Organization of Thesis

This thesis is organized into five chapters:

- Chapter 1 Introduction: An introduction of the thesis focused on the background of CR and FDR construction, the thesis objectives, and the scope of the research conducted.
- Chapter 2 Literature Review: A literature review on the theory behind CR and FDR, how a mixture design is conducted, asphalt acceptance and performance testing for indirect tensile strength, stability, cracking, rutting, and dynamic modulus, and finally full-scale CR and FDR pavement performance.
- Chapter 3 Methodology: Summarizes the CR mixture design method incorporating foamed asphalt as the recycling agent, how as-built samples were mixed, compacted, and tested following construction recorded material properties, how LMLC dynamic modulus specimens were processed and prepared for testing in the laboratory, how PMLC dynamic modulus specimen were processed in the mobile laboratory and prepared for testing, and how PMFC dynamic modulus specimen were recovered from the existing test sections and prepared for testing.

- Chapter 4 Summary of Results: Presents a summary of results comparing the as-built CR and FDR mixtures with respect to the gradations, ITS, MS, IDEAL-CT, and HWT, comparing the mixture design and as-builts to one another, and investigating the impact of the mixture mixing and compacting methods using dynamic modulus testing results.
- Chapter 5 Conclusions and Recommendations: Provides a summarized conclusion for: the CR mixture design results conducted at NCAT as compared to the recommended mixture design requirements, the CR and FDR mixture as-built mixture result comparisons through a combination of laboratory tests conducted, the investigation into the impact of the mixture mixing and compaction methods on specimen performance, the comparison of SS and LS laboratory-mixed dynamic modulus specimens, and recommendations for additional future research for CR and FDR mixtures.

CHAPTER 2 – LITERATURE REVIEW

With the demand for maintaining and rehabilitating existing pavements, recycling of the in-situ pavement has shown promising results at decreasing the impact on the environment and on infrastructure budgets. Two of the recycling methods that are implemented today are CR and FDR. Cold recycling is the process of mixing the RAP millings of an existing pavement with a recycling/stabilizing agent and paving it back down as a bound base layer. Full depth reclamation is a rehabilitation technique that incorporates milling the full thickness of an asphalt pavement and a predetermined depth of underlying base or subgrade material and mixing with a stabilizing agent. These methods have reduced costs as they do not require virgin aggregates to be processed and only incorporate a fraction of virgin asphalt binder as compared to an HMA. Furthermore, additional aggregate materials are not needed to haul to the construction site except when corrective aggregates are required (ARRA 2015). The addition of an asphalt recycling/stabilizing agent to CR and FDR mixtures can increase the overall strength as compared to the pre-existing road in need of rehabilitation.

There are two methods of CR: CIR and CCPR. CIR uses a single or multiple equipment train for milling, crushing, and screening of the existing pavement, introducing a recycling agent to the material, and repaving it as a base lift. Figure 2 shows an example of a CIR equipment train. Cold in-place recycling does not require any hauling of processed material from a plant to the jobsite. Cold central plant recycling is similar to CIR except that material is processed and mixed at a mobile or stationary plant. This method does require hauling of the recycled mixture to the jobsite (ARRA 2015). Figure 3 shows an example of a mobile CCPR plant.

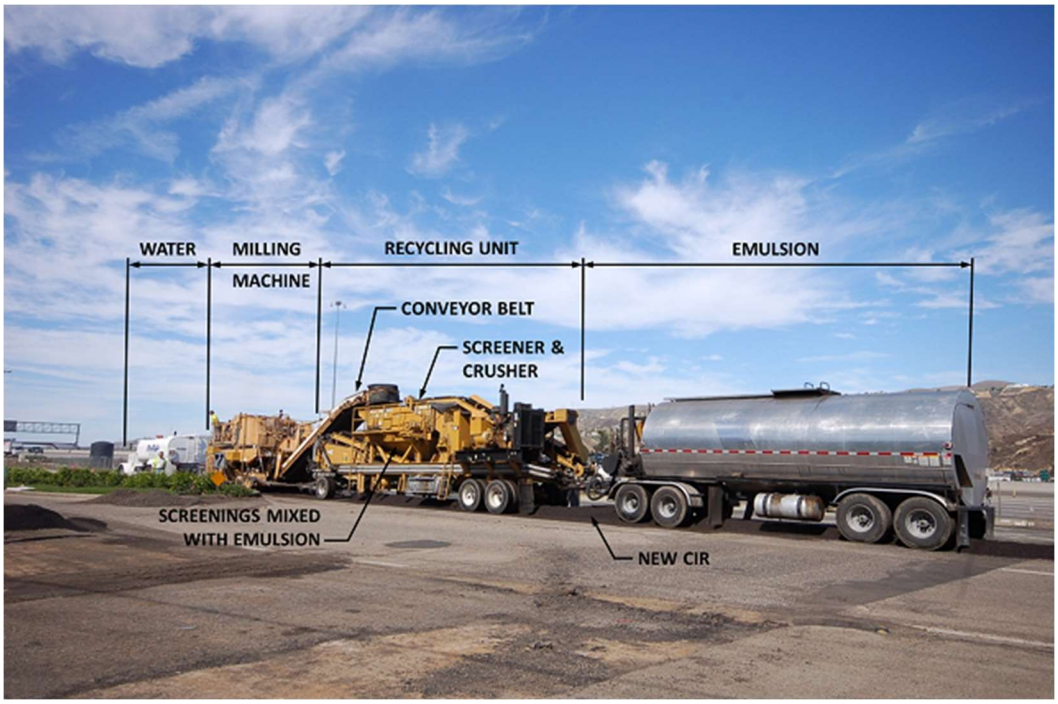

Figure 2: CIR multi-unit recycling train (Sebaaly et al. 2018).

Figure 3: CCPR mobile recycling plant (Diefenderfer & Apeagyei 2014).

2.1 Cold Recycling and Full Depth Reclamation

Cold recycling allows for correction of the geometry of the roadway during recycling (Scherocman 1983). The use of CR also provides sustainable and economic benefits. The reduction in materials needed from a quarry lowers the emissions of haul trucks and other construction equipment, as well as limiting the amount of non-renewable material sources required to complete

projects (Stroup-Gardiner 2011). A typical HMA drum plant uses natural gas or other fuel burners to heat and evaporate water from the virgin aggregate, and to achieve the desired mixing temperature for the HMA. For aggregate drying, the inside temperature of the drum is usually around 1400°F (Brown et al. 2009), which allows the aggregate to dry and reach the desired mixing temperature at the time it exits. Ma et al. (2016) concluded that the production phase of asphalt pavement construction accounts for 54% of the total greenhouse gas (GHG) emissions in a specific project. Environmental concerns of GHG have affected larger construction projects due to the practicality of being sustainable (Kim et al. 2012). Cold recycling is advantageous because the process is performed on ambient RAP millings, reducing the amount of GHGs that are produced for a project.

Cold central plant recycling is a similar process to CIR, except that mixing of the RAP is completed at a mobile or stationary central plant instead of on the roadway. This method allows for a more controlled mixture to be prepared due to the control over the RAP gradations incorporated in the mixture by using crushers, screens, and appropriate blending of RAP. Additionally, because the CCPR material is produced off-site, errors in the material identified during mixing can be corrected prior to hauling and/or placement, unlike CIR whose recycled mixture is placed immediately after processing and mixing. Cold central plant recycling can be paved in multiple lifts while CIR can only be paved in one lift.

Full depth reclamation is a rehabilitation technique consisting of milling and reclaiming bound and unbound materials at ambient temperatures. An FDR reclaimer should have the capacity to pulverize a minimum of twelve inches below the pavement surface. One of the purposes of using FDR instead of CR is to correct structural issues found anywhere in the existing pavement

structure. The FDR material will have aggregate base or subbase soil mixed in with the RAP due to the depth of pulverization (ARRA 2015).

2.2 Recycling/Stabilizing Agents

The two most common types of asphalt recycling agents in CR or stabilizing agents in FDR are emulsified and foamed asphalts (ARRA 2015). Each of these agents are added to the ambient temperature RAP along with a specified amount of additional water to aid in compactive efforts and coating of the millings.

2.2.1 Emulsified Asphalt

Emulsified asphalts are a mixture of water, an emulsifying agent, and asphalt cement. Emulsions are categorized as either cationic (positively charged) or anionic (negatively charged) and the charges keep the asphalt droplets from coalescing. An anionic or cationic emulsion is selected based on the composition of aggregate materials. Table 1 summarizes the effects of using the two emulsion types mentioned against various aggregate types that can be found. The cationic emulsion has a fast break rate for either of the aggregate types while the anionic emulsion has a slow to medium break rate depending on the aggregate blend. Additionally, the adhesion of an anionic emulsion can have significantly different results between the two aggregate types, while the cationic emulsion can have good to excellent adhesion results from the aggregate types.

Table 1: Emulsion/aggregate type compatibility (Wirtgen 2012).

Emulsion Type	Aggregate (Rock) Type	Trends	
		Breaking rate	Adhesion
Anionic	Acidic	Slow	Poor
Anionic	Alkaline	Medium	Good
Cationic	Acidic	Fast	Excellent
Cationic	Alkaline	Fast	Good

An emulsified asphalt breaks when the excess water begins to evaporate, and the asphalt residue starts to coalesce. Cold weather and high in-situ moisture can delay the time for an emulsion to break, causing delays in constructing a surface layer (Stroup-Gardiner 2011). Engineered emulsions (EE) are a specialized emulsion that can be modified for specific properties required to complete a job, such as cold weather or adverse construction conditions. It is typical to find an EE to be slow setting and cationic (ARRA 2015). The setting time of the emulsion is based on how quickly all of the water evaporates, leaving only asphalt residue.

2.2.2 Foamed Asphalt

Foamed binder was first developed for stabilizing soils by Ladis Csanyi in 1957. Csanyi found that when steam is introduced to hot asphalt binder it causes the binder to foam and expand, lowering the viscosity and increasing the surface area. Csanyi also developed a nozzle that combined the steam and hot binder together instead of the earlier method of adding water to binder and heating the mixture up (Csanyi 1957). Figure 4 shows how a foamed asphalt is produced by incorporating water and pressurized air into the hot asphalt binder.

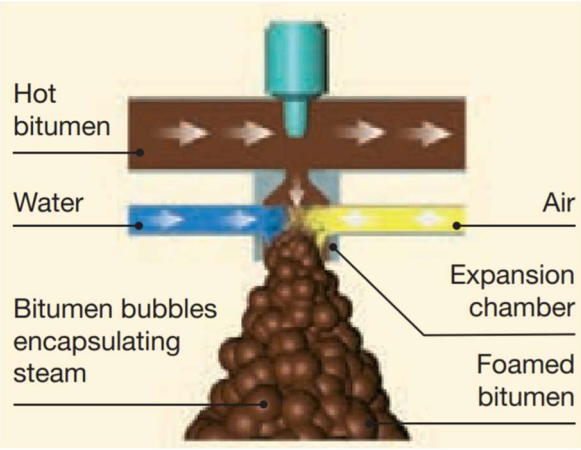

Figure 4: Foamed asphalt binder creation (Wirtgen 2012).

Research has found that incorporating aggregate and foamed binder is done best when the foam is "unstable." This refers to the foamed binder's characteristic of its expansion and half-life. When the binder is expanded to its maximum volume prior to it collapsing with bubbles of asphalt bursting, it is considered "unstable" (Wirtgen 2012). After these bubbles burst, they create tiny bitumen spot-welds between aggregates which creates a mastic as seen in Figure 5 (Wirtgen 2012; Asphalt Academy 2009).

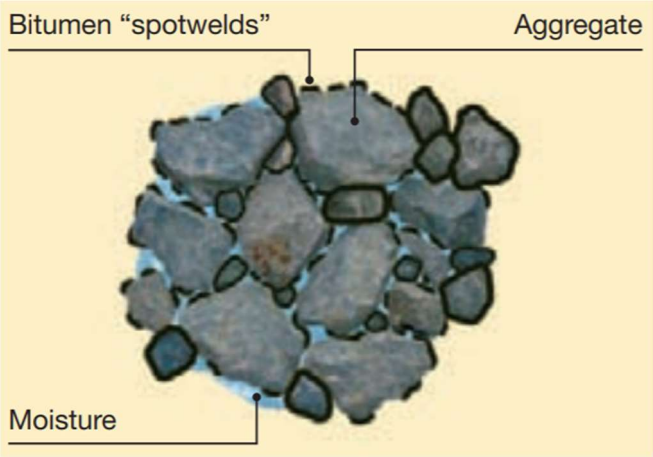

Figure 5: Foamed binder mastic (Wirtgen 2012).

Asphalt needs to meet two distinctive properties to be selected for use in a foamed asphalt design. The first is the expansion ratio, which is the ratio of the volume of foamed asphalt to the un-foamed counterpart. The expansion ratio is determined using a pre-calibrated bucket with a known volume and a calibration dipstick specific for foamed asphalt testing. The half-life is the measure of time in seconds that it takes for the unstable foamed asphalt to collapse to half of the maximum volume achieved. Research shows that the temperature is one of most influential factors in the quality of the foamed binder. It is recommended to identify a target binder temperature that can be achieved in the field for constructing a foam CR or FDR mixture. Additionally, the amount of water injected into the hot asphalt binder will affect the two properties. Testing of the foamed asphalt should include multiple water contents and binder temperatures so that an educated

selection of both can be made. The expansion ratio and half-life must be a minimum of 8:1 and 6 seconds, respectively (Wirtgen 2012). The Wirtgen Cold Recycling Manual (2012) provides a diagram of how to select an optimum foamed water content (OFWC) at a specific binder temperature, seen in Figure 6. Vertical lines are placed at the minimum required expansion ratio and half-life as indicated by the yellow lines. The OFWC, shown as the green vertical line, is selected as the point equidistant from either vertical yellow line drawn.

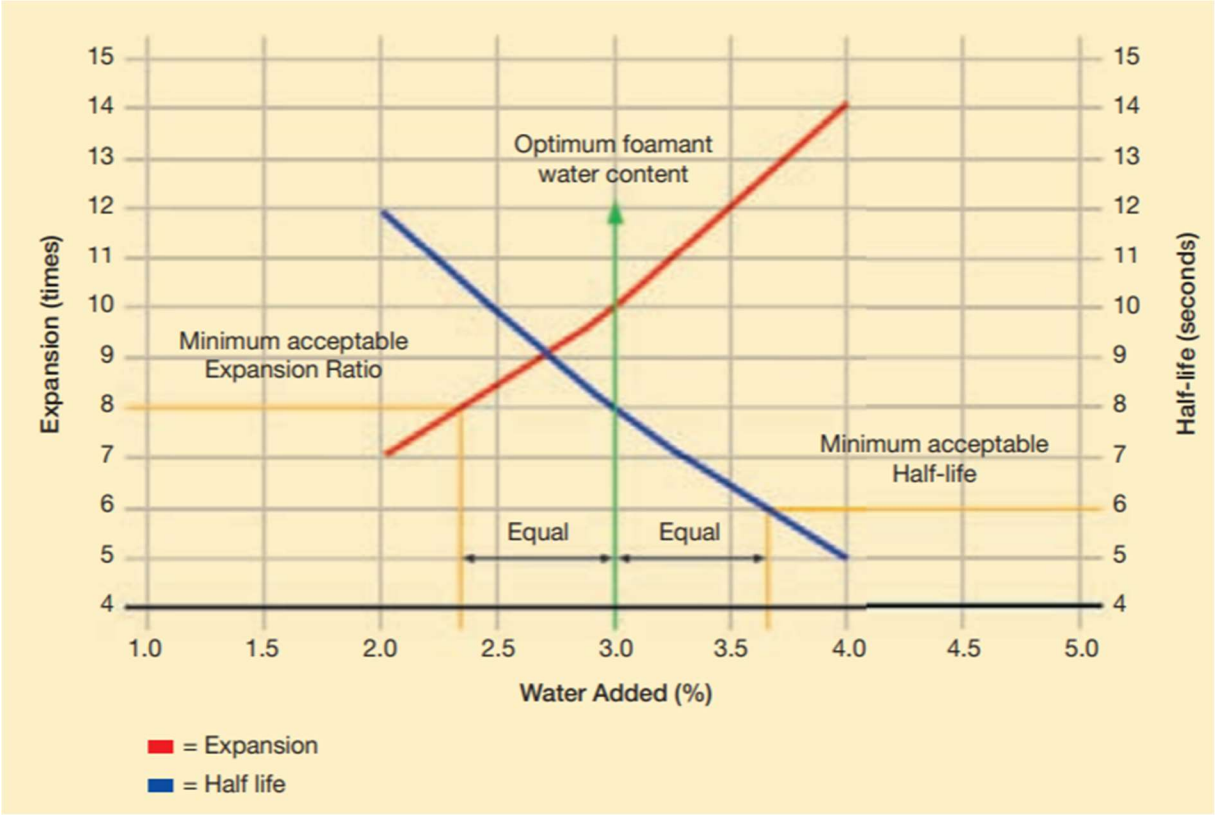

Figure 6: OFWC determination (Wirtgen 2012).

2.3 Mixture Design Process

A CR and FDR mixture design consists of selecting an appropriate RAP, recycling/stabilizing agent, and additional water content that meets specified recommended testing requirements. Several contractors are performing mixture designs using their own methods because there is not currently a standard design method for CR and FDR. Some of these methods

produced by agencies are empirical tests while others test the performance for acceptance of a CR mixture design (ARRA 2015). Cold in-place recycling and FDR mixture designs will vary based on the project because of the variation of material properties for in-place RAP. Additionally, a mixture design can be modified in the field by an experienced person to meet adequate mixing and compacting (ARRA 2015). This section covers RAP sampling, establishing a water/density relationship, selection of recycling/stabilizing agent content, use of active filler, and preparing and testing specimens.

2.3.1 RAP Sampling

Obtaining a representative sample of material for the mixture design process is essential because of the effect gradation is presumed to have on the final mixture performance. The gradations of the obtained RAP will be determined in accordance with AASHTO T27 (ARRA 2015). For a proper mixture design, several hundred pounds of RAP material should be collected from each pavement layer included in the recycling operation. FDR should include bound and unbound materials for which they will be processed during construction (ARRA 2015; Wirtgen 2012).

Recycled asphalt pavement used for the mixture design process needs to be sampled with proper techniques to minimize variation. For all recycling methods, the surface should either be milled or have cores cut and crushed from the proposed project site to obtain enough representative material to conduct proper mixture design procedures (Wirtgen 2012). Recycled asphalt pavement can be collected from existing stockpiles for CCPR mixture designs. It is important to obtain samples from the same stockpile that construction RAP will be processed from. There is a misconception that RAP stockpiles are highly variable, and that when increasing amounts of RAP are used, the mixture will perform unexpectedly. Even when stockpiles consist of various types of

RAP, good practices of stockpiling and sampling can minimize the variation (West 2015). For CCPR mixture designs using a stockpile of existing RAP it is important to ensure proper stockpile sampling. The best practice is to use a front-end loader to make a smaller stockpile from the larger one, flatten out the mini-stockpile, and sample from multiple locations along the surface of the flattened area until a few hundred pounds have been collected.

2.3.2 Establishing a Water/Density Relationship

Additional water in emulsified mixtures is required to aid in the coating of RAP particles while foamed mixtures used the additional water to aid in compactive effort (ARRA 2015). The water content that achieves a maximum dry density (MDD) is considered the optimum moisture content (OMC) of the RAP. The OMC and MDD are determined following the modified AASHTO T180 (Wirtgen 2012). It is typical for an emulsified and foamed mixture to require between 1.5 and 2.5% additional water added, and in some circumstances higher water contents can be needed (ARRA 2015).

2.3.3 Selection of Recycling/Stabilizing Agents

Selection of the appropriate performance graded (PG) binder is primarily centered on the in-service pavement temperatures found for a specific project. Cold recycling projects will select emulsifying agents based on their coating ability, initial strength, and breaking times. Foamed asphalt has recently been incorporated more often as CR mixtures continue to gain popularity. For FDR mixtures, the selection of emulsion versus foam is typically based on the percentage of fines found in the reclaimed material. An FDR mixture with 5 to 20% passing the No. 200 sieve may use foamed asphalt. When the fine particles passing the No. 200 sieve are between 0 and 20%, an emulsion may be used (ARRA 2015).

It is recommended that a range of three to four recycling/stabilizing agent contents be used during the mixture design process to find the optimum content meeting stability and strength requirements. It is typical for an emulsified mixture to include contents ranging from 0.5 to 4.0%, and a foamed mixture to include contents ranging from 1.5 to 3.0% by dry weight of RAP (ARRA 2015).

2.3.4 Active Fillers

The use of cement as an active filler in CR and FDR can improve early strength with the addition of 0.25% to a maximum of 1.0% of the dry RAP weight (ARRA 2015; Wirtgen 2012). The cement can be added in CIR and CCPR in a dry or slurry form. If the cement content is too high, it can cause the mixture to become too brittle (ARRA 2015) and can encourage shrinkage cracks similar to a concrete pavement during its curing process (Wirtgen 2012).

2.3.5 Preparing and Testing Specimen

2.3.5.1 Mixing and Compacting

To achieve a properly mixed material in a laboratory sized pugmill, such as a Wirtgen WLM-30, 20 to 30 kilograms of RAP are needed (Wirtgen 2012). After determining an OMC and percent of active filler, three to four recycling/stabilizing agent contents should be tested to determine the optimum content that meets all testing requirements (ARRA 2015). The standard compactive effort for cold recycled and full depth reclaimed mixture designs is 30-gyrations using a Superpave gyratory compactor immediately after mixing (Cross 2003; ARRA 2015) and 75-blows using a Marshall hammer (ARRA 2015). For testing of tensile strength and moisture sensitivity, a minimum of six specimens at each recycling/stabilizing asphalt content are

compacted (ARRA 2015; Wirtgen 2012) to a diameter of 100 mm and height of 63.5 mm (Wirtgen 2012).

2.3.5.2 Curing

For CR and FDR mixtures to fully cure and obtain their maximum strength, all water in a compacted specimen must evaporate. Curing is defined as the process of the water evaporating out of a mixture, and as a result the mixture tensile strength increases. It is typical for emulsified mixtures to have longer curing periods than foamed mixtures because they contain more water by the nature of its composition (Wirtgen 2012). In the laboratory, specimens are typically cured at a temperature of 60°C for emulsion and 40°C for foam recycled mixes (ARRA 2015). Curing is considered complete after a recommended maximum of 48-72 hours, and when no mass change is recorded, indicating evaporation of the water is complete (ARRA 2015; Wirtgen 2012).

2.3.5.3 Strength and Moisture Sensitivity Testing

Testing for ITS and Marshall stability (MS) are the two most common practices for identifying strength and moisture sensitivity in recycled mixes currently (ARRA 2015). While ITS testing is not the most repeatable method for flexibility and flexural strength of a specimen, it can be one of the most economical methods (Wirtgen 2012). Two sets of multiple specimens at each recycling/stabilizing agent content are selected for running dry and conditioned testing. The dry specimens for ITS shall be tested at 25°C while the specimens for MS shall be tested at 40°C (ARRA 2015).

Indirect tensile strength testing uses cylindrical compacted asphalt specimen with a continuous compressive load being applied on opposite sides of the specimen as seen in Figure 7. Kennedy found that the conditioning temperature of the specimen and the loading rate of the steel

loading strips applied can have a significant impact on the average test result (Kennedy and Hudson 1968). Therefore, having consistent testing protocols will provide the more reliable results. Cross' ITS testing resulted in a higher ITS values when 3:1 flat and elongated particles were found in the RAP. The specimen curing time and RAP physical properties did not seem to correlate to any significant differences in recorded ITS values (Cross 2003). Valentin et al. concluded that an increase in foam and/or emulsion asphalt contents resulted in an increased material flexibility but lowered the ITS and stiffness values (Valentin et al. 2016). No current standard is in place for a minimum ITS; however, ARRA recommends that the minimum CR mixture's ITS be 45 psi at the optimum recycling agent content (ARRA 2015).

Figure 7: Indirect tensile strength breaking head.

Marshall stability uses cylindrical specimens loaded into the breaking head and a continuous compressive load is applied on opposite ends of the specimen. The maximum load carried by a compacted asphalt specimen is considered the stability of the mixture. This value represents the measure of mass viscosity an asphalt mixture has. Viscosity is typically dependent on the binder grade, so increasing or decreasing the performance grade (PG) of an asphalt binder will increase or decrease the stability of the mix, respectively (Brown et al. 2009). Cox identified issues with emulsified CIR mixtures with regards to the stability of various emulsion contents. It was noted that repeatability of MS testing was poor. Cox had three replicate design curves with entirely opposite results, all with identical materials and testing procedures (Cox and Howard 2018). Identical to ITS, MS has no currently accepted standard for minimum required stability of a recycled/reclaimed mixtures, though ARRA (2015) recommends a minimum MS of 1,250 psi.

For identifying moisture susceptibility issues in mixtures, tensile strength ratio (TSR) and Marshall stability ratio (MSR) can be calculated. The ratios are the average maximum conditioned specimen's ITS/MS divided by the average dry specimen's maximum ITS/MS. The Asphalt Recycling and Reclaiming Association notes that the resistance to moisture induced damage using a TSR or MSR shall be a minimum of 0.70 but can be reduced to 0.60 if the ITS or MS exceed the minimum dry ITS/MS recommended requirements (ARRA 2015).

2.4 Performance Testing

2.4.1 IDEAL-CT

The IDEAL-CT was developed by Zhou et al. (2019) at the Texas A&M Transportation Institute because of the need for an economical and simplistic test for identifying the cracking resistance of a mix. It is similar in testing to ITS, but the IDEAL-CT test derives a cracking

tolerance index (CT_{Index}) from the measured load applied versus a displacement curve. Zhou et al. stated that the IDEAL-CT is rugged when the four properties of the specimen (height, air voids, loading rate, and test temperature) remain similar regardless of the mixture tested (Zhou et al. 2019). Dong and Charmot identified that within CR mixtures, the CT_{Index} increases when emulsion content increases and when cement content decreases. Conversely, CR mixes with increasing amounts of cement tended to become more brittle, consequently having a lower CT_{Index} (Dong and Charmot 2019). Diefenderfer et al. (2019) conducted a cracking analysis on CR mixtures using IDEAL-CT procedures. The results of the study showed that for a slow setting CR pavement recycled with emulsion, the average CT_{Index} was 29.8 when no cement was included. A reduction of 20.2 in the average CT_{Index} was found when cement content was raised from 0 to 1% within a CR mixture.

2.4.2 Hamburg Wheel Track

The HWT helps identify the rutting and stripping potential in asphalt surface mixtures because the test is conducted in a hot water bath. The prediction of rutting in the field is reduced, so the HWT test is used primarily to note any potential rutting issues for a specific mixture (Brown et al. 2009). Currently, AASHTO T324 is the standard test method for HMA using a HWT device. Testing is generally conducted at 50°C with a conditioning period of 45 minutes prior to starting wheel passes on the specimen. Figure 8 shows a typical curve from Hamburg testing with various parameters and points of interest. Consolidation of the asphalt materials within testing specimens occurs within the first few hundred passes. A rutting creep is usually identified, and when a significant increase in rut depth occurs, a stripping point can be visualized, indicating that stripping had begun in the mix. An example of a passing HMA mixture with 1 to 3 mm of rutting after 20,000 passes is shown in Figure 9.

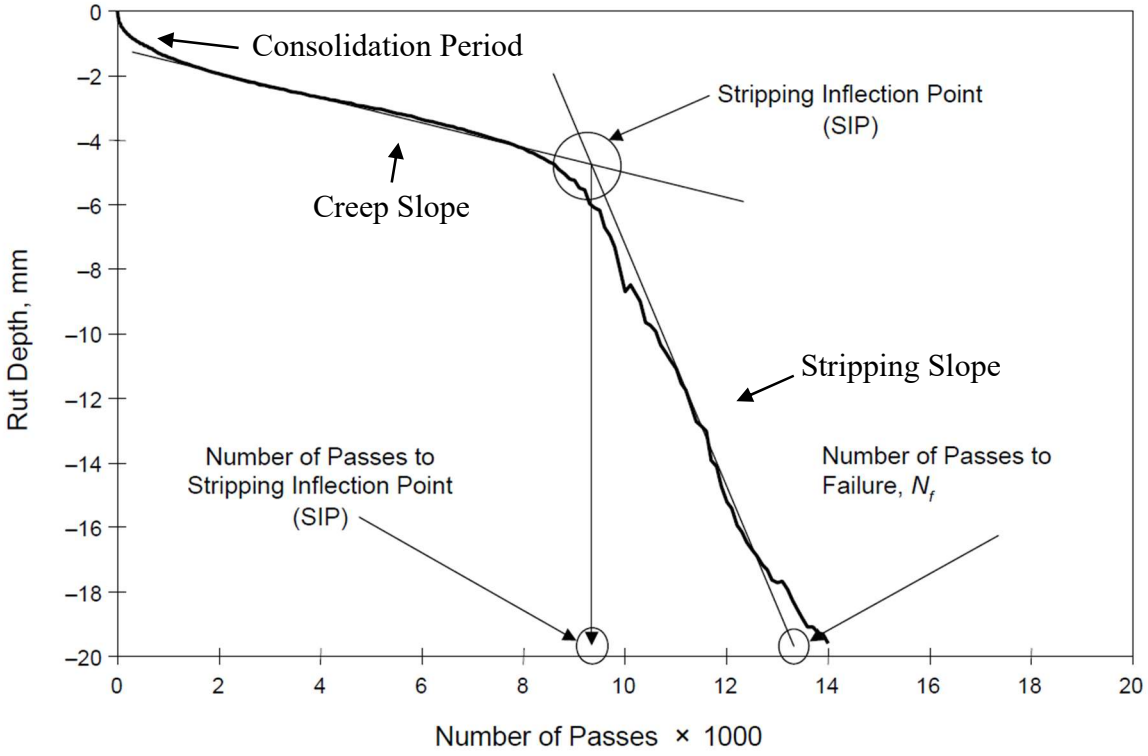

Figure 8: Hamburg curve with test parameters (AASHTO T324-19 2020).

Figure 9: Hamburg HMA specimen example after 20,000 passes with good rutting resistance.

2.4.3 Dynamic Modulus

Dynamic modulus for asphalt mixtures is defined as the stress to strain ratio under repetitive compressive traffic loads. It is a common means for predicting and analyzing pavement performance for laboratory produced and field cored specimen under various kinds of traffic and climates (Witczak et al. 2002). The modulus can be found using an Asphalt Mixture Performance Tester (AMPT) or similar device. The standard test method for determining dynamic modulus of a mixture using an AMPT is found in AASHTO T378. Specimens designated for testing of the dynamic modulus are prepared in accordance with the standard method of practice in AASHTO R83. Additionally, SS specimen measuring 50 mm in diameter and 110 mm in height can also be tested, as compared to the LS specimen measuring 100 mm in diameter and 150 mm in height. Because most cold recycled layers are not generally paved with lift heights of 150 mm or greater, coring and cutting a LS specimen is not a practical option (Schwartz et al. 2017; Diefenderfer et al. 2015). Strong correlation between the LS and SS specimens were found for dynamic modulus testing (Schwartz et al. 2017; Diefenderfer et al. 2015). Research was conducted comparing the SS and LS dynamic modulus results of various hot mix asphalt mixtures. The statistical results of the study showed that no significant difference in the dynamic modulus of SS and LS was identified at all temperatures, reduced frequencies, and nominal maximum aggregate sizes (Bowers et al. 2015).

2.4.4 Recycled Pavement Performance

During the NCAT Test Track's Phase V cycle, three sections (N3, N4, and S12) sponsored by the Virginia Department of Transportation (VDOT) were studied to characterize the field performance of CCPR as a recycled base material. The cross sections of the three test sections are provided in Figure 10. The CCPR lifts were constructed using 100% RAP, 2% foamed asphalt of

PG 67-22, and 1% hydraulic cement. The CCPR lifts were overlaid by a combination of HMA and SMA ranging from an average of four inches. Rutting of the three test sections was tracked between October 2012 and October 2014, with a maximum resulting rut depth of 0.30 inches. The N3 and N4 section's backcalculated modulus for the AC/CCPR lifts together were calculated and the combined AC/CCPR lift's response to temperature was similar to a conventional HMA material (West et al. 2018).

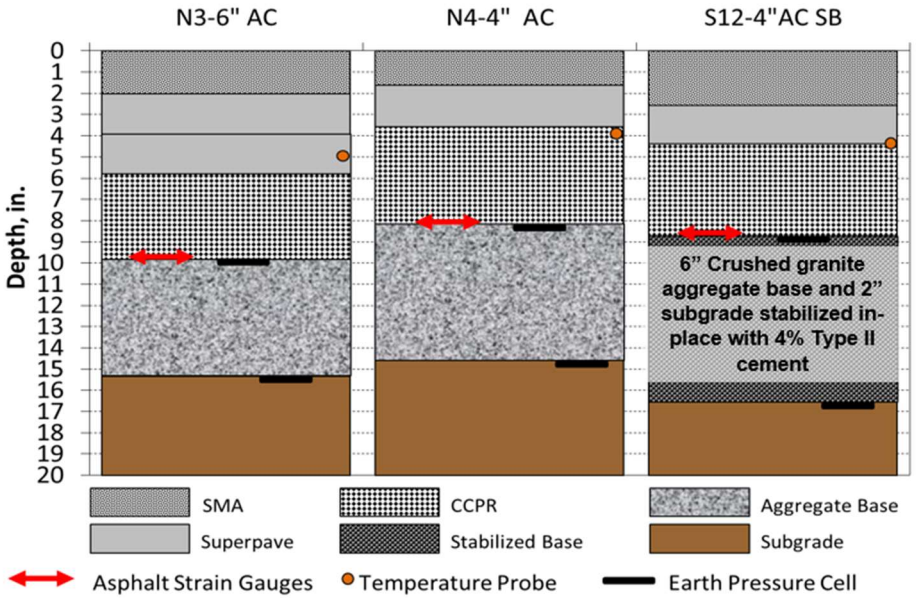

Figure 10: NCAT Test Track Phase V, VDOT experiment average as-built thicknesses and depth of instrumentation (West et al. 2018).

A second research cycle of 10 million equivalent single axle loads (ESALs) was conducted during Phase VI research cycle on the same section as Phase V. At the conclusion of Phase VI, 20 million total ESALs had been applied to the three sections. Excellent performance of these sections was realized when there was no observed cracking and the backcalculated moduli of the sections remained similar in response to temperature as it had in the previous research cycle. It was expected that the sections would be able to handle many more years of service before rehabilitation was necessary (West et al. 2019).

The Virginia Department of Transportation conducted a study along Interstate 81 in Virginia that consisted of CIR, CCPR, and FDR constructed as seen in the cross section in Figure 11. One of the objectives of this project was to study the structural performance during a three-year period following construction to establish a baseline for future CR and FDR pavement performance evaluation. The field performance evaluation of these two lanes showed that after 34 months of service, the left and right lanes had rut depths of less than 0.1 and less than 0.05 inches, respectively (Diefenderfer and Apeagyei 2014).

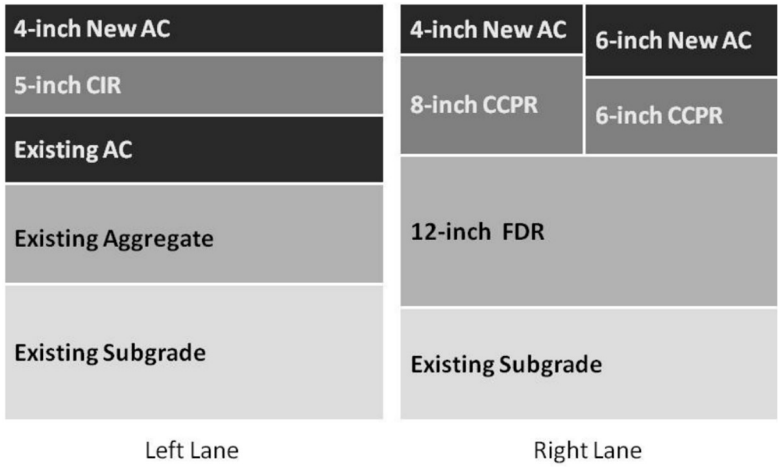

Figure 11: VDOT I-81 cross sections for left and right lanes (Diefenderfer and Apeagyei 2014).

In 2015, a study on the performance of CR pavements on US Highway 280 began when four sections were built. The objective of the study was to evaluate the structural contribution of the CR lifts. Cross sections of the pavement sections containing the CIR and CCPR lifts are in Figures 12 and 13, respectively.

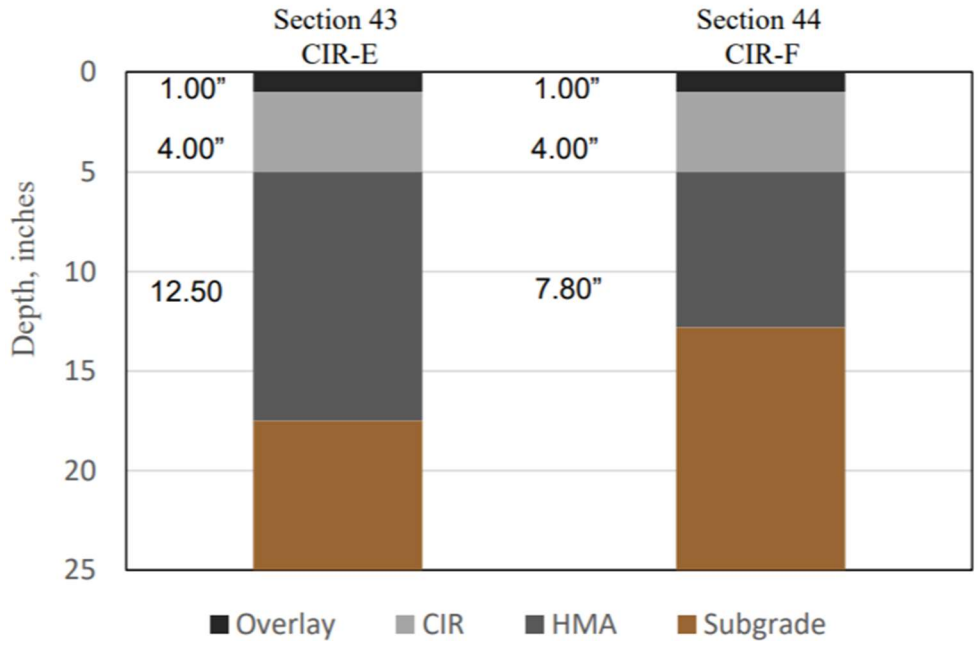

Figure 12: NCAT pavement preservation CIR test sections' cross sections (Martinez 2020).

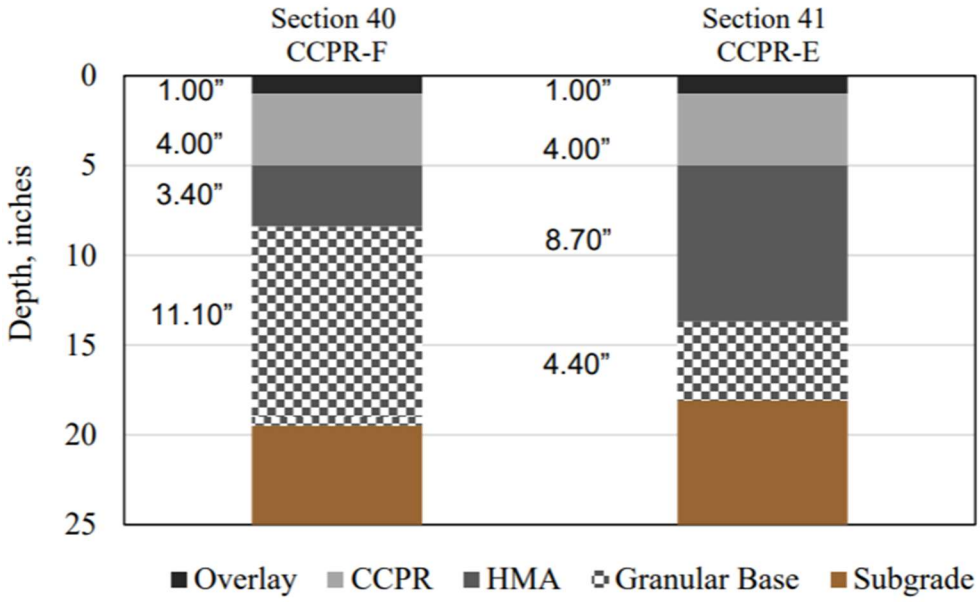

Figure 13: NCAT pavement preservation CCPR test sections' cross sections (Martinez 2020).

Martinez (2020) found that each of the four sections exhibited good cracking resistance for the majority of the 4.5-year study, but towards the end, the CCPR-F section began cracking more as compared to the other three sections. The composite pavement modulus was backcalculated and

the CIR-E and CIR-F exhibited a strong influence between pavement temperature and the backcalculated modulus. The CCPR-E and CCPR-F sections modulus slowly decreased overtime.

2.5 Summary of the Literature Review

Cold recycling and full depth reclamation are processes that incorporate cold milled RAP materials with recycling and stabilizing agents to construct strengthened base layers from existing roads. Asphalt binder needs to meet specific expansion and half-life requirements to be considered for foaming purposes, and the selection of an emulsion is dependent on construction application and material properties. The acceptance testing of ITS and MS is currently only a recommended requirement, and the IDEAL-CT and HWT performance tests are used to determine cracking resistance and rutting potential specifically for HMA mixtures. The usage of CR and FDR mixtures as strengthened base layers is currently being studied in NCAT and MnROAD's Pavement Preservation projects. The test sections that incorporated these sustainable layers have shown results similar to conventional HMA pavements, indicating that the potential for these materials to be used in more paving projects is promising.

CHAPTER 3 – METHODOLOGY

This chapter focuses on the methodology for conducting a CR mixture design with foamed asphalt as the recycling agent, the as-built mixture and LMLC specimen production and performance testing, the PMLC specimen production and performance testing, and PMFC specimen production and performance testing.

3.1 Mixture Design

The mixture design process was conducted at NCAT for the CIR and CCPR foamed test sections. NCAT used a Wirtgen WLB-10S laboratory-scale foamed asphalt plant to determine foaming properties of the provided asphalt binder. The laboratory WLB-10S was used in conjunction with a laboratory-scale plant pugmill, Wirtgen WLM-30, to mix the recycled material with water, foamed asphalt, and cement. These two machines together are shown in Figure 14. The ITS was determined using a Marshall press. Conditioned and dry specimen ITS results were compared to determine the moisture susceptibility using the TSR. The design optimum recycling agent content was selected as the mixture at which the minimum dry strength and TSR recommended requirements were achieved.

Figure 14: Wirtgen WLB-10S laboratory foamer and WLM-30 laboratory pugmill.

3.1.1 Obtaining Materials

To conduct a proper mixture design for the CIR foam section, multiple cores were taken at random locations inside the proposed construction bounds. Cores were then crushed by an industry partner and multiple five-gallon buckets of the processed RAP were shipped to NCAT. For the CCPR foam section, multiple five-gallon buckets of RAP were collected from a pre-designated RAP stockpile to be used during the construction phase. Recycled asphalt pavement collection was performed by an outside source and steps were taken upon receiving the material to properly homogenize it.

The recycling agent selected for the project, a PG 58-28 binder, was collected in multiple five-gallon buckets from a supplier in Minnesota and shipped to NCAT.

3.1.2 Processing and Preparation of Materials

3.1.2.1 RAP Properties

Due to high variability found in most black rock stockpiles and segregation that occurred during the shipment of materials, all RAP materials were homogenized by hand. A mini-stockpile of the CIR RAP was built on a smooth dry concrete floor. The stockpile formed was kept flat and without a peak to reduce the chance of segregation. The mini-stockpile was split into four quadrants, seen in the Figure 15. A single quadrant was selected, and half of the empty buckets were filled with a single scoop from that selected quadrant. Then the quadrant diagonal to the first was used to fill the remaining empty buckets with one scoop. The mini-stockpile was re-homogenized at this point. This process of creating quadrants and filling buckets a single shovel at a time was continued until the mini-stockpile was nearly empty. The remaining material left behind after each bucket was filled equally was recycled at a local asphalt plant. The material experienced fluffing after homogenization; therefore, there appeared to be more material remaining at the end of mixing than what was originally provided, resulting in a small excess of RAP. The CCPR was homogenized in the same method as the CIR above.

Figure 15: Mini-stockpile of RAP split into quadrants during the homogenization process.

Due to the high temperature volatility of RAP, instead of drying moisture out by an oven, the RAP was dried in an ambient temperature warehouse with multiple box fans. The RAP was occasionally stirred to encourage the drying process. The drying stage was completed no sooner than one-week after initially being placed in front of the fans. A hydroscopic moisture content of the RAP was not recorded for the mixture design process. After drying, the RAP was screened over a one-inch sieve to remove any oversized particles and returned to their buckets.

The black rock (or coated) gradation of the RAP was determined following AASHTO T27 for sieve analysis. Prior to conducting the sieve analysis, two buckets of RAP were selected and reduced to appropriate testing size by a mechanical splitter following standard practices from AASHTO R76. Following the black rock sieve analysis, the sample was burned in an NCAT

ignition oven following the standard test from AASHTO T308. The remaining aggregate after the test was used to determine a burn gradation. Due to ashing that can occur during the ignition process, samples were washed following the standard test from AASHTO T11, prior to conducting the sieve analysis.

3.1.2.2 Moisture-Density Relationship

An OMC was needed to conduct a mixture design for each of the cold recycled materials. To determine the OMC, a modified Proctor following the standard test method of ASHTO T180-D was conducted with varying moisture contents. A single bucket of RAP was mechanically split into portions of nearly six-kilograms each. The RAP was not dried by low temperature ovens to determine a hydroscopic moisture content prior to this process. Each sample of RAP was weighed, and varying amounts of ambient temperature tap-water were mixed by hand into the pre-weighed RAP on a smooth metal sheet. Target moisture contents that were tested varied from 3.0 to 6.0% by weight of RAP. Two replicates at each moisture content were tested and averaged. Material was collected for each of the tests run following the specification procedures and moisture contents of the RAP were calculated. Wet and dry density values for each were calculated with Equations 1 and 2, respectively. A graphical approach was used in determining the OMC. The point at which the maximum dry density was achieved was noted as having the OMC for construction.

$$W_1 = (A - B)/V \tag{1}$$

Where:

W_1 = Wet density of compacted soil, lb/ft^3

A = Mass of the mold base plate, and wet soil, lb

B = Mass of the mold, base plate, lb

V = Mold volume, ft^3

$$W = \frac{W_1}{w+100} \times 100 \quad (2)$$

Where:

W = Dry density of compacted soil, lb/ft^3

W_1 = Wet density of compacted soil, lb/ft^3

w = Moisture content of the specimen, %

Significant difficulties were met during the modified Proctor such as excess water seeping from the base of the mold (Figure 16), lowering the intended water contents of the RAP. Additionally, slicing the compacted sample with respect to the procedures in T180-D was difficult due to the presence of large RAP particles. This caused issues with sampling which in turn affected the sample collection for determining the actual moisture contents for each water content tested.

Figure 16: Modified Proctor test, seeping excess moisture.

3.1.2.3 Foamed Asphalt Characteristics

The properties of the foamed asphalt binder, expansion ratio and half-life, were tested following standard procedures provided by Wirtgen's Cold Recycling Technology Manual (2012). The expansion ratio and half-life of a foamed asphalt binder varies due to the temperature of the binder and water content injected into the binder. The binder temperatures tested were 150°C, 160°C, 165°C, and the water contents tested were 1%, 2%, and 3%.

3.1.3 Mixing and Compacting

A single five-gallon bucket of RAP was used for each asphalt content tested because the Wirtgen WLM-30 pugmill is recommended to have 20 to 30 kilograms of material in each batch for optimum mixing. After the asphalt binder was heated to 150-160°C in a separate oven to reduce the viscosity, it was poured into the heated kettle inside the WLB-10S foaming machine. The

temperature of the foaming machine's components was set to the optimum binder temperature for foaming and the water content was adjusted to the OFWC.

Mixing of the recycled material using foamed asphalt was performed in three rounds of 60-second mixing. The weighed RAP sample was poured into the pugmill, along with 1% cement by weight of dry RAP. The first round was performed on the RAP and cement mixture only. Figures 17 and 18 show the raw RAP and RAP-and-cement mixtures in the pugmill, respectively.

Figure 17: Raw RAP in the WLM-30 pugmill for laboratory foamed asphalt recycling.

Figure 18: RAP-and-cement mixture in the WLM-30 pugmill for laboratory foamed asphalt recycling.

The additional water required to achieve the OMC was then added to the pugmill, and the second round of mixing began. Immediately after completing the second round of mixing, the pugmill was aligned with the laboratory foamer and the third round of mixing began. After 10-seconds of mixing in the pugmill the foamer was activated so that the foamed binder would coat the mixture during the 'unstable' period of the asphalt for maximum coverage, Figure 18. Mixing continued until the pugmill finished the third 60-second round of mixing. Figures 19 and 20 show the recycled asphalt mixture before and after introducing the foamed asphalt, respectively.

Figure 19: Recycled asphalt mixture in the WLM-30 pugmill before foamed asphalt injected.

Figure 20: Completed foamed recycled asphalt mixture in the WLM-30 pugmill.

The recycled mixture was visually inspected to ensure that it was homogenous. A handful of the CR mixture was squeezed by hand to check for mixture cohesion and for dispersion of the asphalt foam seen in Figure 21 and 22, respectively. If after squeezing a sample of the mixture by

hand produces a loose mix that falls apart, cohesion of the mix is poor. Additionally, small spots of foamed asphalt should remain indicating proper foamed binder dispersion, instead of large clumps that would indicate poor foaming of the asphalt binder.

Figure 21: Cohesion check of foamed cold recycled material.

Figure 22: Dispersion of foamed asphalt check by hand.

The completely mixed CR mixture was then placed into a tub with a sealable lid so that it did not begin to lose moisture and cure prior to compaction. The ITS test to be conducted on the mixtures required a 100 mm diameter specimen with a height of 63.5 ± 1.5 mm. The specimens were compacted using 30 gyrations. Because the mixture design for cold recycled material is specified to be completed with 30 gyrations (ARRA 2015), the height of the specimens was dependent on the weight of material added to the mold. A minimum of two specimens were compacted for each CR method to dial in the precise amount of CR mixture to be within the height tolerance.

3.1.4 Indirect Tensile Strength Verification

After compacting of a minimum of eight specimens within the allowed height tolerances, they were each cured in an oven at 40°C for 72 hours. The ITS testing was conducted on conditioned and dry specimen so that moisture susceptibility could be evaluated. At the completion of the curing period, the specimens were weighed and measured for their height and diameter using calipers. The specimens designated for conditioned testing were placed into a 25°C water bath, seen in Figure 23, while the dry specimens were placed into a 25°C oven, both for 24 hours.

Figure 23: Water bath for conditioning samples for ITS or MS.

At the end of the 24-hour conditioning regime the dry specimens were removed from the oven and tested according to the specification. For each conditioned specimen, they were gently dried to saturated surface dry (SSD) condition and tested according to the specification. The Marshall apparatus seen in Figure 24 was used for the ITS and MS testing, along with the four-inch strength-loading fixture. The tensile strength (S_t) values were determined using Equation 3. Additionally, the TSR was determined using Equation 4 for evaluating moisture susceptibility of the mixture designs (AASHTO T283 2018).

$$S_t = \frac{2P}{\pi t D} \quad (3)$$

Where:

S_t = Tensile strength, psi

P = Maximum load, lbf

t = Specimen thickness, in.

D = Specimen diameter, in.

$$TSR = \frac{S_2}{S_1} \quad (4)$$

Where:

TSR = Tensile strength ratio

S_1 = Average tensile strength of the dry subset, psi

S_2 = Average tensile strength of the conditioned subset, psi

Figure 24: PINE Marshall apparatus used for ITS and MS testing.

The cold recycled mixture is considered passing if the required foaming properties are met, the dry ITS is greater than the 45-psi requirement, and the TSR is greater than 0.70. Foamed asphalt contents for recycled mixtures typically are within the ranges of 1.5 to 3% (ARRA 2015). Three foamed asphalt contents of 2.0, 2.3, and 2.6% were selected for testing. Because one of these met the ITS and TSR requirements, no other foamed binder contents were tested.

3.2 As-Built Mixture Specimen Production and Testing

During the construction process in Minnesota, rainfall affected the in-place moisture content for some of the test sections and as a result, changes of the mixture design targets were made as seen in Table 2 and 3 for emulsion and foamed mixtures, respectively. Additionally, the RAP stockpile initially selected for the CCPR construction phase was changed prior to placement. During construction of the FDR foam section, the reclaimer was not processing the material properly and cement was tossed into the raw material before sampling for PPLC specimen could take place. Therefore, the raw processed RAP in the FDR foam stabilized section was not collected for testing as-built mixture specimens, and PPLC specimens were not delivered to NCAT to be tested.

Table 2: Emulsion mixture design and as-built mixture properties.

Mixture	CIR-E			CCPR-E		FDR-E	
Method	Medium Mix Design	Coarse Mix Design	As-Built	Mix Design	As-Built	Mix Design	As-Built
Agent Content, %	3.0	2.5	2.8	3.5	3.5	3.0	3.0
Active Filler Content, %	N/A	N/A	N/A	N/A	N/A	N/A	N/A
Moisture Content, %	3.00	2.83	4.91	3.66	5.4 & 7.1	3.70	6.16

Table 3: Foam mixture design and as-built mixture properties.

Mixture	CIR-F		CCPR-F	
Method	**Mix Design**	**As-Built**	**Mix Design**	**As-Built**
Agent Content, %	2.6	2.6	2.3	2.3
Active Filler Content, %	1.0	1.0	1.0	1.0
Moisture Content, %	4.50	3.60	4.50	4.94

Tests conducted from the as-built mixtures were more abundant due to the quantity of material provided. Table 4 summarizes the testing conducted for each recycling methods, split by asphalt recycling/stabilizing agent type.

Table 4: Testing regime for each stabilizing agent used.

Asphalt Agent	Indirect Tensile Strength	Marshall stability	Hamburg Wheel Track	IDEAL-CT	Dynamic Modulus (SS and LS)
Emulsion		X	X	X	X
Foam	X		X	X	X

3.2.1 Obtaining RAP Samples

During construction of the test sections, samples of processed RAP for CIR and FDR were collected after the in-situ pavement was milled by the recycler and reclaimer, respectively. The CCPR RAP materials were collected from the newly designated stockpile at the central plant during construction. All RAP materials were collected and sealed in multiple five-gallon buckets and delivered to NCAT for as-built testing. Additionally, multiple buckets of PG 58-28 binder for the foaming sections were collected at the supplier. The EE used for the emulsion recycled and

stabilized sections was a cationic slow setting solution mixed with PG 58-28 binder. Multiple jugs of the EE were delivered to NCAT for use in the laboratory.

3.2.2 Processing and Preparation of Materials

The unexpected rainfall during the week of construction resulted in the RAP having high moisture contents. The samples of RAP were dried and homogenized in the same manner as the mixture design RAP in section 3.1.2.1.

To verify that homogenization of the mini stockpiles was performed properly, a black rock sieve analysis was completed on multiple buckets from each section. Selected buckets were split down to a proper testing size using a mechanical splitter. Once verification of similar gradations was performed, buckets were stored and numbered for use. If the gradation analysis showed a large difference between buckets, homogenization would be completed again until acceptable. Additionally, gradations of the raw RAP recorded during construction were compared to the homogenized RAP in the laboratory for verification of similar material gradations. All material was screened over a one-inch sieve to remove large chunks of RAP.

3.2.3 Mixing and Compacting

Mixing of the foamed recycled mixtures was performed in the same manner as the mixture design, section 3.1.3. The foamed asphalt, cement, and the additional water contents used in the laboratory mixing process were based on the as-built mixtures. The additional water contents were the recorded moisture contents of the mixtures during construction, as reported in section 4.3.

Mixing of the emulsion recycled and reclaimed mixtures was performed with the laboratory-scale pugmill. The mixing of the emulsified samples was performed in two 60-second rounds. Prior to weighing the appropriate EE contents for mixing, the EE was stirred with a glass

rod to ensure that there were no clumps of asphalt residue separated from the rest of the sample. The weighed RAP was added to the pugmill along with the additional water to achieve the recorded moisture contents of the mixtures during construction. The first round of mixing began, and after completing it, the weighed portion of EE was added to the mixture in the pugmill and mixed for a final 60-second round. After mixing, the recycled mixture was inspected visually for complete homogenization during mixing, and then placed into a tub with a sealable lid so that it did not lose moisture and break early.

Various specimen diameters and heights were required to be compacted. Therefore, two different gyratory compactors were used to compact the specimen. Table 53 summarizes the specimen sizes needed for each performance test along with the gyratory compactor used.

Table 5: Performance test specimen dimension requirements.

	MS/ITS	HWT	IDEAL-CT	Dynamic Modulus
Diameter, mm	100	150	150	150
Height, mm	63.5 ± 1.5	62 ± 1.5	62 ± 1.5	180 ± 10
Gyratory Compactor		Pine 125X		Troxler 5850v2

3.2.4 Curing

After compacting the specimen using the Superpave gyratory compactor (SGC), they underwent a curing regime depending on their designated test. Specimens with foamed asphalt as the recycling agent were cured at 40°C for ITS testing, while those with EE as the recycling/stabilizing agent were cured at 60°C for MS testing. All specimens except those designated for MS cured in an oven at the aforementioned temperatures for a minimum of 72 hours and until a constant mass was met.

The ITS specimens followed the same procedures for curing, conditioning, and testing as in section 3.1.4. The results from the ITS tests were recorded as the as-built's ITS test results and were later compared to the mixture design results.

The MS specimens were cured in an oven at 60°C for 48 hours. The heights of the MS specimens were measured with calipers and the weights were recorded. Specimens for conditioned testing were placed into a 25°C water bath for 23 hours, and then a 40°C water bath for 1 hour. They were gently dried to SSD and tested. The dry specimens were placed into a 25°C conditioning chamber for 22 hours, and then a 40°C oven for 2 hours. Specimens were removed from the oven and tested according to the specification.

Prior to any cutting, coring, or conditioning, specimens had their heights measured using calipers and their weights recorded. The dry density of the specimens could then be evaluated to verify that specimens prepared from the same component materials and designs were not different. These dry densities were also used to compare to cored specimen whose dry density should be greater at the center of a specimen compacted using a Superpave gyratory compactor.

3.2.5 Performance Testing

3.2.5.1 Indirect Tensile Strength & Marshall Stability

Similar to section 3.1.4, the foamed asphalt specimens were conditioned and ITS tested to verify if they passed the minimum requirement for the designs with a TSR of 0.70 and a dry tensile strength of 45 psi. The conditioned and dry emulsion specimen were tested for MS. Similar to TSR from the indirect tensile strength testing, MSR should be determined. The MSR should be greater than 0.70 and the average dry MS is recommended to be a minimum of 1,250 pounds (ARRA 2015).

3.2.5.2 IDEAL-CT

Each of the mixtures had five replicate specimens tested. Some of these were made in the same mixing and compacting batches while other mixtures were made on separate days following the same procedures. Similar to the Hamburg specimens, IDEAL-CT specimens were allowed to cool in an ambient temperature room for two to three days after curing was completed. A minimum of five specimens were placed into a 25.0°C conditioning chamber for a minimum of two hours. Specimens were placed into the TestQuip loading cell, seen in Figure 25, following protocols in the TestQuip IDEAL-CT software. The hydraulically loaded frame was set to displace 50 mm/min. The CT_{Index} was calculated by the software on the laptop and the data was recorded.

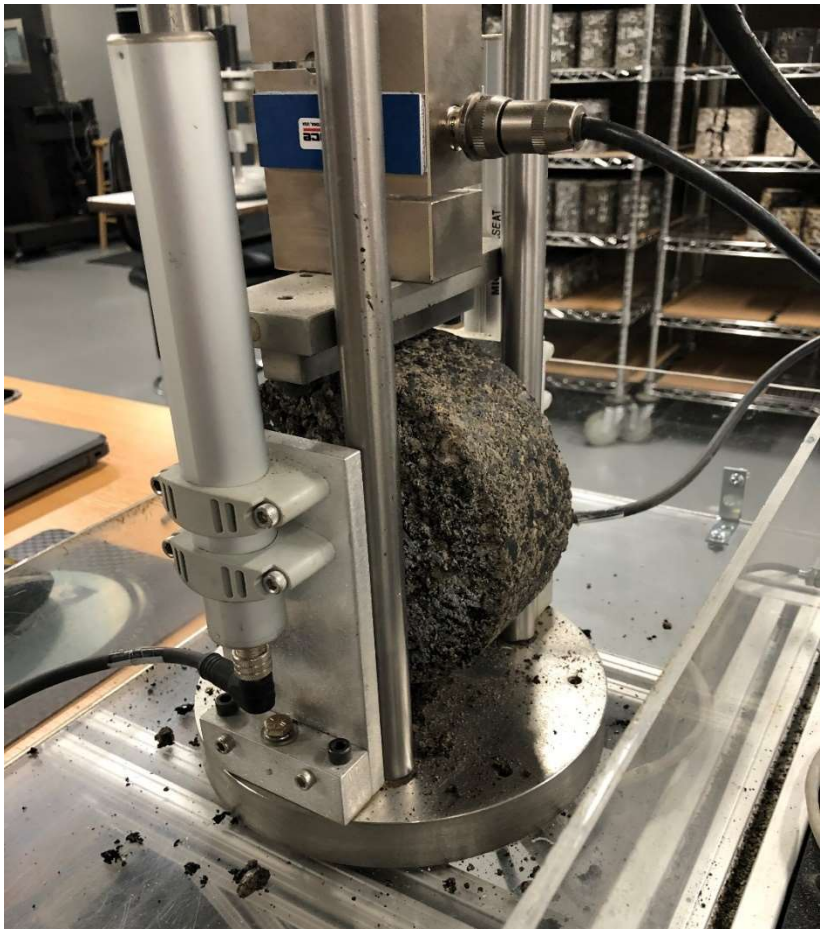

Figure 25: TestQuip load frame with a CCPR-F specimen.

3.2.5.3 Hamburg Wheel Tracking

After curing, the HWT specimens were allowed to cool to ambient temperatures for two to three days, and were then cut with a wet masonry saw, and placed into the cylindrical specimen mounting system seen in Figure 26. The specimens were placed in the James Cox & Sons HWT device, seen in Figure 27, and conditioned for 45 minutes under a 50°C water bath prior to testing. Two replicate pairs of specimens for each recycled/reclaimed mixture were tested. Specimens were tested until a rutting depth of 13.0 mm was reached for both sets in a single test.

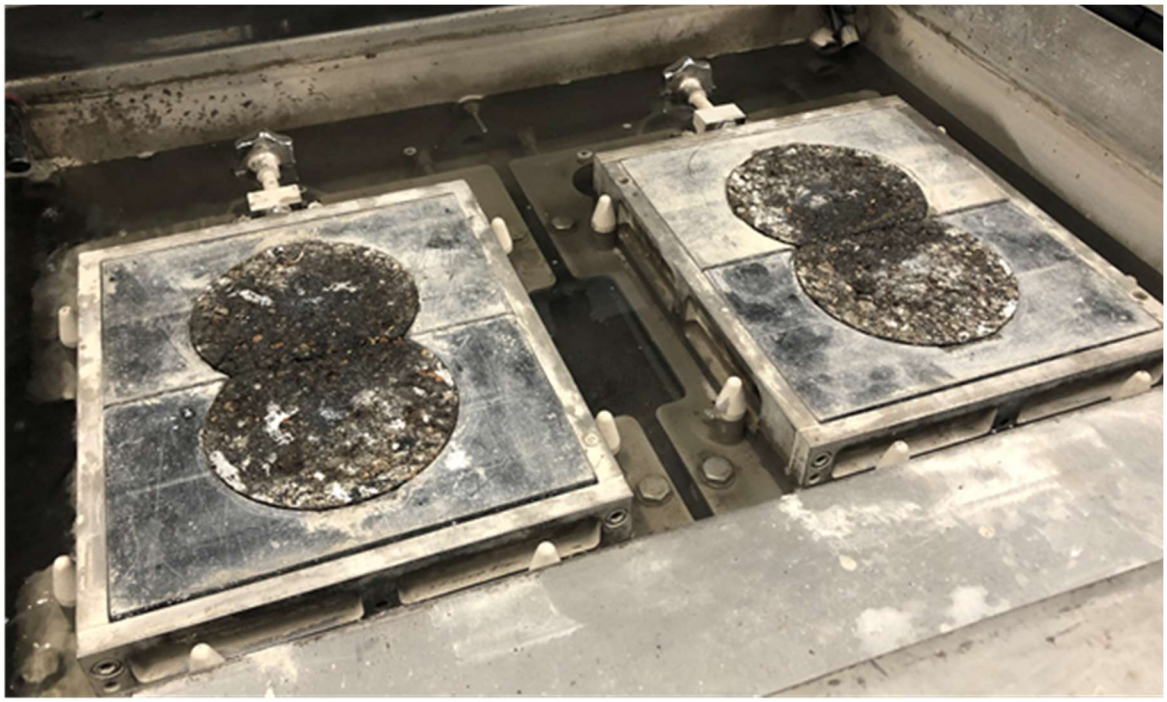

Figure 26: HWT specimens loaded into the cylindrical specimen mounting systems.

Figure 27: James Cox & Sons Hamburg Wheel Tracker (James Cox and Sons 2018).

3.2.5.4 Dynamic Modulus

Dynamic modulus testing was performed on 50 mm and 100 mm tall specimens, identified as SS and LS, respectively. Prior to coring, samples were placed on shelves indoors to remain at ambient temperature for a minimum of two weeks to ensure the curing process was complete. From a 180 ± 10 mm tall sample, the SS and LS specimens were cored horizontally and vertically, respectively. Coring was completed using the wet coring drill, seen in Figure 28.

Figure 28: Wet coring drill stand with 50 mm core bit and sample.

After coring, specimens were cut on the top and bottom with a wet masonry saw to achieve the 110 mm and 150 mm heights required for the SS and LS specimen, respectively. These SS and LS specimen will also be referred to as LMLC-S and LMLC-L, respectively, when comparing the mixing and compacting specimen types. After coring and cutting, specimens were placed on a rack to dry in front of fans for a minimum two weeks to remove excess water. Specimens' dimensions

were measured using calipers, their weights were recorded, and they were studded using the IPC Global Gauge Point Fixing Jig in Figure 29.

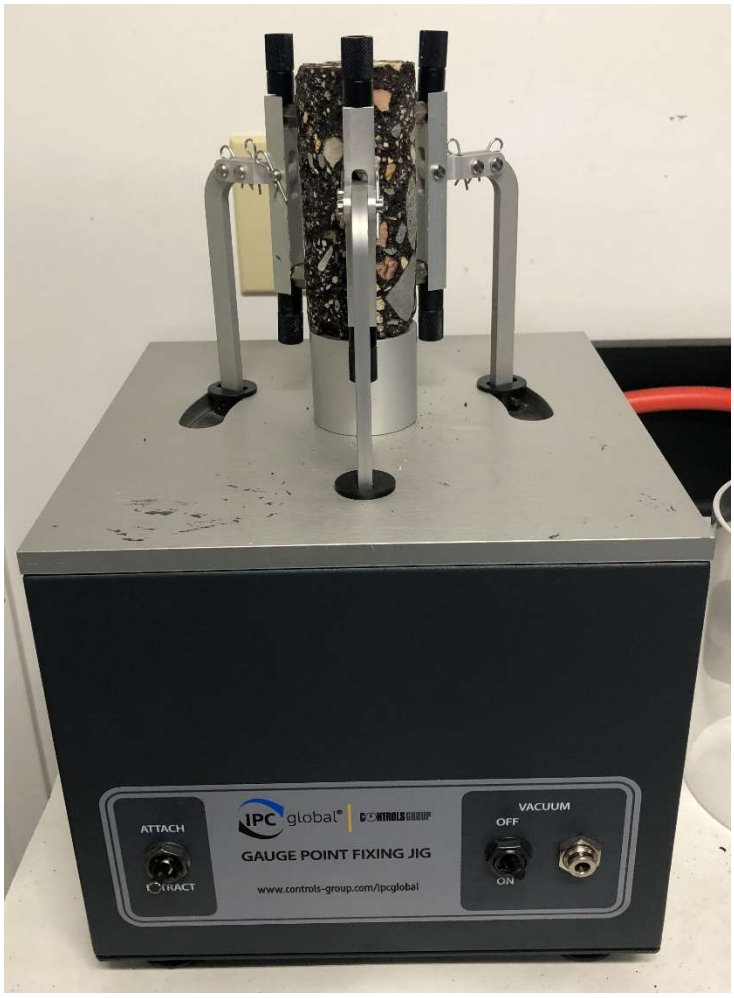

Figure 29: IPC Global gauge point fixing jig.

Recording the dynamic modulus of specimens was performed with IPC Global's AMPT PRO. Three testing temperatures of 4.4°C, 21.1°C, and 37.8°C and six testing frequencies of 25, 10, 5, 1, 0.5, and 0.1 Hz were used based on cold recycled dynamic modulus research completed in the NCHRP project 09-51 (Schwartz et al. 2017). To reduce the possible risk of damage to the specimens, they were each tested in an increasing order of temperature and decreasing order of frequency. LS were placed in a conditioning chamber overnight for the 4.4°C, two hours for the 21.1°, and three hours for the 37.8°C tests. SS were placed in a conditioning chamber for a

minimum of two hours prior to testing for each of the three testing temperatures. Three spring-loaded linear variable differential transformers (LVDTs) were placed on the glued studs around the specimen and were loaded into the AMPT chamber. Teflon sheets were placed on the top and bottom of the specimen to reduce friction between it and loading platens. Specimens were conditioned at the testing temperature for an additional thirty minutes inside the AMPT PRO testing chamber prior to starting the dynamic modulus testing. A specimen prepared for testing in the AMPT PRO chamber can be seen in Figure 30. Verification of the specimen data after testing at each temperature was done with the data quality characteristics in Table 6.

Figure 30: IPC Global AMPT PRO with a large dynamic modulus specimen in the conditioning chamber.

Table 6: Data quality characteristics (AASHTO T378).

Data Quality Statistic	Maximum Value Tolerance
Load Standard Error	10%
Deformation Standard Error	10%
Deformation Uniformity	30%
Phase Uniformity	3°

3.3 Plant-Mixed Lab-Compacted Specimen

During construction of the recycled pavements, a mobile asphalt laboratory was used to compact samples using a SGC. Processed CIR, CCPR, and FDR materials were collected from the construction site or CCPR plant after being mixed with the recycling/stabilizing agent, active filler, and water. The processed material was compacted to the wet density recorded in the field from a nuclear density gauge. The SGC in the mobile laboratory was changed in the stopping requirement for the compacted specimen. The laboratory mixed specimens were compacted until 30 gyrations were reached, whereas the mobile laboratory mixed specimens were compacted until a specific height was reached. This small change in the SGCs system settings resulted in the mobile laboratory specimens achieving the required height in around five gyrations. Three replicates for each test section were made. Specimens were delivered to NCAT and cored vertically for LS dynamic modulus testing, also referred to as PMLC-L. The conditioning and testing regime used for these specimens was identical to the LMLC dynamic modulus specimen in section 3.2.5.4.

The FDR-E samples began breaking apart during the coring process as seen in Figure 31. Only one of the three FDR-E PMLC-L specimens remained intact enough for testing. Dynamic modulus testing was performed on the one recovered FDR-E PMLC-L specimen but was not used in the creation of a master curve because a minimum of three specimens were needed for quality results.

Figure 31: FDR-E PMLC sample breakage shown after coring.

The FDR-F test section had PMLC-L specimens compacted, but these were not tested further because raw material for LMLC samples was not collected, therefore comparison between the two could not occur.

3.4 Plant-Mixed Field-Compacted Specimen

The recycled and reclaimed test sections were field cored in October 2020, 14 months after construction was completed. Six field core samples were taken from randomly selected locations within each test section and were delivered to NCAT. The CR lifts were paved with a maximum thickness of 75 mm. Therefore, only one SS specimen could be retrieved from each core, also referred to as PMFC-S. Samples were cored horizontally through the layer and cut to the required

110 mm height for dynamic modulus testing. Field core samples of the CIR and CCPR test sections are seen in Figures 32 and 33, respectively.

Figure 32: CIR field core samples, foam (left) and emulsion (right).

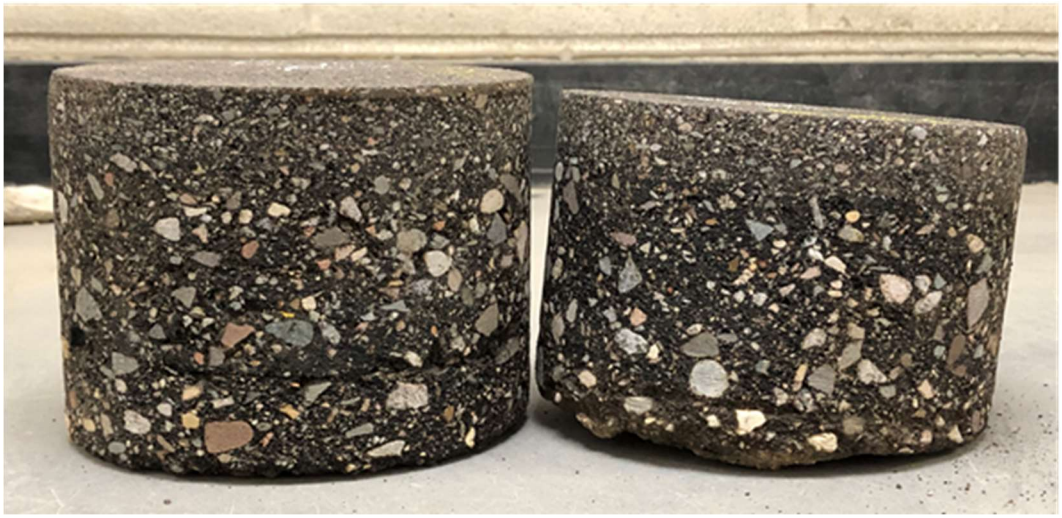

Figure 33: CCPR field core samples, foam (left) and emulsion (right).

Coring small-scale specimens from CR field core samples was difficult in some instances. Figure 34 shows that while the lift thickness was 75 mm, the 50 mm core bit was almost unable to core a complete specimen. In some locations the CR lift was thinner than 75 mm which resulted in the cored PMFC-S specimen being partially deformed from the milled existing surface underneath, as seen in Figures 35 and 36. Additionally, because CIR and FDR is performed on in-situ pavements that are in need of

rehabilitation, it can be common to find strips of crack seal being mixed with the RAP. Figure 37 shows a CIR-E PMFC-S specimen that had a line of crack seal run along its longitudinal axis. All the specimens were still tested for their dynamic modulus.

Figure 34: Cold recycled field core sample showing a thin lift.

Figure 35: Cold recycled field core sample with the milled pavement surface exposed as a result of too thin a lift.

Figure 36: Cold recycled field core with milled pavement surface imposed on the specimen.

Figure 37: CIR-E PMFC-S specimen with crack seal along its longitudinal axis.

The FDR-E sections were paved with a maximum layer thickness of 175 mm; therefore, two SS specimen could theoretically be extracted horizontally from each of the six field cores. Unfortunately, during coring with the wet core drill, these samples began to disintegrate, and none were recovered for dynamic modulus testing. Figures 38 and 39 show an FDR field core sample and the resulting FDR-E PMFC-S specimen after coring, respectively. Dynamic modulus testing was not performed on the FDR-E PMFC-S specimens because none of the specimens were recovered intact.

Figure 38: FDR-E field core specimen.

Figure 39: FDR-E PMFC-S specimen broken during coring.

3.5 Summary of the Methodology

The foamed CR test section's mixture designs were conducted at NCAT. Foamed binder properties and optimum moisture contents were determined. After construction of the test sections on 70th Street, material was collected and sent to NCAT for as-built testing. Samples were mixed and compacted at NCAT using the recycling/stabilizing agent, water, and active filler contents recorded during the construction phase.

The acceptance testing was conducted for foamed mixture using the ITS method and the emulsion mixtures using the MS method. Cracking resistance of the mixtures was determined by performing the IDEAL-CT. Rutting potential of the mixtures was determined by running HWT in a 50°C water bath until a failure limit of 12.5 mm was reached.

Dynamic modulus of the mixtures was conducted on LMLC-L, LMLC-S, PMLC-L, and PMFC-S specimen to investigate whether the different mixing and compacting methods affects the modulus recorded.

CHAPTER 4 – RESULTS

The first section of the results chapter is focused on presenting the findings of the mixture design process. Within this section, sub-sections cover results on the foamed binder properties, gradations, moisture-density relationship, ITS, and MS for the foam (FDR) and emulsion mixture designs performed by Ingevity and AET. The second section of the results chapter focuses on the comparison of the CR and FDR mixes within sub-sections covering gradations, MS, ITS, HWT, and IDEAL-CT testing. The third section presents the comparison of the mixture design to the as-built mixture using their gradations and ITS. The fourth section covers the impact of the mixing and compaction methods used to create the four specimen types, and the comparison between lab-mixed SS and LS dynamic modulus specimens.

4.1 Mixture Design

4.1.1 Foamed Binder Properties

The asphalt used for the foamed mixtures was a PG 58-28. The OFWC and binder temperature test results at 165°C, 160°C, and 150°C are shown in Figures 40-42, respectively. A summarization of the binder testing temperatures and OFWC are in Table 7. The OFWC was determined as the water content equidistant between the passing water contents for each expansion ratio and half-life requirements, indicated by the blue arrows in each figure.

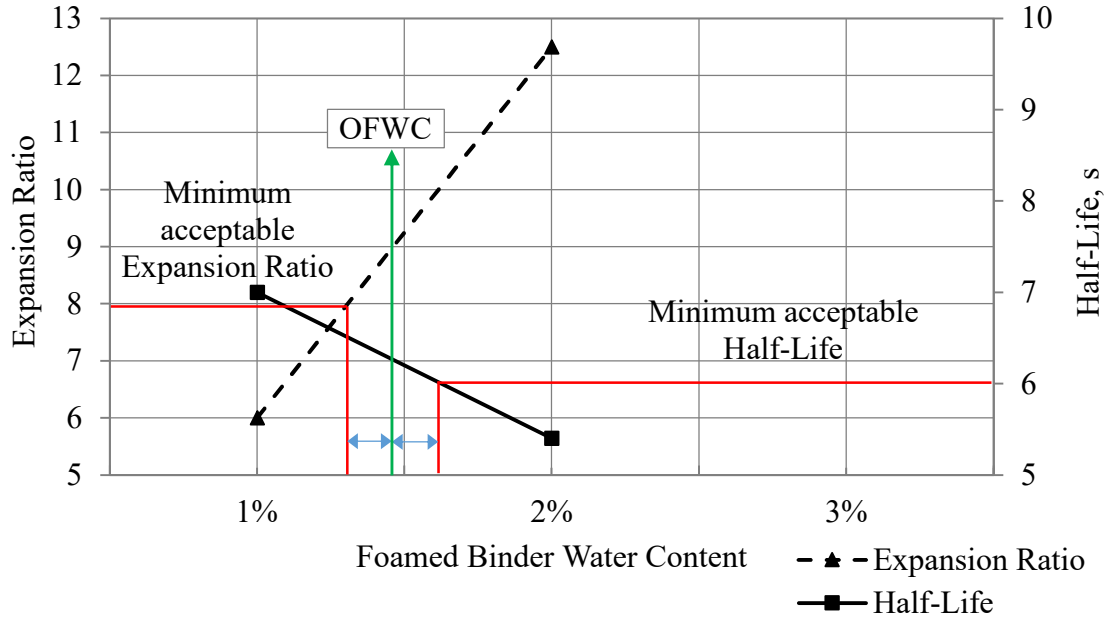

Figure 40: OFWC at a 165°C binder temperature.

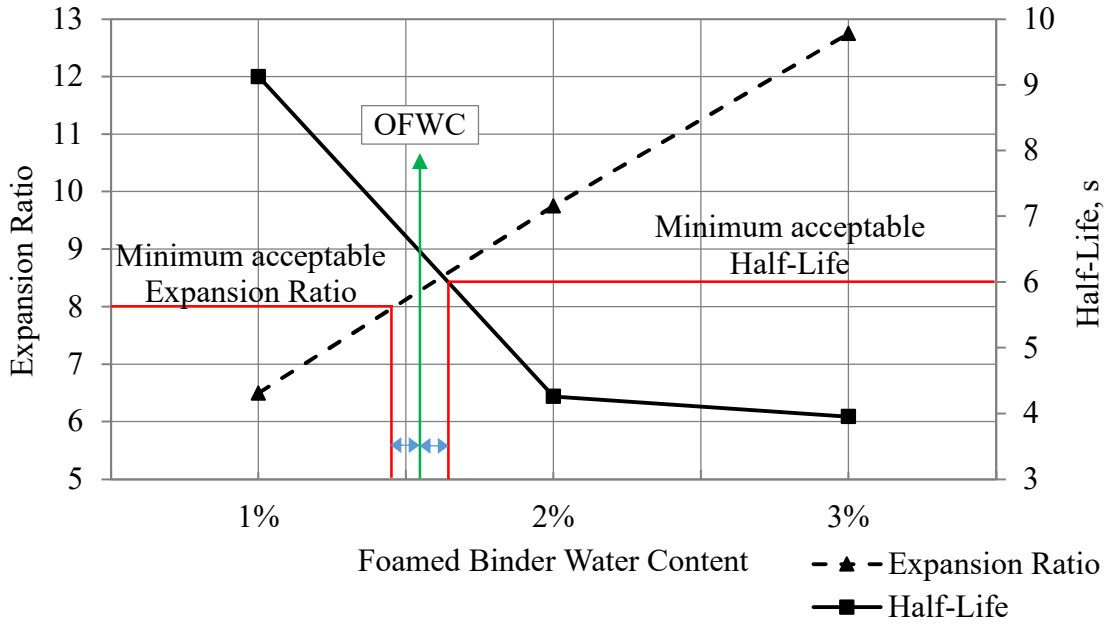

Figure 41: OFWC at a 160°C binder temperature.

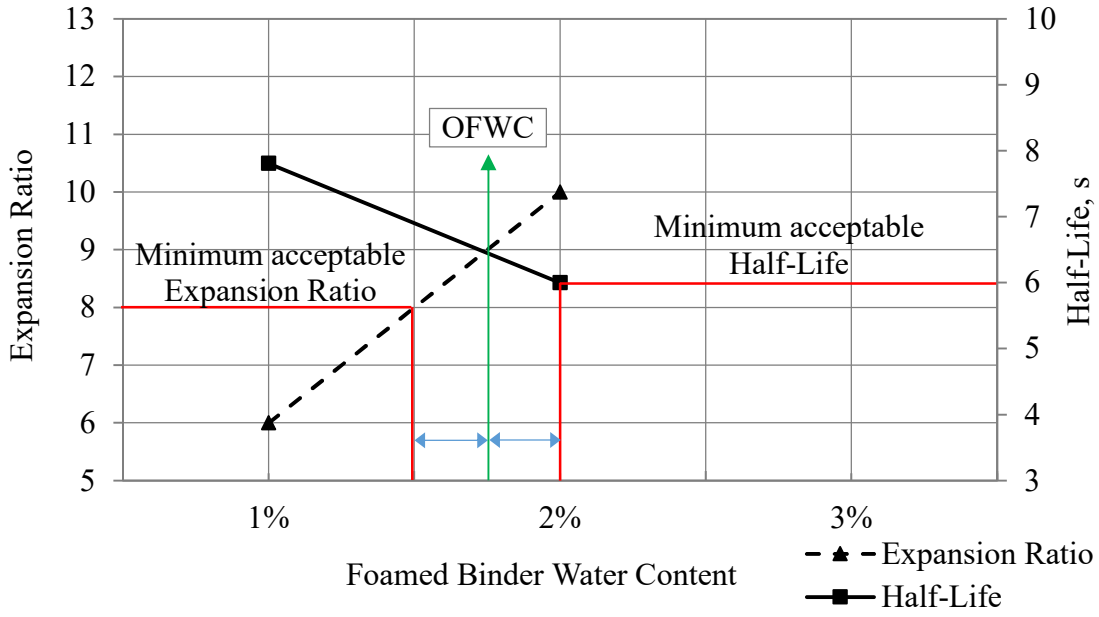

Figure 42: OFWC at a 150°C binder temperature.

Table 7: OFWC summarized results.

	Binder Temperature, °C		
	165	160	150
Optimum Water, %	1.47	1.55	1.75
OFWC Range, %	1.31 - 1.63	1.46 - 1.64	1.50 - 2.00

The OFWC selected for the mixture designs was 1.5%. This water content was acceptable for each of the three temperatures tested. The optimum temperature selected was 165°C because the foamed binder met the half-life and expansion requirements, and a factor of safety is incorporated if the asphalt binder temperature does not reach 165°C during construction.

4.1.2 Gradations

The black rock and uncoated gradations of the CIR-F and CCPR-F mixtures are provided in a 0.45 power chart in Figure 43. The black rock gradations were performed on the RAP after screening over a one-inch sieve and prior to mixing with the recycling agent. Additionally, the

uncoated gradations were the same samples after they were placed in the NCAT ignition furnace for burning of the asphalt. Two replicates for each CR mixture were performed and averaged into each of the gradations seen.

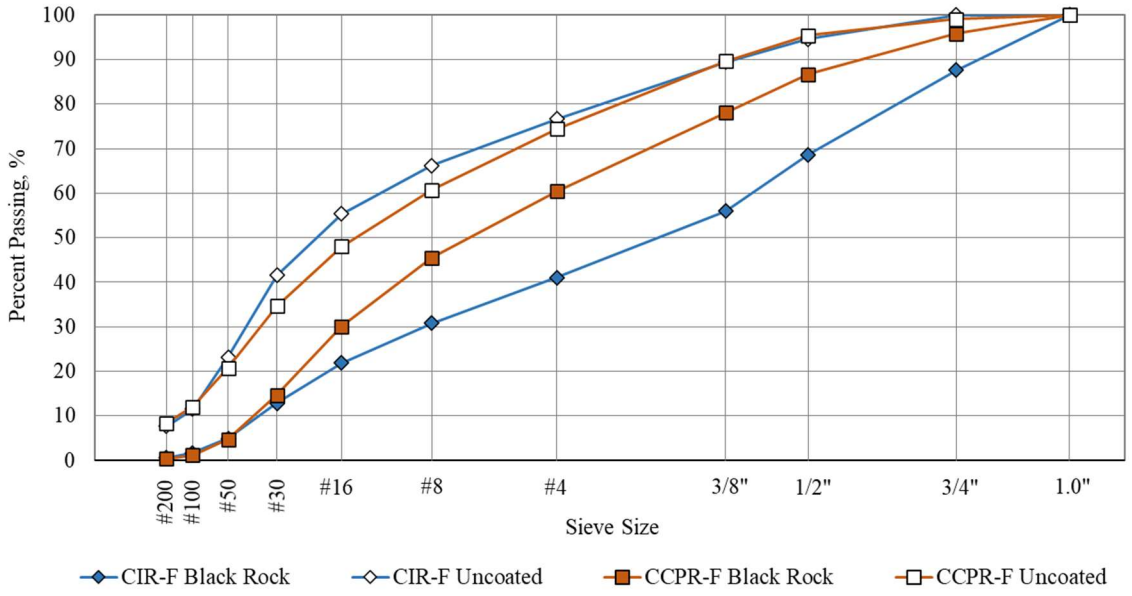

Figure 43: Mixture design gradations for CIR-F and CCPR-F.

The CIR-F black rock gradation was coarser than the black rock CCPR-F between the 3/4-inch and #16 sieves. Because the CIR-F RAP for the mixture design was conducted on crushed field cores instead of being milled, the gradation was drastically different than it would be during construction. The CCPR-F black rock gradation was coarser than the uncoated CCPR-F gradation, but not as much as the CIR-F. This is most likely due to the way RAP milling are collected, processed, and stockpiled. It is common for RAP stockpiles to be comprised of the milling of a mill and fill project since these projects are the most common methods of rehabilitation. A mill and fill project typically removes only the surface lift of a pavement, which has a finer gradation by design. Because the millings are comprised of smaller aggregates, it is more common to find stockpiles of finer gradations. The CIR-F and CCPR-F uncoated gradations show a difference

between the #8 and #30 sieves. The shift in the sieves ranging in different percent passing material is most likely due to the RAP particles consisting of smaller aggregates still coated and bound in binder. These coated aggregate particles were not completely separated during the milling and processing, and only became apparent when the binder holding the aggregate together was burned off. Each of the black rock gradations had between 0 and 1% dust, while the uncoated gradations had between 7 to 9% dust.

4.1.3 Moisture-Density Relationship

The results of the modified Proctor to find the OMC to maximize the compactive effort of the sample is in Figure 44. RAP can be difficult to get clear results for the moisture-density relationship, as seen for both mixtures. The CCPR RAP OMC was selected to be nearly 4.5%. Because of the wide gap between the second and third data points on the CIR OMC plot, an engineering decision was made to select an OMC of 4.5% to match the CCPR material. A general industry rule of thumb is that if an OMC is not specified for a mixture, an assumed OMC of 5% may be used. Because the CCPR-F mixture used 4.5%, the decision for keeping the mixtures OMC the same was made.

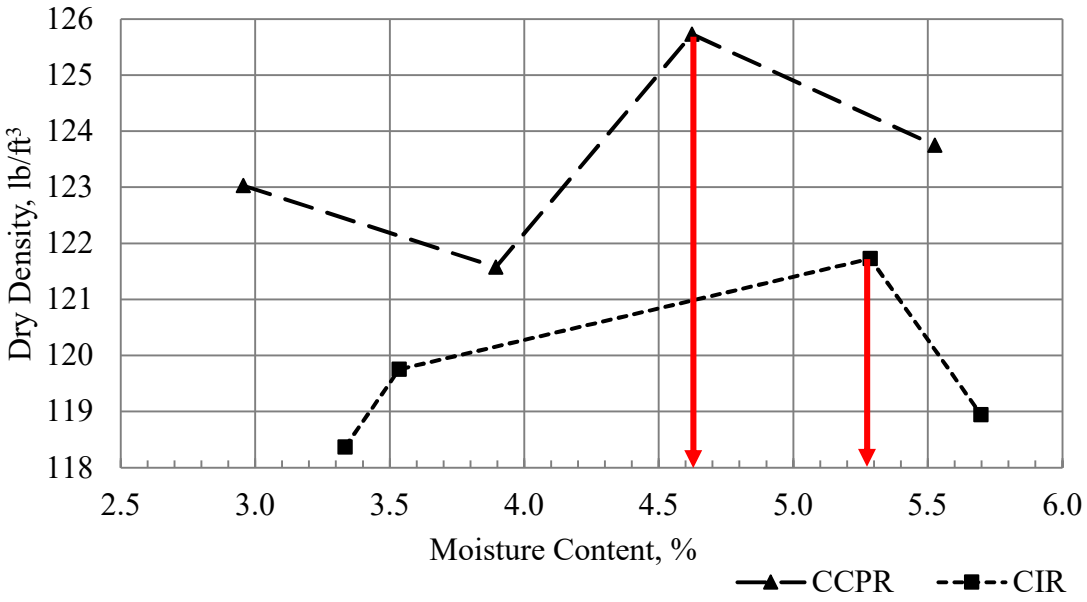

Figure 44: Modified Proctor test results for the foamed CR mixture designs.

4.1.4 Indirect Tensile Strength Testing

Indirect tensile strength results of the conditioned and dry samples are provided in Figures 45 and 46 for CIR-F and CCPR-F, respectively. Summarized ITS results for the foamed mixture designs is in Table 8. The recommended requirement for the 100 mm diameter dry specimen is a 45 psi tensile strength, which is indicated with a horizontal red line. Each of the mixtures tested had eight specimens made. Four were conditioned and the remaining four were dry during testing. In some instances, a specimen's test result was not recorded due to errors in collecting the data from the Marshall apparatus. The TSR was calculated for each of the asphalt contents in each CR mixture design and the results are also provided in Table 8.

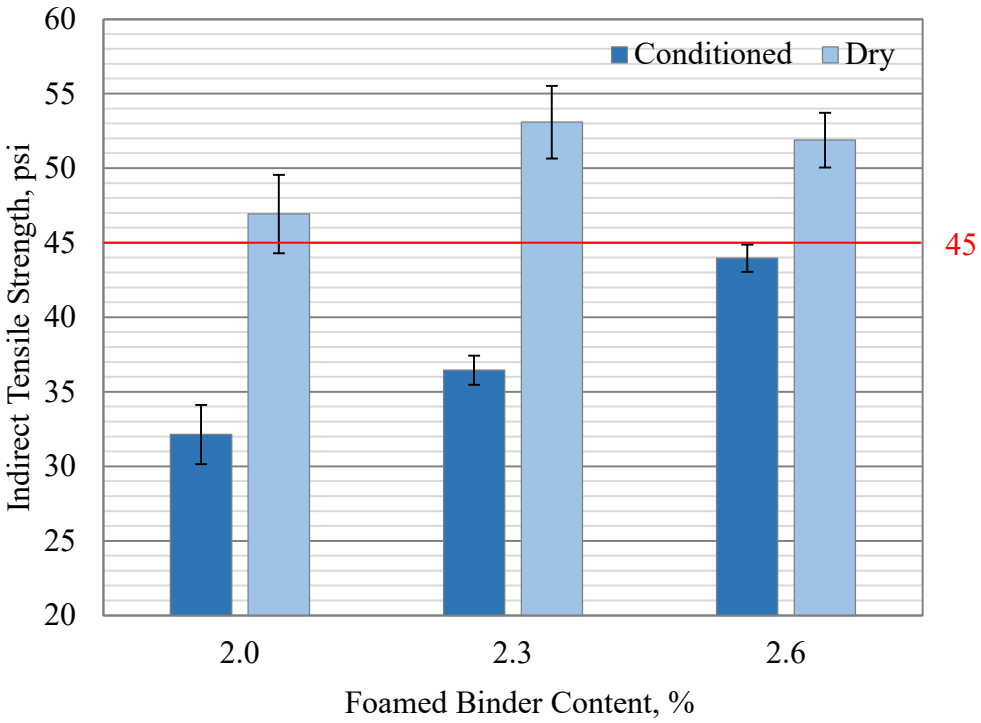

Figure 45: ITS results for the CIR-F mixture design.

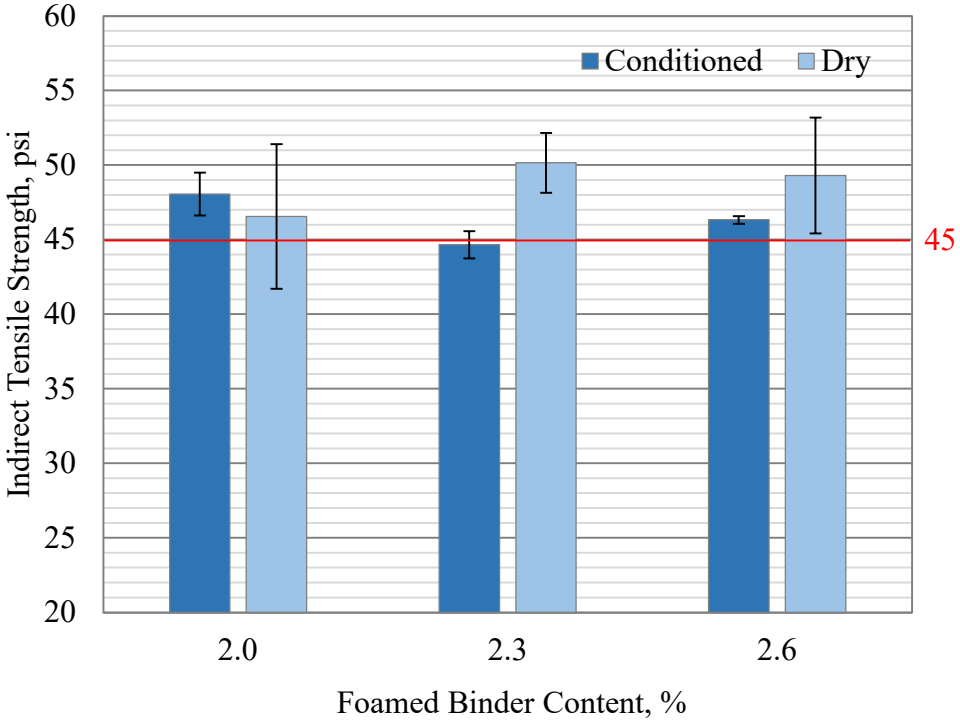

Figure 46: ITS results for the CCPR-F mixture design.

Table 8: ITS mixture design results summarized.

Mixture	CIR-F			CCPR-F			Minimum Req.
Foamed Asphalt Content, %	2.0	2.3	2.6	2.0	2.3	2.6	N/A
Dry ITS, psi	46.9	53.1	51.2	46.6	50.2	49.3	45.0
Conditioned ITS, psi	32.1	36.5	44	48.1	44.7	46.3	N/A
TSR	0.68	0.69	0.86	1.03	0.89	0.94	0.70

*Red cells indicate failure to meet criteria.

The CIR-F ITS results indicated a drop in strength when conditioned in the water bath as compared to the dry specimen. The 2.3 and 2.6% foamed asphalt mixes passed the 45 psi ITS recommended requirement for the dry specimens, while the 2.0% foamed asphalt mixture showed a dry tensile strength just over the 45 psi mark. The conditioned strength increased gradually as the asphalt content was increased in each mixture design. The CIR-F optimum foamed asphalt content selected was 2.6% because it passed the 45 psi dry ITS requirement and the 0.7 TSR requirement. The CCPR-F ITS results showed that both the dry and conditioned specimens had similar tensile strengths as compared to that of CIR-F. The foamed asphalt content did not seem to have much influence on the conditioned or dry specimen tensile strengths. The CCPR-F 2.0% foamed asphalt design closely passed the minimum dry ITS and TSR requirements, but the 2.3% foamed asphalt content was selected to add an extra level of safety for construction variability.

4.1.5 Marshall Stability Testing

The CIR, CCPR, and FDR emulsion designs were performed by other entities: Ingevity and AET. The CIR-E section had two designs made for a medium and coarse gradation material, because of the variable material gradation during construction that could occur. Because these were not performed at NCAT, only the final designs were reported. The mixture design acceptance criteria results for the final mixture designs are shown in Table 8.

Table 9: Marshall stability mixture design results.

Mixture	CIR-E - Medium	CIR-E Coarse	CCPR-E	FDR-E	Minimum, Req.
Emulsion Content, %	3.0	2.5	3.5	3.0	N/A
Dry MS, lbf	2335	2190	2113	2382	1250
Conditioned MS, lbf	2030	1870	1765	3825	N/A
MSR	0.87	0.85	0.84	0.62	0.70

*Red cells indicate failure to meet criteria.

The only mixture design that did not pass MS requirements was the FDR-E design. The stability recorded for the design was well above the requirement. However, the MSR below the requirement shows that the final mixture design may have moisture susceptibility issues.

4.2 As-Built Mixtures

The construction of the five recycled/reclaimed sections of the MnROAD research sites used in this study were completed, and the reported as-built mixture data was provided and is summarized in Table 10.

Table 10: As-built constructed mixture properties.

	Mixture				
	CIR-E	**CCPR-E**	**CIR-F**	**CCPR-F**	**FDR-E**
Construction Date Completed	8/22/2019	8/22/2019	8/21/2019	8/20/2019	8/22/2019
Recycling/Stabilizing Agent	Emulsion	Emulsion	Foam	Foam	Emulsion
Emulsion Content, %	2.8	3.5	N/A	N/A	3
Foamed Asphalt Content or Emulsion Residual Asphalt Content, %	1.9	2.2	2.6	2.3	1.9
Cement Content, %	N/A	N/A	1	1	1
Added Water, %	2	0.5	2	0.5	2.5
In-Situ Water, %	n/a	3.6	2.5	4.3	n/a
Design Optimum Water, %	2	2.5	4.5	4.5	6
Recorded Moisture Content, %	4.91	5.40 & 7.10	3.6	4.94	6.16

In some instances, the in-situ water contents were not recorded. However, the construction of the as-built mixtures was based solely on the recorded moisture contents. Due to the rainfall that occurred during the week of construction, the in-situ water impacted achieving the optimum water content in several test sections. For example, the CCPR-E test section had a selected design optimum water of 2.5%. The in-situ moisture content was 3.6% due to the weather, but a minimum water content of 0.5% was needed to achieve adequate coating of the RAP in the EE. The EE also added 1.3% water into the mixture because of its chemical makeup. This resulted in a moisture content recorded of 5.4 and 7.1. Two separate entities recorded the moisture contents, and both were tested for MS to verify which should for the remaining tests.

4.2.1 Comparison of CR and FDR Mixtures

4.2.1.1 RAP Properties

After the RAP millings were received in five-gallon buckets, homogenized, and dried, multiple gradations were performed to verify that each of the mixture's RAP was truly homogenized and similar to the gradation recorded in the field for both black rock and uncoated. Figures 47-51 provide the gradations on a 0.45 power chart of field performed and laboratory performed sieve analysis to verify that the RAP was relatively similar for CIR-E, CCPR-E, CIR-F, CCPR-F, and FDR-E, respectively. Variations of up to 5.0% in the median sieve is expected with proper stockpile management for CCPR RAP. CIR RAP should have tight gradations because the material is collected from the same project (West 2015). Two and four black rock gradations were performed in the laboratory to obtain a representative gradation and to verify that the material was similar to the field material. Two samples were burned in an ignition furnace and used for an uncoated laboratory sieve analysis test. A single test for black rock and uncoated gradation was performed in the field during construction.

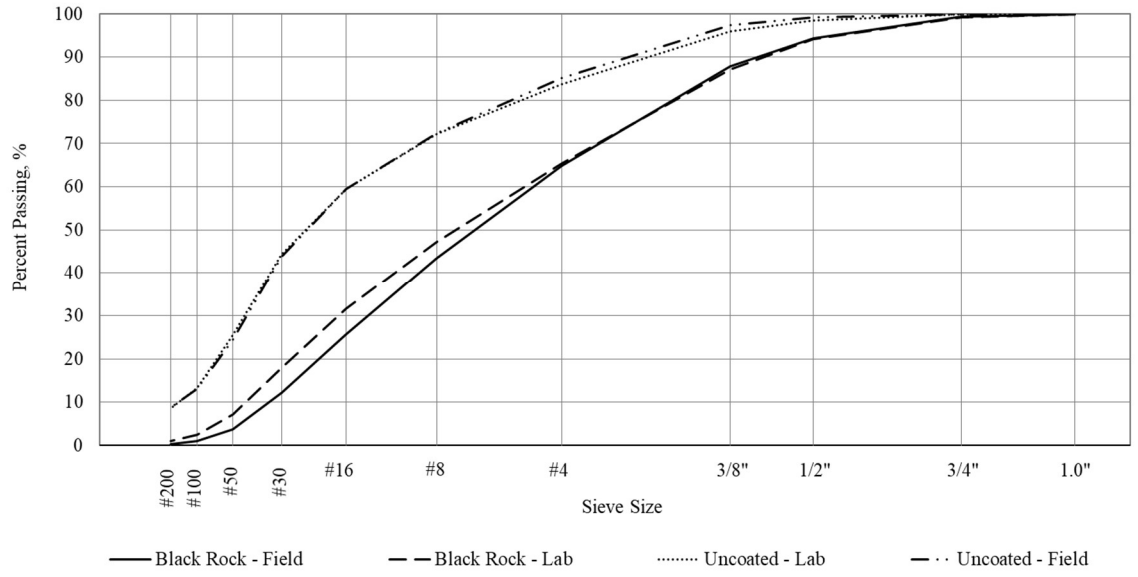

Figure 47: CIR-E as-built mixture gradations.

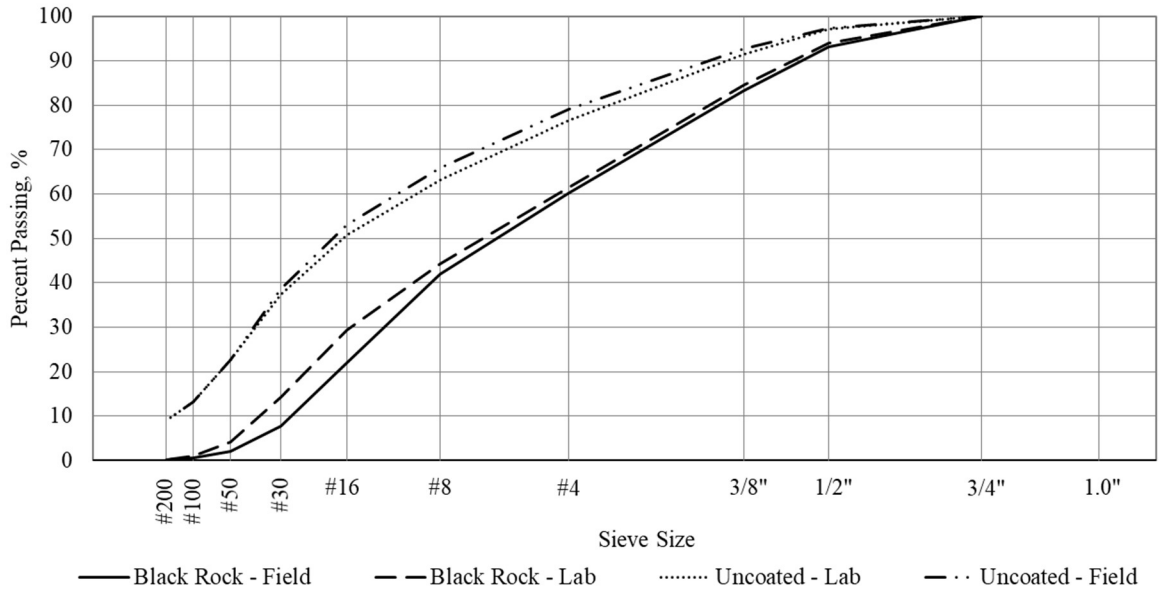

Figure 48: CCPR-E as-built mixture gradations.

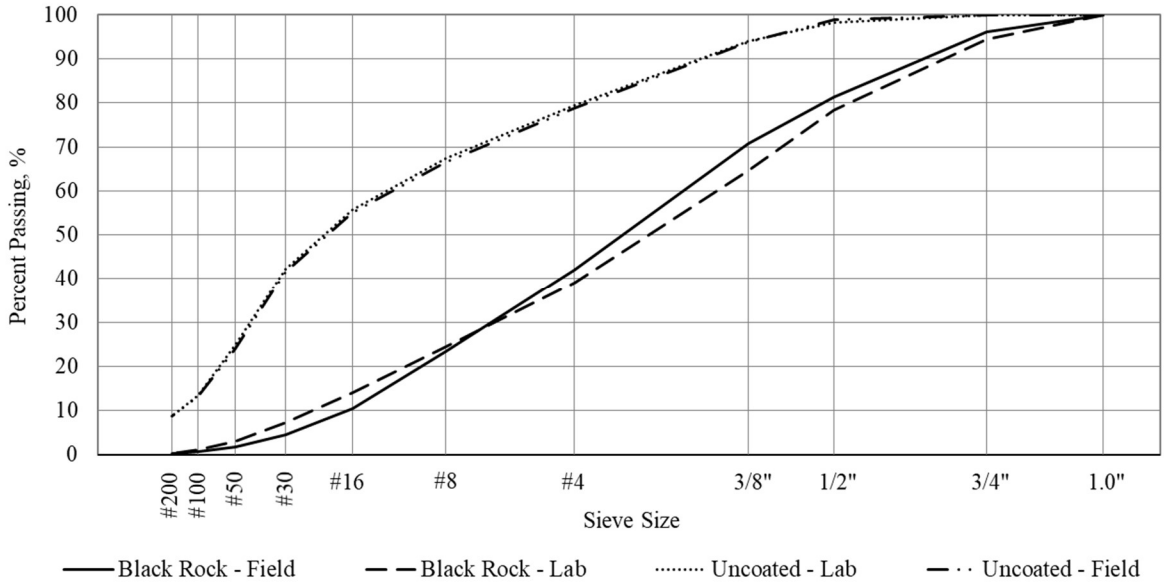

Figure 49: CIR-F as-built mixture gradations.

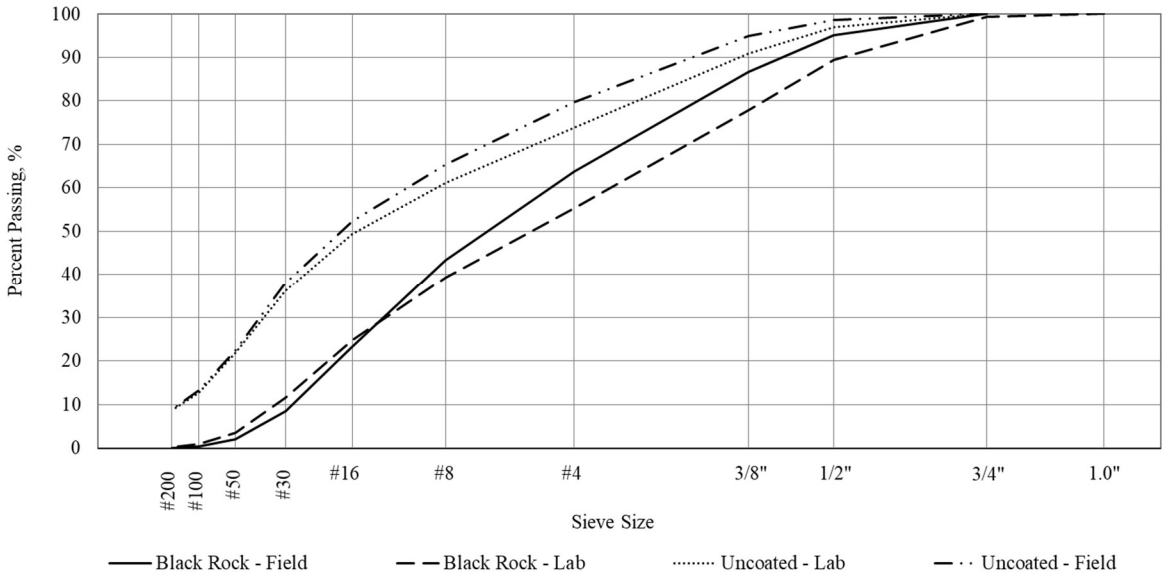

Figure 50: CCPR-F as-built mixture gradations.

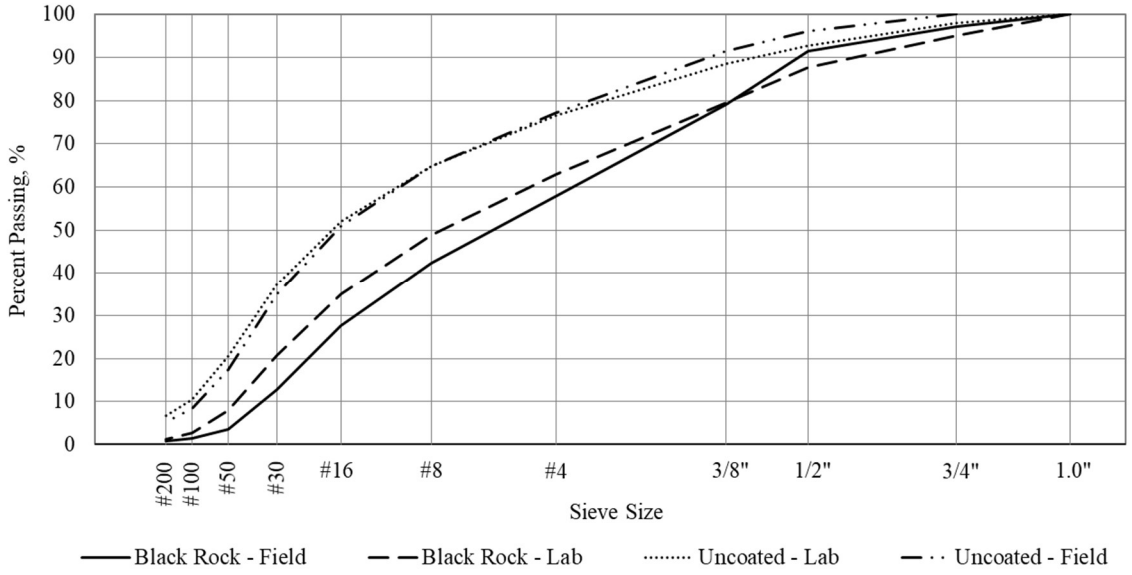

Figure 51: FDR-E as-built mixture gradations.

The results of the CCPR-F gradations in Figure 50 show a visual difference between the 1/2-inch and #4 sieve. This difference was not seen in the CCPR-E mixture in Figure 48, even though the gradations should be identical for the as-built materials regardless of the recycling agent. The difference in the CCPR-F uncoated gradations along with the black rock gradations suggests that there were either errors in the field testing, stockpile sampling occurred in a particularly fine or coarse part of the stockpile, or separate stockpiles were unintentionally used for material collection.

Fundamentally, CIR gradations should be similar between the foamed and emulsified test section because it is performed on in-place material. If patching occurred in one section and not the other, the gradation may show a difference. Additionally, there are many different variables during the CIR construction phase that could affect the resulting gradation of identical sections (ARRA 2015):

- Rotation speed of the cutting drum

- Forward speed of the milling machine
- Condition of the existing pavement
- Ambient temperature

Figure 52 shows the comparison of the CIR black rock gradations between the field and laboratory tests. The CIR-F section was recycled one day after the CIR-E section and historical weather data shows that there was 0.75 inches of rainfall the day that the CIR-F section was recycled. It is possible that construction was performed more quickly on the CIR-E section because of a delay due to the weather from the day prior, or that the milling teeth of the CP could also have cut differently for different moisture contents in the pavements.

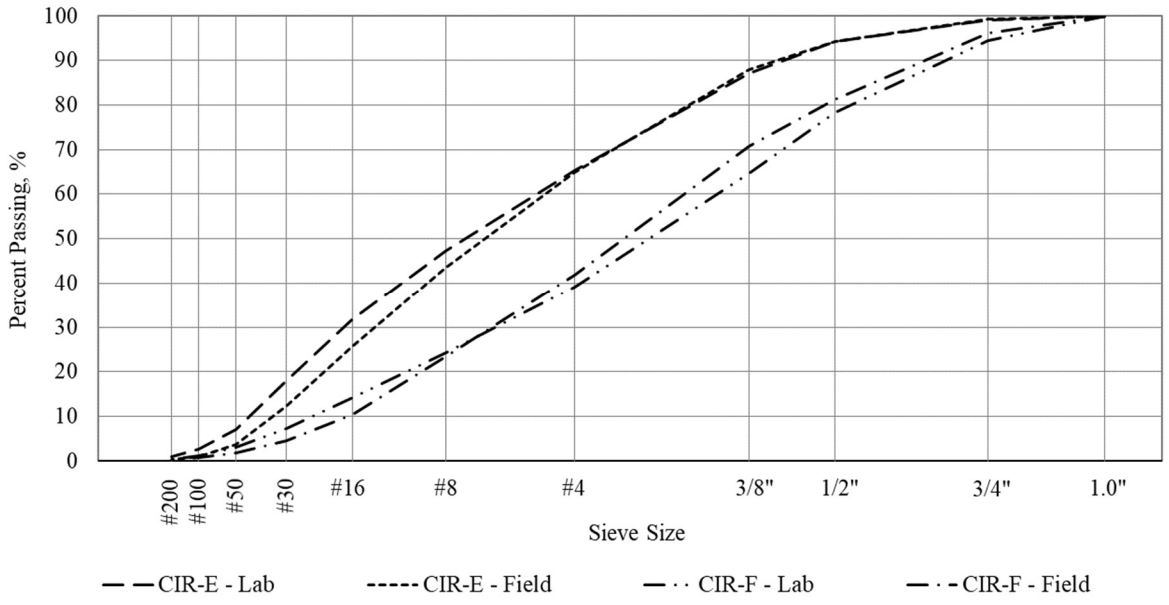

Figure 52: CIR as-built mixture black rock gradations.

A difference in the field and laboratory reported black rock gradations for CCPR can be seen in Figure 53. The CCPR RAP was collected at the same central plant stockpile for both CCPR-E and CCPR-F, therefore the RAP material should be similar with the allowed variation identified

from West (2015). Figure 53 was created to visually detect if the difference in CCPR-F RAP occurred due to poor homogenizing in the laboratory materials, stockpile sampling at the plant, or possible differences in sampling the RAP for sieve analysis in the field. As shown on the 0.45 power chart, the CCPR-F field gradation is coarser than the other three samples, especially between the 0.5-inch and #4 sieves. Each of the four gradations should be nearly identical because the source stockpile was kept the same during construction. Possible reasons for the gradation deviation in the RAP are:

- Poor stockpile sampling techniques for the CCPR-F laboratory RAP
- Miscalculation or loss of material coarser than the #4 sieve during testing

No information was reported on errors during the field gradation testing or stockpile sampling; therefore, these reasons are only speculative.

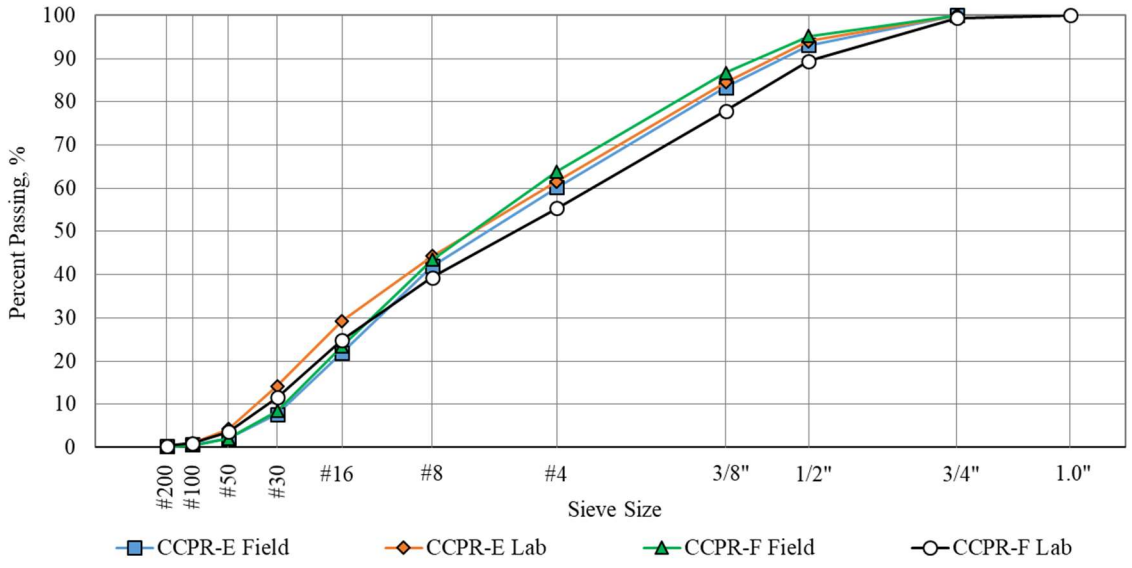

Figure 53: Comparison of CCPR-E and CCPR-F as-built black rock gradations.

Finally, all as-built mixture gradations recorded in the laboratory are plotted in Figure 54. The CIR-F mixture had the coarsest material of all the CR and FDR mixtures.

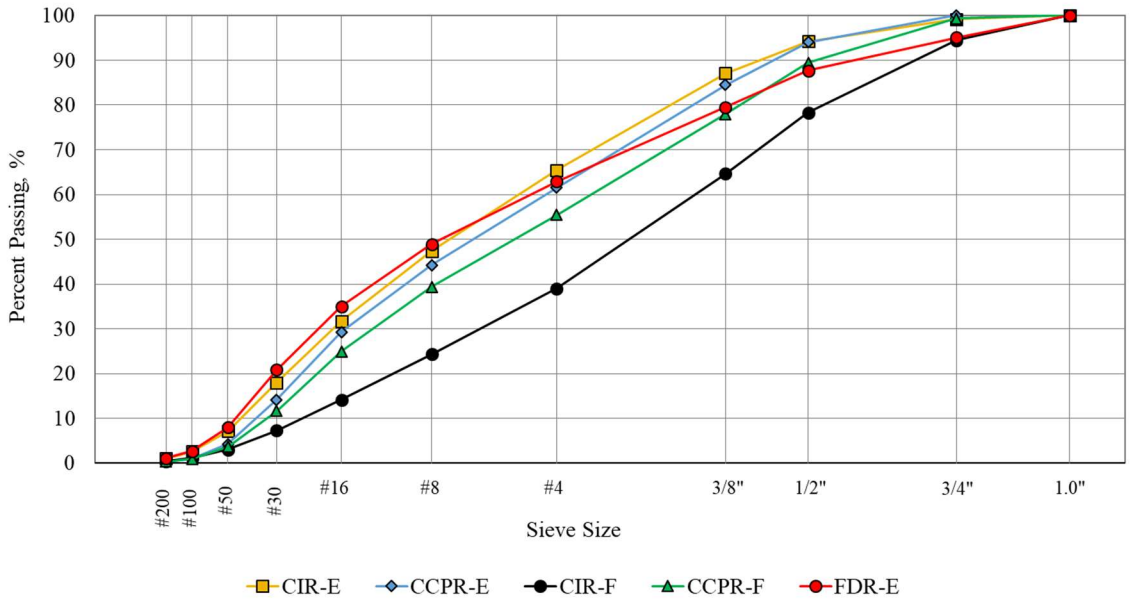

Figure 54: As-built mixture laboratory recorded gradations.

4.2.1.2 Compacted Density Requirements

Moisture contents were recorded for each of the mixtures before and after the recycling/reclaiming process. The wet and dry densities of the paved CR and FDR lifts are in Table 11. "Raw" is the RAP milling after the recycling/reclaimer prior to being mixed with any additional water, recycling/stabilizing agents, or active fillers. "Processed" is after mixing the raw RAP with the recycling/stabilizing agent, additional water, and active fillers.

Table 11: Mixture moisture contents and target densities as recorded from construction.

	Moisture Content, %		Target Density, pcf	
	Raw	Processed	Wet	Dry
CIR-E	2.7	4.9	130.0	124.1
CCPR-E	5.0	7.1	138.0	129.9
CIR-F	0.9	3.6	130.0	125.4
CCPR-F	4.3	4.9	135.1	129.2
FDR-E	3.8	6.2	135.0	127.8

Each of the samples that were compacted in a SGC aimed for the field recorded target wet density after 30 gyrations. After curing, the dry density of each sample was determined by recording the weight and using calipers to record the outer dimensions. The comparison between the target and sample dry densities mixture is in Figure 55. The dynamic modulus dry densities presented in Figure 55 are from the pre-cored 180 ± 10 mm tall, compacted samples.

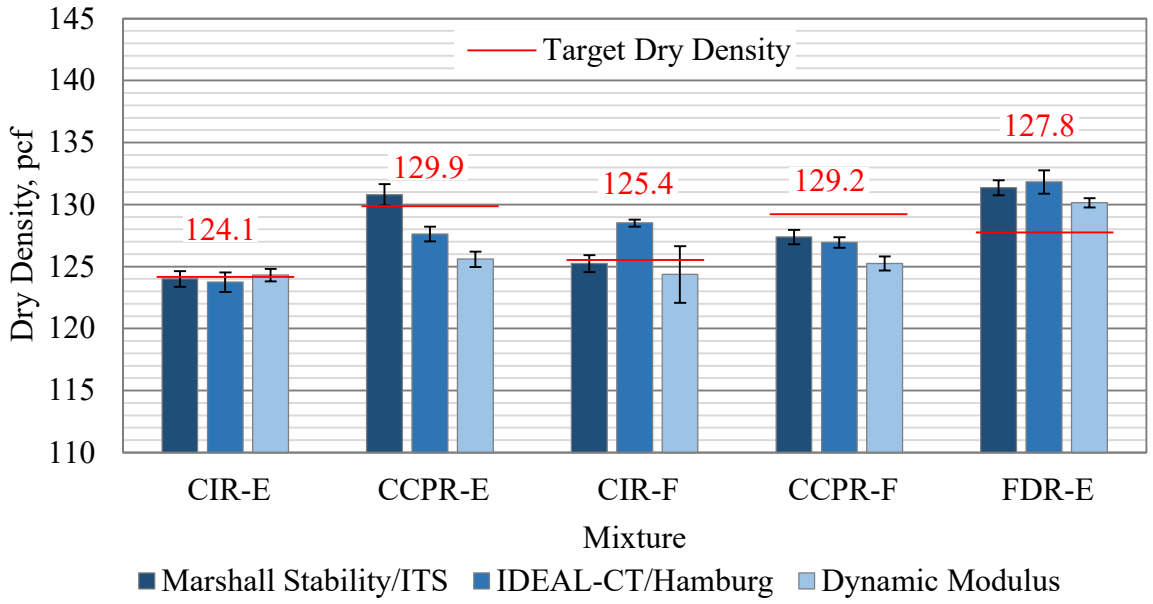

Figure 55: Laboratory samples dry density comparisons to the mixture target dry density.

Mixture CIR-E was the only mixture that had each of the three specimen sizes with means nearly identical to the dry density. The smaller the sample size for the CCPR-E, the higher the recorded dry density became. The CIR-F had relatively close dry densities between the MS/ITS and dynamic modulus specimens. The CCPR-F laboratory specimens were all less dense than the target dry density. The FDR-E laboratory specimens had some of the highest dry densities recorded. It was the only mixture that resulted in all three specimen sizes with dry densities higher than the target. In general, deviations between the laboratory and field densities could be from slight changes of material or from differences in compaction methods and efforts.

4.2.1.3 Indirect Tensile Strength

The as-built mixture's average ITS testing results are presented in Figure 56 and summarized in Table 12. Four specimens were designated for dry and conditioned specimen testing each. During testing, human error with beginning the test prior to resetting the Marshall apparatus caused the ITS data to be lost. Because of these errors, some of the data averages considered only three specimens.

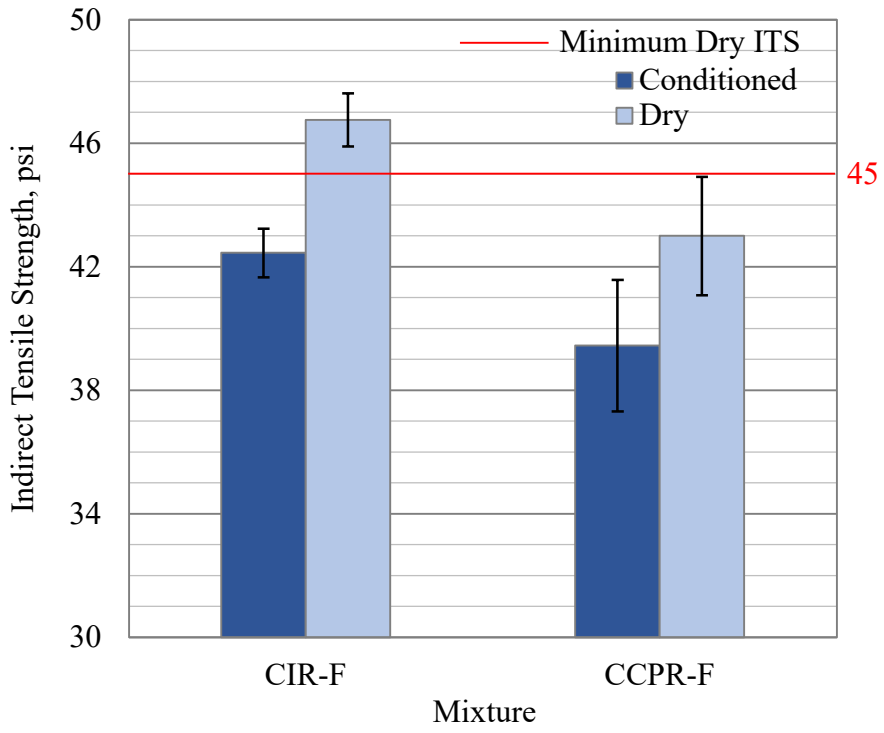

Figure 56: As-built mixture's ITS test results with the 45 psi dry requirement.

Table 12: As-built mixture's ITS test results summarized.

Mixture	Method	ITS, psi	St. Dev., psi	45 psi Req.	TSR
CIR-F	Conditioned	42.6	0.8	N/A	0.91
	Dry	46.8	0.9	Pass	
CCPR-F	Conditioned	39.5	2.1	N/A	0.92
	Dry	43.0	1.9	Fail	

*Red cells indicate failure to meet criteria.

The CIR-F passed the 45 psi recommended requirement for the dry specimen. The TSR is higher than the 0.70 requirement, showing that there is not a moisture susceptibility issue for the CIR-F mixture. The as-built CCPR-F design did not pass the minimum required 45 psi required with the dry specimens. However, the TSR was above the 0.70 requirement for CR mixtures.

4.2.1.4 Marshall Stability

The MS of the as-built mixtures was recorded and are shown in Figure 57 and summarized in Table 13.

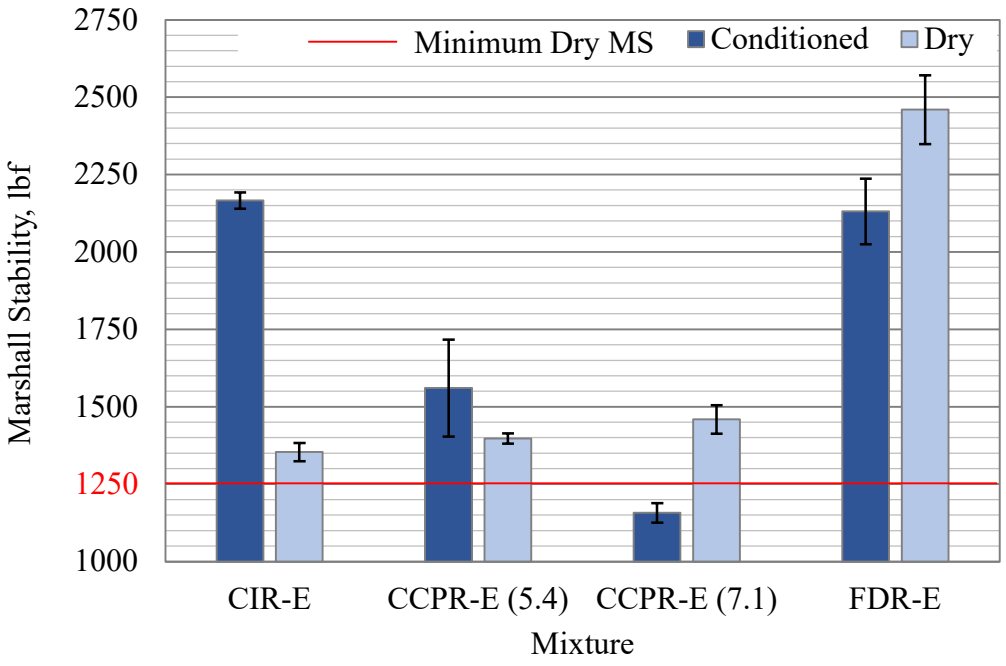

Figure 57: As-built mixture's MS test results with the 1,250 lbf dry requirement.

Table 13: As-built mixture's MS test results summarized.

Mixture	Method	MS, lbf	St. Dev.	1250 lbf Req.	MSR
CIR-E	Conditioned	2166.2	26.7	N/A	1.60
	Dry	1353.9	29.3	Pass	
CCPR-E (5.4)	Conditioned	1560.6	157.0	N/A	1.12
	Dry	1397.4	16.5	Pass	
CCPR-E (7.1)	Conditioned	1157.3	31.3	N/A	0.79
	Dry	1459.6	46.0	Pass	
FDR-E	Conditioned	2131.3	105.9	N/A	0.87
	Dry	2459.8	111.4	Pass	

During construction, two different moisture contents were recorded for the CCPR-E mixture, 7.1% and 5.4%. Both moisture contents were experimented with in the laboratory to identify if a difference in the MS or MSR was present between the two. As shown in Table 13, both of the CCPR-E mixtures passed the 1,250 lbf requirement. The conditioned specimens acted differently under the two moisture contents. When the moisture content was 7.1%, the MS was lower than the dry specimen. Although the large difference in stability values can be seen, the MSR was 0.79, which indicates that moisture susceptibility was not an issue in this recycled mixture. The lower moisture content CCPR-E had a dry specimen stability just slightly lower than the higher moisture content mixture. The difference between the two was the conditioned specimen resulted in higher stability values than the dry. Because both the 5.4 and 7.1% moisture contents for the CCPR-E passed the minimum requirements, the remaining performance test samples were mixed at the 5.4% moisture content. Additionally, after switching to the moisture content of 5.4% the large CCPR-E samples had EE and water squeezed from the mold during compaction in the SGC, as seen in Figure 58. This caused concerns with the amount of residual asphalt remaining in the specimen after compaction. Because of this issue, the additional water content added to the mixture was reduced by 20%, resulting in a moisture content of 4.32%. The CIR-E and CCPR-E

mixtures have higher conditioned specimen stabilities than the dry specimen. This phenomenon is not an uncommon occurrence in emulsion CR mixes, but the reason has not been adequately documented.

Figure 58: Engineered Emulsion and water seepage from compacting the 5.4% moisture content as-built CCPR-E mixture.

4.2.1.6 IDEAL-CT

The IDEAL-CT results for each of the five mixtures are shown in Figure 59 and summarized in Table 14. Five samples were tested for each of the mixtures, and the CT_{Index} values reported are the averaged results.

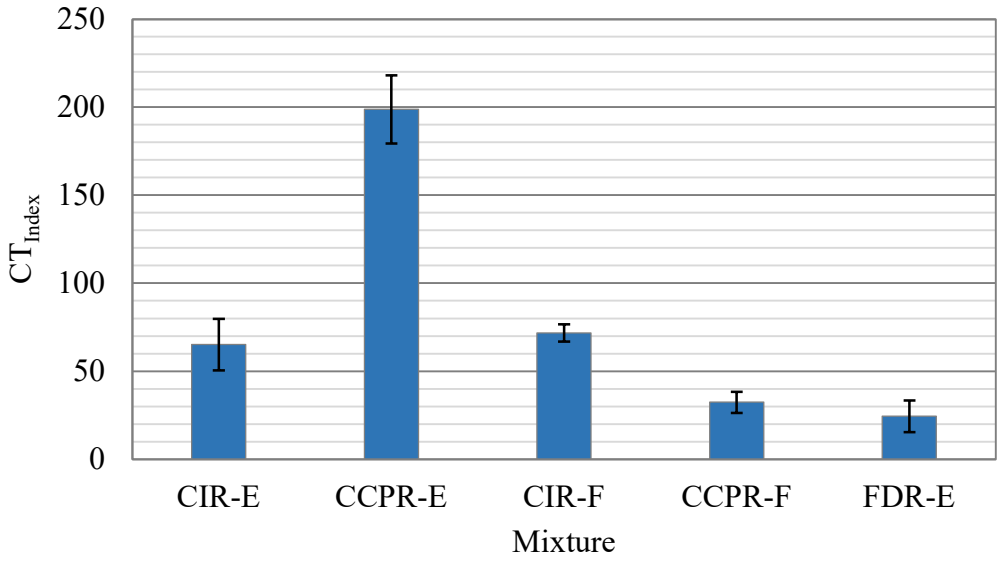

Figure 59: IDEAL-CT mixtures results.

Table 14: Summarized IDEAL-CT mixture results.

Mixture	CIR-E	CCPR-E	CIR-F	CCPR-F	FDR-E
CT_{Index}	65.1	198.8	71.8	32.4	24.6
Std. Dev.	14.6	19.3	4.9	6.0	9.0

The CIR-F mixture had a 10% higher average CT_{Index} value than CIR-E but it will most likely not create a noticeable difference in cracking resistance in the field between the two mixtures. The CCPR-E mixture had an average CT_{Index} value 514% higher than the CCPR-F mixture. It is expected that the CPPR-E test section will resist cracking much longer than the other four test sections. The FDR-E mixture had the lowest CT_{Index} value of the sections. It is expected that the FDR-E mixture will show cracking throughout the section much faster than the others. Zhou et al. found that a typical HMA using PG 58-28 virgin binder with a 40% RAP binder content reached an average CT_{Index} of 160.0 and COV of 19.9%. Comparatively, the CCPR-E CT_{Index} had a better crack resistance than the HMA that had similar virgin PG binder. Additionally, he found that an HMA using PG 64-22 virgin binder and 20% recycled asphalt shingles binder content resulted in a CT_{Index} of 45.2 with a COV of 7.9 (Zhou et al. 2019). The CCPR-E mixture provides

a similar cracking resistance as compared to the HMA mixture with 40% RAP binder content. The FDR-E mixture IDEAL-CT results indicate that it may be the least effective mixture tested at resisting cracking as compared to the CR mixtures tested and the referenced HMA mixtures.

4.2.1.7 Hamburg Wheel Tracking

The averaged results for each of the five recycled/reclaimed mixtures are presented in Figure 60 after testing two replicates per mixture. The failure rutting depth specification in a HWT test can vary by agency. A rutting failure depth of 12.5 mm is used for this thesis because Ingevity had previously used this specification for other CR and FDR tests. If a mixture does not rut to the specified failure depth within 20,000 passes, it is assumed to be relatively good at preventing rutting. Each of the five mixtures resulted in exceeding the maximum rut depth within 1,600 and 3,800 passes at the 50°C specimen and water temperature. Failing Hamburg test samples for CIR-E, CIR-F, CCPR-E, CCPR-F, and FDR-E are seen in Figures 61-65, respectively. For comparison, a stiff HMA mixture with little rutting after 20,000 passes is shown in Figure 9 in section 2.4.2.

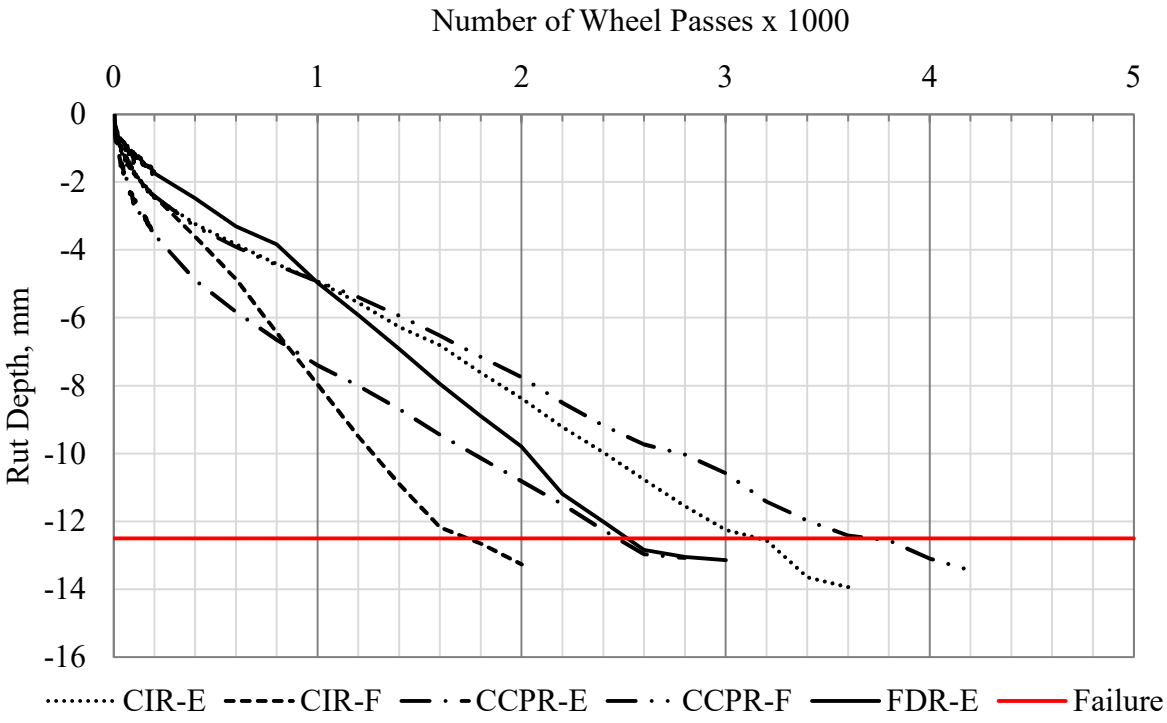

Figure 60: Hamburg wheel track test results.

Figure 61: CIR-E Hamburg test specimen after failure.

Figure 62: CIR-F Hamburg test specimen after failure.

Figure 63: CCPR-E Hamburg test specimen after failure.

Figure 64: CCPR-F Hamburg test specimen after failure.

Figure 65: FDR-E Hamburg test specimen after failure.

Exposed uncrushed aggregate after a HWT test can indicate that failure occurred by stripping of the asphalt from the aggregate due to the moisture susceptibility of the mixture. Moisture susceptibility can weaken the bond between the aggregate and binder mastic. Occasionally, it can be hard to identify whether the CR specimen stripped or that the air voids collapsed under the weight of the HWT steel wheels. Figure 61 shows a small amount of exposed fine aggregate on the CIR-E failed specimen. The specimen having little to no exposed aggregate along the rutting failure wall could indicate that the mixture did fail in rutting and that only few RAP particles were crushed directly under the steel wheel. It is difficult to discern whether the failure for the CIR-F specimen occurred due to rutting or moisture susceptibility because the image in Figure 62 was taken while the sample had standing water on it. Figure 63 shows that the CCPR-E specimen did not have any exposed or crushed aggregate, therefore the failure in the specimen was likely due to rutting. The CCPR-F specimen in Figure 64 had some exposed aggregate along the raised rutting failure wall that indicated some stripping may or may not have occurred. Figure 65 shows that the FDR-E specimens had excessive amounts of exposed uncoated aggregate. This mixture is combination of bound and unbound materials, so it cannot be confirmed that the specimen failed due to stripping.

A typical Hamburg test result for HMA can have three identifiable parts to failure: a consolidation period, a creep slope, and a stripping slope as seen in Figure 8 of section 2.4.2. All of the mixtures except FDR-E showed a slight consolidation period within the first 400 wheel passes. Additionally, an inflection point, which indicates the point at which a mixture begins stripping, seen in Figure 8, could not be identified for any of the mixtures. For each mixture, a linear regression line was fitted to each of the mixture's HWT test result curves, as seen in Figure 66 for CIR-E. The equations and R^2 results for the regressions are tabulated in Table 15. The high

R^2 show that throughout the entirety of rut testing, a near linear path to failure was expressed. Creep and stripping slopes were not identifiable for any of the mixtures tested.

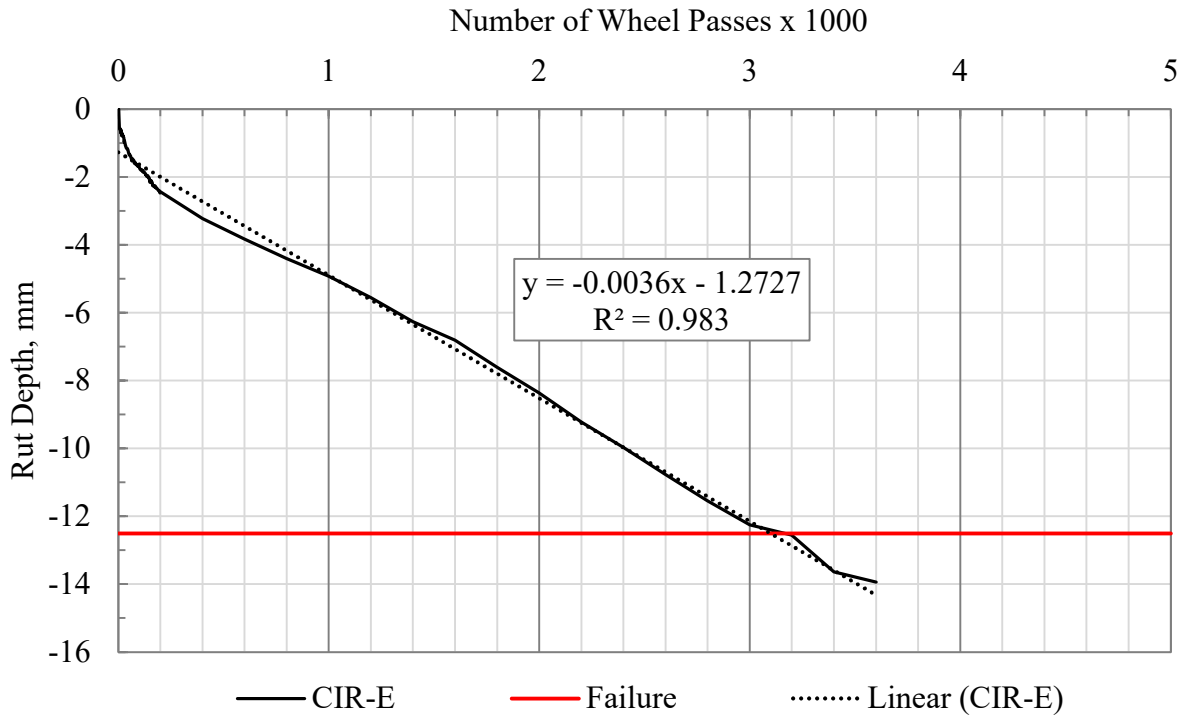

Figure 66: Hamburg rutting test data plotted with linear regression line and R^2 value.

Table 15: HWT mixture result trendline values.

Mixture	Equation	R^2
CIR-E	-0.0036x-1.2727	0.984
CCPR-E	-0.0045x-1.9085	0.933
CIR-F	-0.0068x-0.9101	0.985
CCPR-F	-0.0031x-1.2775	0.976
FDR-E	-0.0045x-0.6862	0.994

The HWT test was developed to indicate rutting potential in surface mixtures. Each of these five mixtures tested were used as a base layer with a one-inch HMA overlay as the surface layer. The recycled/reclaimed base mixture's specimen may have resulted in less rutting if they were overlaid with the one-inch thin HMA lift identical to what was constructed in field. The overall

confining benefit of the surface mixture on top of the recycled/reclaimed base layers in the field may prove to be sufficient against the potential for rutting. Moisture would also not become an issue as easily with the dense surface overlay.

4.3 Comparison of the Mixture Designs and As-Built Mixtures

4.3.1 Foamed Mixtures

The CIR-F mixture design and as-built mixture's black rock gradations were plotted on a 0.45 power chart in Figure 67 to compare material gradations from the mixture design and construction phases. The figure shows that the mixture design RAP had coarser material between the 3/8 and 3/4-inch sieves with the highest percent passing difference of 9.62% at the 1/2-inch sieve. Seven of the eleven sieves had percent passing differences greater than 5%, which was higher than the limit for acceptable tolerance at the median sieve for a properly maintained stockpile (West 2015). It is uncertain whether the seven sieves with differences greater than 5% will affect the performance of the mixture. The as-built material had fewer fine RAP particles, which could indicate that a lower foamed binder content could possibly have been used in the construction of the test section.

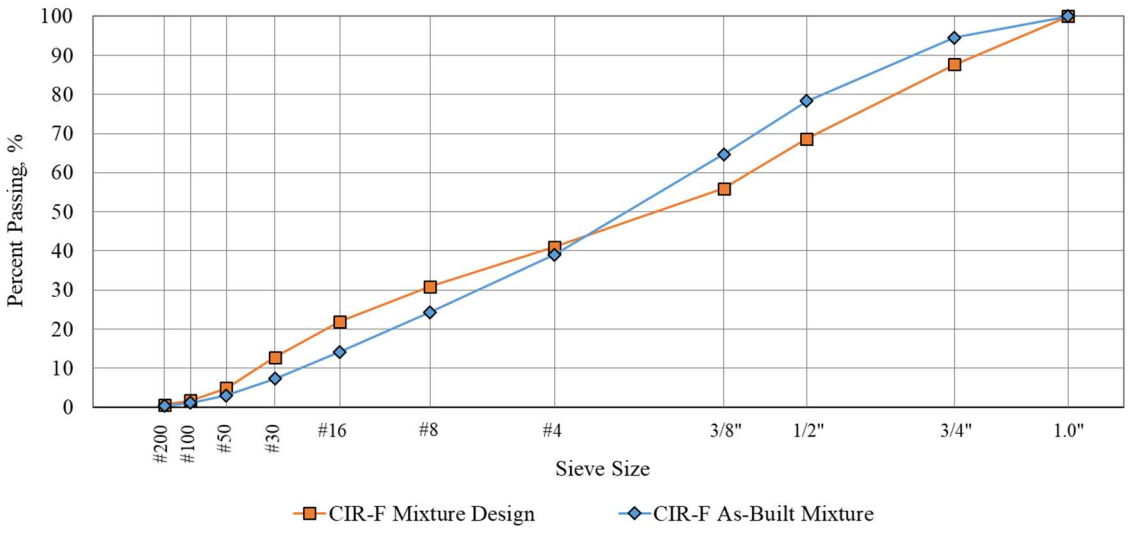

Figure 67: Comparison of CIR-F mixture design and as-built mixture black rock gradations.

The CCPR-F mixture design and as-built mixture black rock gradations were plotted on a 0.45 power chart in Figure 68 to compare material gradations during the mixture design and construction phases. The figure shows that the as-built mixture RAP had coarser material between the #4 and 3/4-inch sieves with the highest percent passing difference of 8.65% at the 3/8-inch sieve. Only four of the eleven sieves had percent differences greater than 5%. Again, it is uncertain whether the four sieves with differences greater than 5% will affect the performance of the material. The CCPR-F as-built material also had fewer fine RAP particles than the mixture design, similar to the CIR-F. This could have allowed a lowered foamed asphalt content during construction.

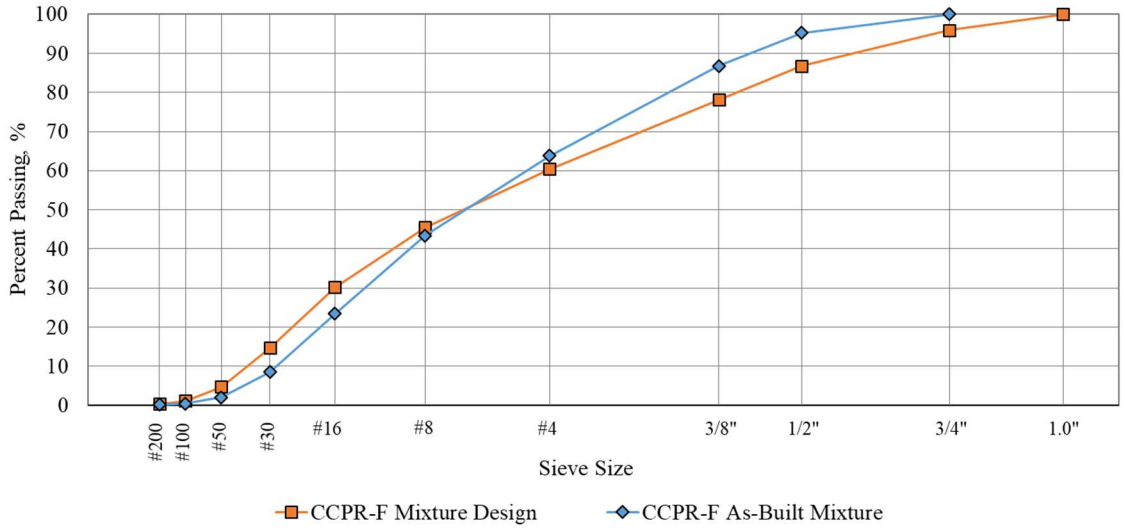

Figure 68: Comparison of CCPR-F mixture design and as-built mixture black rock gradations.

A comparison between the mixture design and as-built mixture ITS results were conducted. Figure 69 and 70 show the comparison of the ITS results for CIR-F and CCPR-F, respectively. Table 16 summarizes the ITS and TSR findings for each mixture and phase.

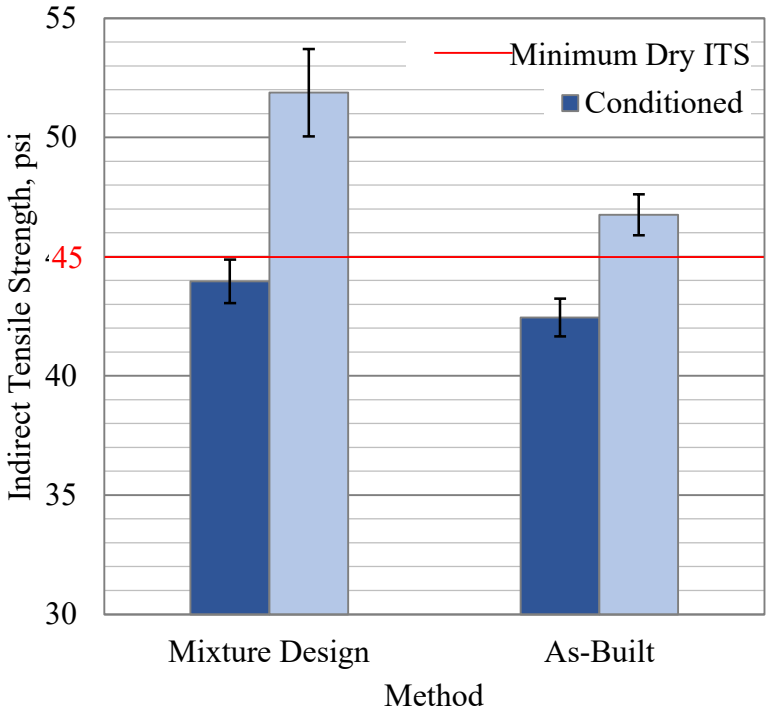

Figure 69: CIR-F ITS comparison between mixture design and as-built mixture.

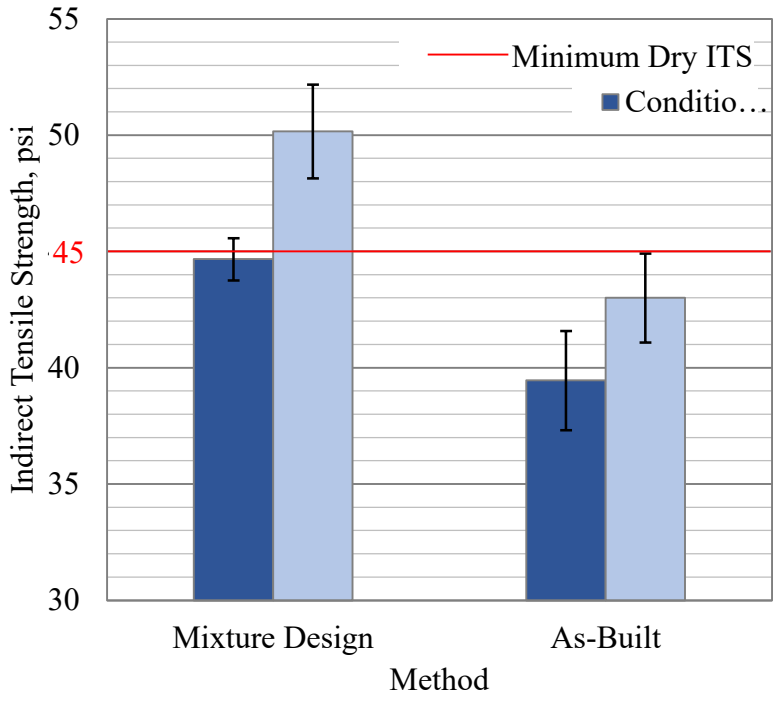

Figure 70: CCPR-F ITS test result comparison between mixture design and as-built mixture.

Table 16: Foamed CR ITS result comparison between mixture design and as-built mixtures.

Mixture	CIR-F		CCPR-F	
Method	**Mix Design**	**As-Built**	**Mix Design**	**As-Built**
Dry ITS, psi	51.9	46.8	50.2	43.0
Conditioned ITS, psi	44.0	42.5	44.7	39.5
TSR	0.85	0.91	0.89	0.92

*Red cells indicate failure to meet criteria.

The figures show that the TSR ratios remained consistent between the mixture designs and as-built mixtures. However, a decrease in the dry and conditioned ITS was recorded for both of the as-built mixtures. This result was not expected, however, the change in gradation between the two phases (mixture design and construction) for the mixtures in combination with the moisture content differences may have affected these results. Even with the decrease in tensile strength, the average dry strength for CIR-F remained above the minimum recommended 45 psi limit. The average CCPR-F dry ITS decreased from 50.2 psi to 43.0 psi from the mixture design to the as-built mixture. It is concerning that the acceptance criteria was not met from the material constructed following the as-built mixture material properties. This result shows that the paved CCPR-F test section may have issues with its strength. However, the 45 psi requirement is a recommended value from ARRA based on experience, so this result showing unacceptable tensile strength may ultimately not be of concern.

A two-sample *t*-test performed in Minitab 19 was used to compare the mixture design and as-built mixture's ITS results for the CIR-F and CCPR-F dry and conditioned specimen. A confidence interval of 95% was used to indicate whether the mixture design's and as-built mixture's ITS results had statistically equal means. The p-values from the two-sample *t*-tests are in Table 17, and the grey cells indicate that the null hypothesis of equal means between mixture

design and as-built mixtures was rejected. This table shows that there were differences in the ITS means between the two methods. This may have occurred because the RAP was collected in a different method for the CIR-F and a different stockpile for CCPR-F. The difference in ITS means may also have been caused by the change in the moisture contents after the construction phase.

Table 17: Two sample t-test p-values comparing the means of ITS mixture design and as-built mixtures.

Mixture/Condition	p-value
CIR-F ITS Dry	0.002
CIR-F ITS Conditioned	0.046
CCPR-F ITS Dry	0.005
CCPR-F ITS Conditioned	0.004

*Grey cells indicate a rejected null hypothesis.

4.3.2 Emulsified Mixtures

The emulsion mixture designs were not conducted at NCAT, therefore the complete set of data for the designs were not acquired. A statistical analysis comparing the means of each of the mixtures and their methods could not be conducted because of the limited amount of data available from the mixture designs. Table 18 summarizes the resulting MS values for the mixtures from their respective final mixture designs completed by Ingevity and AET and the post-construction as-built mixtures tested at NCAT. The CIR-E mixture was constructed using an emulsion content of 2.8% most likely because the RAP millings were found to be between the medium and coarse mixture design gradations. Based on the construction material properties recorded, the FDR-E mixture ultimately ended up passing the minimum MSR requirement, as compared to the mixture design that failed. This was an unexpected result because the moisture content of the FDR nearly doubled during construction. From the as-built testing, MSRs for the CIR-E mixture nearly doubled and the CCPR-E mixture increased by 33%, which were

unexpected results. It is possible that the increased moisture contents during construction from these three mixtures caused the increase in MSR, however, this phenomenon was not studied further.

Table 18: Emulsion CR and FDR MS result comparison between mixture design and as-built mixtures.

Mixture	**CIR-E**			**CCPR-E**		**FDR-E**		
Method	**Medium Mix Design**	**Coarse Mix Design**	**As-Built**	**Mix Design**	**As-Built**	**Mix Design**	**As-Built**	**Minimum Req.**
Emulsion Content, %	3.0	2.5	2.8	3.5	3.5	3.0	3.0	N/A
Dry MS, lbf	2335	2190	1354	2113	1397	3825	2460	1250
Conditioned MS, lbf	2030	1870	2166	1765	1561	2382	2131	N/A
MSR	0.87	0.85	1.60	0.84	1.12	0.62	0.87	0.70

*Red cells indicate failure to meet criteria.

4.4 Impact of Mixing and Compaction Methods on Specimen Performance

4.4.1 Specimen Density Comparison

A comparison of the LMLC and PMLC sample's dry densities prior to being cored was performed. The comparison for each of the four CR mixture types is presented in Figure 71. The target dry densities recorded from the field listed in Table 11 are shown in Figure 71 as well.

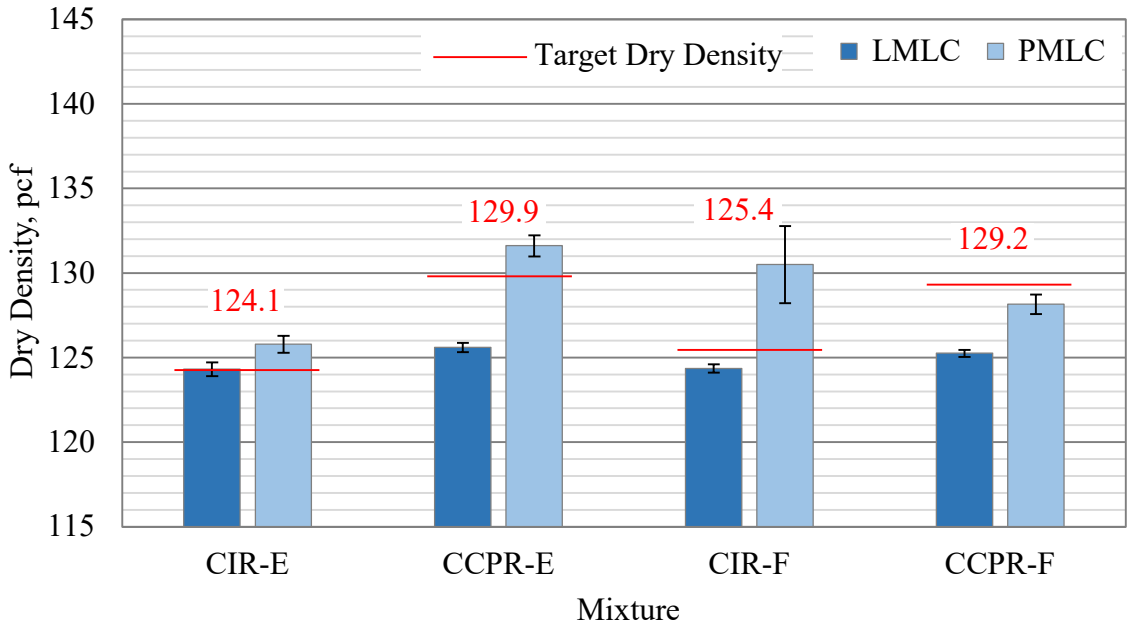

Figure 71: Pre-cored LMLC and PMLC specimen dry density comparisons to their field recorded target dry densities.

The trend for the dry densities in Figure 71 was that the pre-cored PMLC samples had higher dry densities than the LMLC samples. This could have occurred because the compaction setting different in that the PMLC samples were compacted to a specific height, while the LMLC samples were compacted to a specific number of gyrations. Both of the CIR-E lab-compacted specimens had the closest LMLC and PMLC dry densities to the target. The CIR-E, CCPR-E and CIR-F PMLC specimens all had dry densities higher than the target densities. Both of the CCPR-F lab-compacted specimens showed dry densities less than the recorded field dry density.

A two-sample *t*-test statistical comparison was performed in Minitab 19 with a 95% confidence interval for each of the mixtures. Table 19 shows the p-values from statistical testing for each of the four mixtures. The grey cells indicate that the null hypothesis of equal mean dry densities between the two sample types is rejected.

Table 19: Two sample *t*-test p-values comparing the dry densities of the LMLC and PMLC samples prior to coring.

Mixture	p-value
CIR-E	0.005
CCPR-E	0.000
CIR-F	0.022
CCPR-F	0.000

*Grey cells indicate a rejected null hypothesis.

Figure 72 shows the dry density results from each of the four specimen types prepared for dynamic modulus testing for each of the four recycled mixtures. In all mixtures except CIR-E, the LMLC-S specimens had the lowest recorded dry densities of all four specimen types constructed. A few of the SS specimen, regardless of the mixture type, had issues with fragments of the specimen breaking off during the coring and cutting process. The percentage of fine particles in the mixtures added to the possibility of the fragmenting because there was less aggregate skeleton to hold the specimen together. Loss of fragments in the LS specimen also occurred frequently. However, due to the volume of the specimen, the fragments that broke off did not impact the weight as greatly as it impacted the SS specimens.

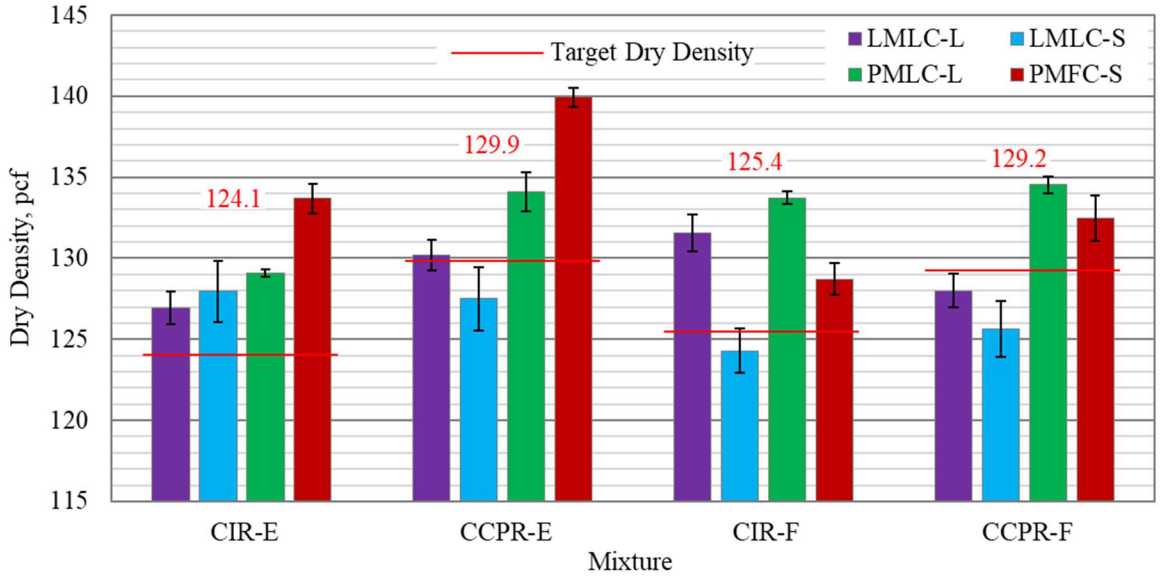

Figure 72: Prepared dynamic modulus specimen dry densities by specimen type.

A statistical comparison between the four specimen types for each of the mixtures was performed in Minitab 19. A one-way ANOVA was used with Tukey methods to create pairwise comparisons between all specimen types. A confidence interval of 95% was used throughout the testing. Table 20 summarizes the p-values for each of the pairwise comparisons. The grey cells indicate that the null hypothesis of equal means between the pairs is rejected.

Table 20: One-way ANOVA Tukey multiple comparison p-values comparing the dry densities of the four dynamic modulus specimen types.

Mixture	CIR-E	CCPR-E	CIR-F	CCPR-F
LMLC-S vs LMLC-L	0.671	0.208	0.000	0.120
LMLC-S vs PMLC-L	0.599	0.011	0.000	0.000
LMLC-S vs PMFC-S	0.000	0.002	0.000	0.000
LMLC-L vs PMLC-L	0.164	0.040	0.107	0.000
LMLC-L vs PMFC-S	0.000	0.002	0.012	0.001
PMLC-L vs PMFC-S	0.001	0.021	0.000	0.151

*Grey cells indicate a rejected null hypothesis.

The p-values shown in Table 20 indicate that most of the specimen types used for dynamic modulus did not have equal means. This was expected due to the different compaction methods used to achieve the dry density targets.

4.4.2 Dynamic Modulus Comparisons

4.4.2.1 Large-Scale and Small-Scale Comparison

A comparison of the dynamic moduli between the LS and SS lab-mixed specimen (LMLC-L and LMLC-S) was performed and graphed on a log-log scale in Figure 73. This was done to identify whether the two different laboratory-mixed specimen sizes tested resulted in similar dynamic moduli. The graph includes dynamic modulus averages from a minimum of three specimen per mixture at each of the six frequencies and the three temperatures tested. The blue

line indicates a perfect theoretical linear relationship between the LS and SS lab-mixed specimen dynamic moduli. However, the figure visually indicates that a higher dynamic modulus was recorded from the LS specimens regardless of the mixture type or recycling/stabilizing agent. The CIR-F mixture had the largest difference between specimen's dynamic moduli as compared to the other mixtures. The CIR-F mixture also had the coarsest gradation as recorded in Figure 54. Being that the SS specimen had much less volume as compared to the LS specimen, any inconsistencies in the material would also be realized far easier for the SS specimen sizes. Additionally, the average dry densities of the SS specimens tended to be lower than the LS specimen, except for the CIR-E, as seen in Figure 71. The dry density of the specimens may directly affect the dynamic modulus, but this was not directly studied from this material.

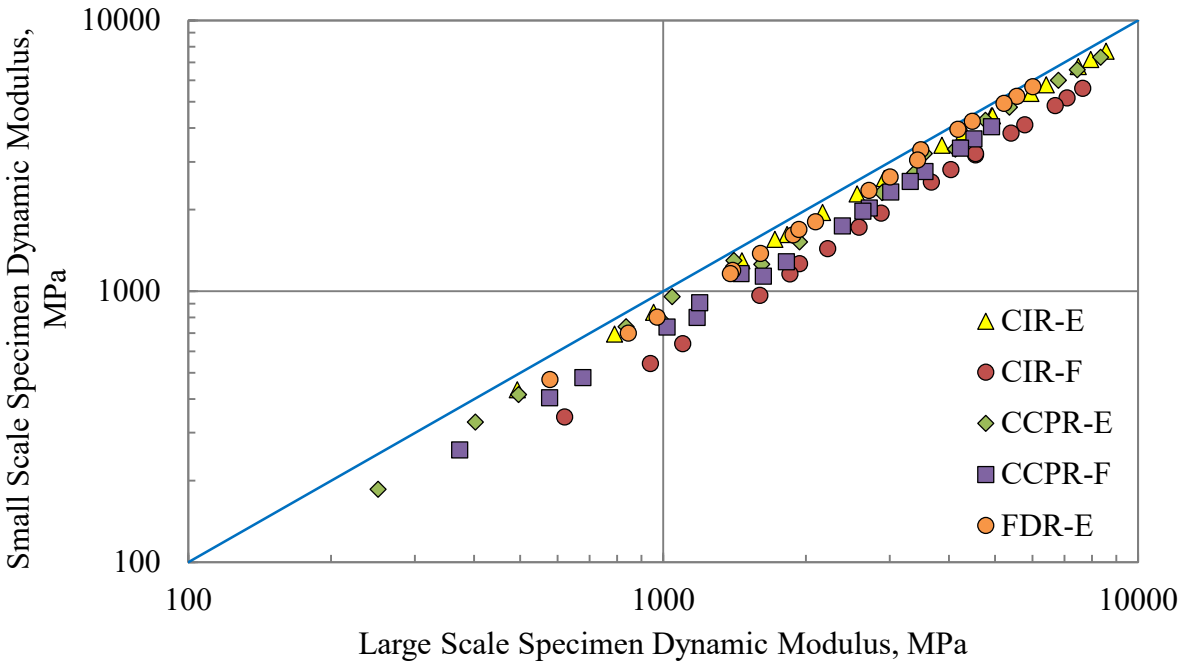

Figure 73: Comparison of dynamic moduli from LMLC-L and LMLC-S specimens for all testing temperatures and frequencies.

4.4.2.2 Dynamic Modulus Statistical Comparison

To validate whether the dynamic moduli were significantly impacted because of the mixing and compacting methods, a one-way ANOVA test was performed in Minitab 19. A 95% confidence interval for the ANOVA test was selected to statistically determine if the sample means were equal, in which case the null hypothesis was not rejected. The omnibus p-values for the four mixtures are in Table 21. The Tukey multiple comparison method was used to consider all pairwise differences and determine which means were equal between them. The p-values for each pair of specimen types created for dynamic modulus testing are summarized in Tables 22 and 23 for CIR and CCPR, respectively. The grey cells in Tables 21-23 indicate that the null hypothesis was rejected and could conclude that a significant difference in the means existed.

Table 21: One-way ANOVA test omnibus p-values comparing the dynamic modulus results for all four specimen types.

Test Temperature, °C	**4.4**	**21.1**	**37.8**
CIR-E	0.004	0.086	0.296
CIR-F	0.000	0.000	0.000
CCPR-E	0.000	0.000	0.006
CCPR-F	0.000	0.000	0.001

*Grey cells indicate a rejected null hypothesis.

Table 22: One-way ANOVA Tukey multiple comparison p-values comparing the dynamic modulus between the four specimen types, CIR.

Mixture	**CIR-E**			**CIR-F**		
Temp., °C	**4.4**	**21.1**	**37.8**	**4.4**	**21.1**	**37.8**
LMLC-S vs LMLC-L	0.194	0.388	0.796	0.000	0.000	0.002
LMLC-S vs PMLC-L	0.004	0.101	0.472	0.000	0.000	0.000
LMLC-S vs PMFC-S	0.009	0.116	0.996	0.001	0.000	0.016
LMLC-L vs PMLC-L	0.207	0.833	0.948	0.068	0.071	0.643
LMLC-L vs PMFC-S	0.581	0.965	0.640	0.183	0.453	0.221
PMLC-L vs PMFC-S	0.678	0.956	0.312	0.001	0.002	0.022

*Grey cells indicate a rejected null hypothesis.

Table 23: One-way ANOVA Tukey multiple comparison p-values comparing the dynamic modulus between the four specimen types, CCPR.

Mixture	**CCPR-E**			**CCPR-F**		
Temp., °C	**4.4**	**21.1**	**37.8**	**4.4**	**21.1**	**37.8**
LMLC-S vs LMLC-L	0.237	0.017	0.713	0.409	0.293	0.500

LMLC-S vs PMLC-L	0.004	0.001	0.006	0.000	0.000	0.001
LMLC-S vs PMFC-S	0.000	0.001	0.591	0.000	0.011	0.421
LMLC-L vs PMLC-L	0.167	0.274	0.029	0.000	0.003	0.005
LMLC-L vs PMFC-S	0.003	0.497	1.000	0.003	0.246	1.000
PMLC-L vs PMFC-S	0.270	0.895	0.018	0.235	0.035	0.003

*Grey cells indicate a rejected null hypothesis.

The dynamic modulus of the CIR-E specimens at both 21.1°C and 37.8°C had Tukey pairwise comparison's p-values show that the means were not statistically different. For the remaining mixtures and test temperatures, the Tukey multiple comparison ANOVA was used to identify all statistically similar pairs of specimen types at each temperature, seen in Table 22.

The CIR-E mixture resulted in 16 of 18 pairs showing not statistically different means. Both of the pairs that reject the null hypothesis included the LMLC-S specimens at the 4.4°C test temperature.

The CIR-F mixture had only 6 of 18 pairs showing not statistically different means. All six of the pairs included the LMLC-L specimens paired with the PMLC-L and PMFC-S specimens. This shows that for the CIR-F mixture, the LMLC-L specimen were accurate at representing the dynamic modulus of the specimen recovered from the test section on 70th Street. The LMLC-S specimens were not reliable at accurately representing specimen recovered from the test section.

The CCPR-E mixture had 9 of 18 pairs showing not statistically different means. The pairs of specimens that had equal means were not the same for each temperature. The LMLC-L and PMFC-S specimen had equal means at the 21.1°C and 37.8°C temperature. The resulting p-values showed that the CCPR-E mixture did not have a dependable way to measure the field dynamic specimen with the laboratory dynamic modulus.

The CCPR-F mixture resulted in the 7 of 18 pairs showing not statistically different means, the lowest number of pairs with equal means for all the CR mixtures. The LMLC-L and LMLC-S specimens were the only pair that had equal means at all three testing temperatures. The LMLC-L and PMFC-S specimen had equal means at the 21.1°C and 37.8°C temperature.

The LMLC-L and PMFC-S pairwise comparison for all four CR mixtures and all testing temperatures had at 10 of 12 pairs with statistically equal means pairs, the most equal mean pairs for all pairwise comparisons. This indicates that if LS specimen are mixed and compacted in the laboratory with the same material properties as recorded during construction, the dynamic moduli may have the most accurately representing results to the SS specimen recovered from field cores.

4.4.2.3 Dynamic Modulus Master Curve Comparison

For each of the four CR mixtures constructed, the four specimen type's (LMLC-L, LMLC-S, PMLC-L, PMFC-S) master curves were graphed together on a semi-log plot to visually show similarities and/or differences in each at different pavement temperatures. The master curves were created by graphing the dynamic modulus against the calculated reduced frequency to measure the response to pavement temperature and traffic loads. The smaller the reduced frequency is, the lower the assumed traffic load and the higher the assumed pavement temperature, and vice versa for the higher reduced frequencies. The traffic load is in terms of vehicle speed. With a vehicle at slow to no speed, the frequency of the compressive load would be low, while a high-speed vehicle would have high frequency loads.

The CIR-E mixture's semi-log master curve is seen in Figure 74. It shows that at the lower reduced frequency, the moduli of all four specimen types are nearly alike. When the reduced frequency of the specimen increases, or the pavement temperature decreases, the dynamic moduli

disperse more. Both LMLC-L and LMLC-S specimen had the lower dynamic moduli for lower temperature and high traffic loadings, with the LMLC-S being the lower of the two. The PMFC-S specimen type has the highest trending modulus at the lowest temperatures. The PMFC-S also had the highest average dry density post coring of the specimen. This was an unexpected results but may indicate that a correlation between the dry density and dynamic modulus for CIR-E materials exists.

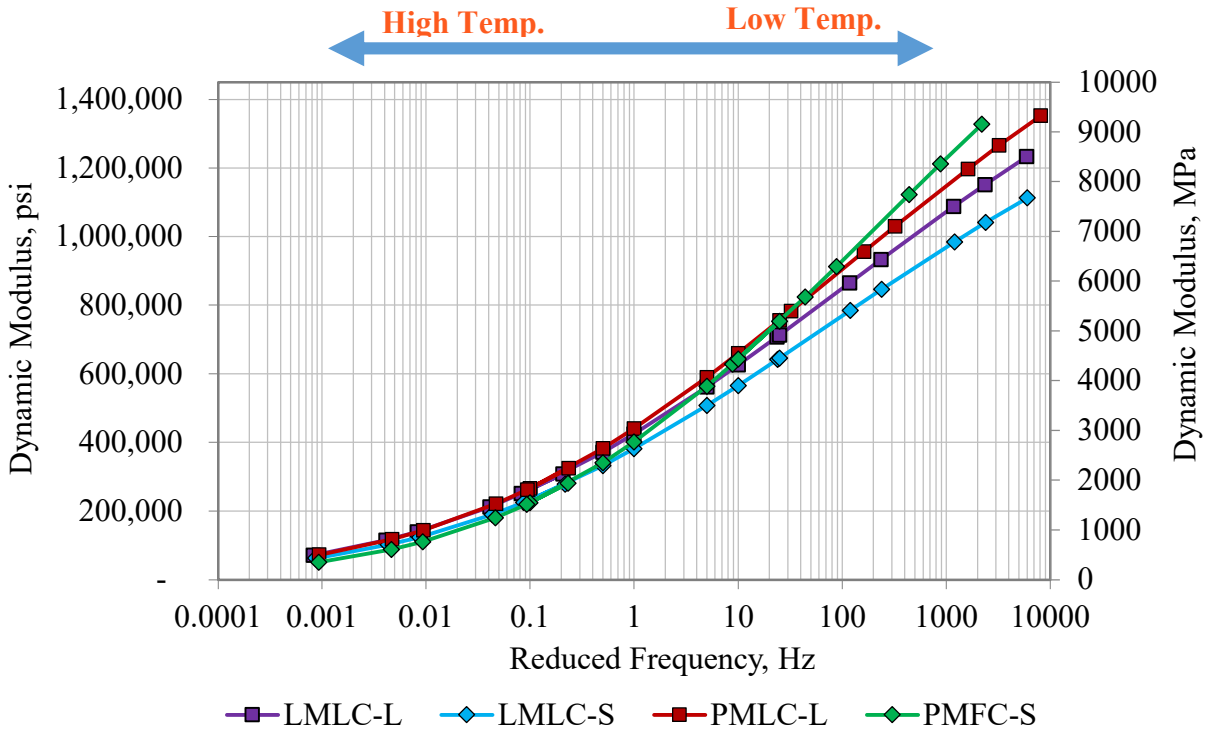

Figure 74: CIR-E semi-log master curves.

The CCPR-E mixture's semi-log master curve is seen in Figure 75. The master curve shows a similar response to the reduced frequency as compared to the CIR-E mixture. The PMFC-S specimen had the highest modulus while the LMLC-S was the lowest throughout the range of frequencies. The dynamic modulus and average dry density of the four specimen types show a trend at lower pavement temperatures. The higher the dry density is, the stiffer the material is at lower temperatures.

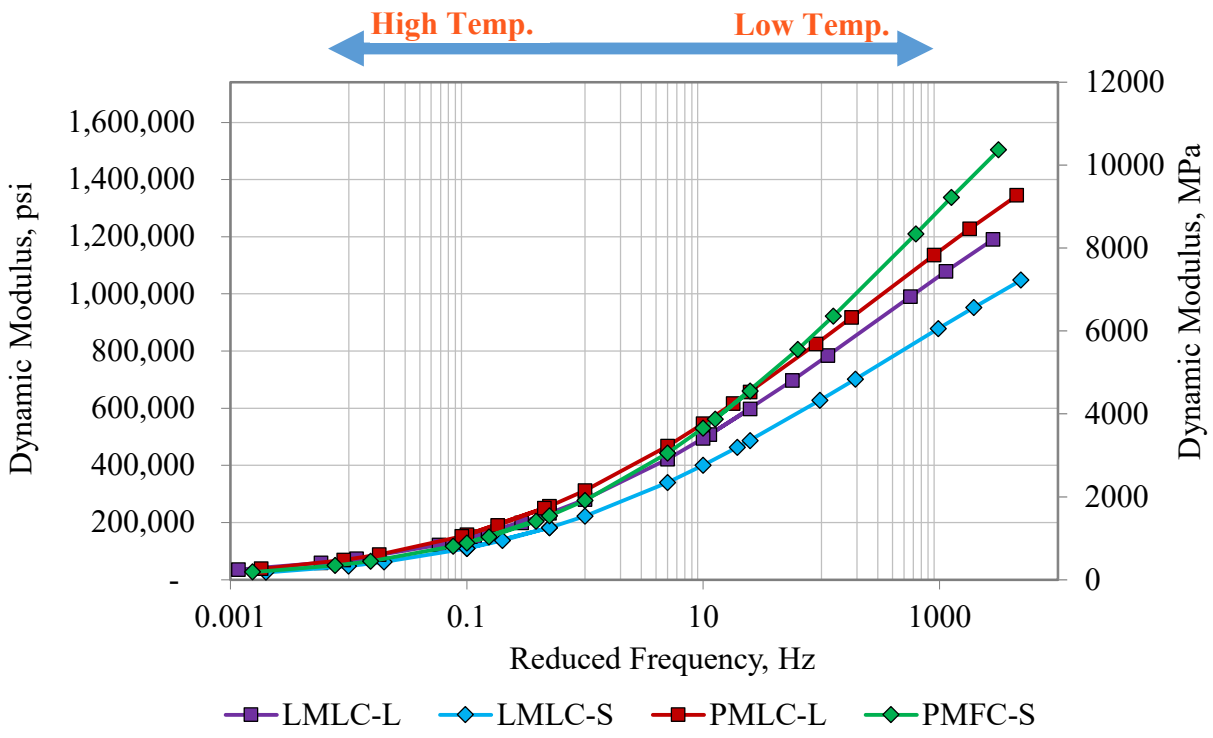

Figure 75: CCPR-E semi-log master curves.

The CIR-F mixture's semi-log master curve is seen in Figure 76. The figure along with the statistical analysis from Table 22 show that the LMLC-S specimens had a significantly different modulus as compared to the other three specimen types. The PMLC-L specimen had the highest modulus recorded for all reduced frequencies as compared to the CIR-E and CCPR-E specimen which had the PMFC-S having the higher modulus across most reduced frequencies. Again, the dry density and dynamic modulus correlation at lower pavement temperatures is exhibited for the CIR-F mixture.

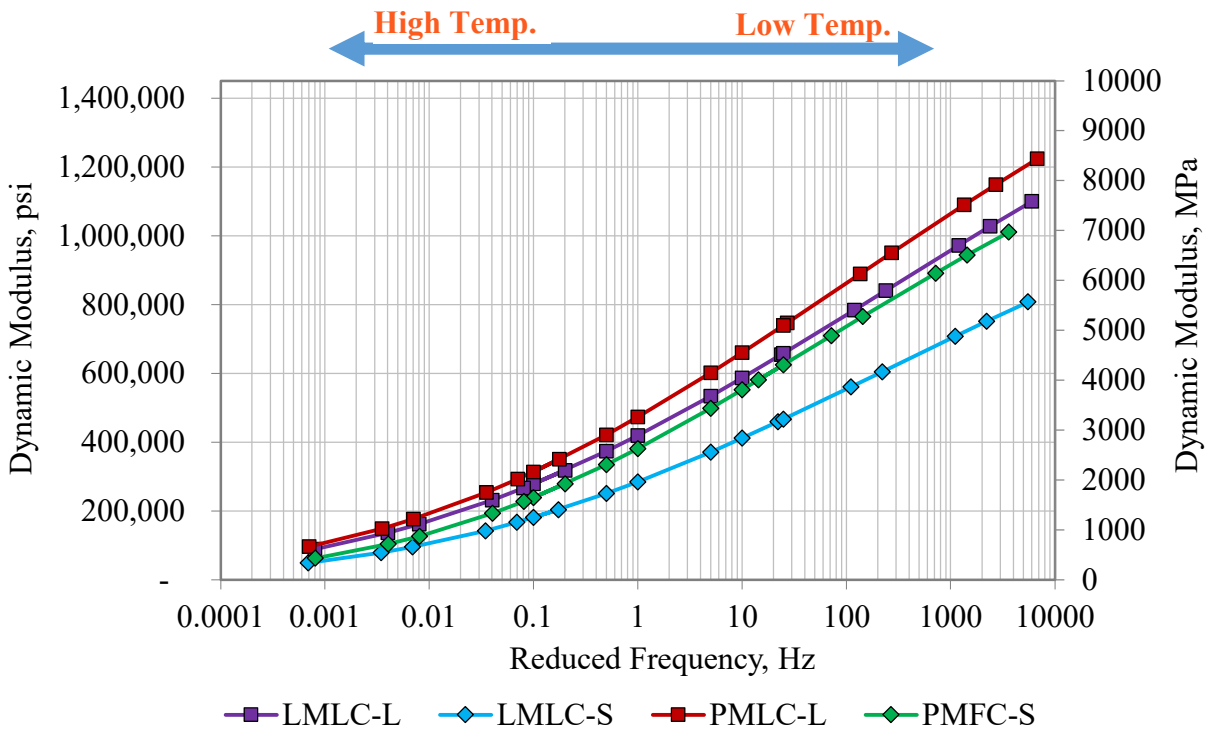

Figure 76: CIR-F semi-log master curves.

The CCPR-F mixture's semi-log master curve is seen in Figure 77. It visually confirms that the PMFC-S specimens had the highest modulus recorded across all reduced frequencies. Both LMLC-S and LMLC-L specimen trends were similar to one another at the higher reduced frequencies, with LMLC-L being slightly higher. The PMFC-S specimens had the highest moduli at all reduced frequencies. The PMLC-L moduli was similar to the LMLC-L at the lower reduced frequencies, until around 10 Hz when it began to respond to far stiffer than either lab-mixed specimen. The CCPR-F mixture again shows a correlation between the dry density and dynamic modulus at the lower pavement temperatures, which was unexpected.

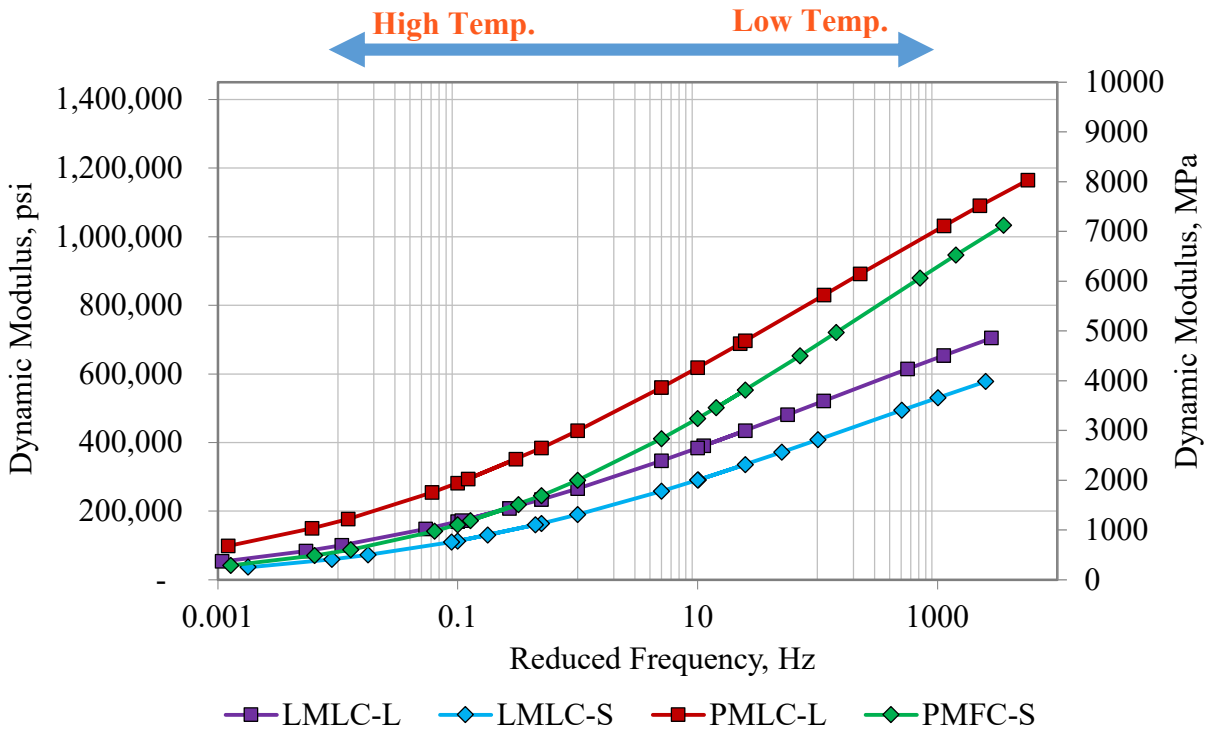

Figure 77: CCPR-F semi-log master curves.

The general tendency for the master curves for any of the mixture types was that the lower moduli were the LMLC-S specimen. At lower pavement temperatures, the PMFC-S specimens had the highest modulus when the recycling agent was emulsion, and the PMLC-L specimens had the highest modulus when the recycling agent was foamed asphalt. A correlation between the dry density and dynamic modulus at low pavement temperatures was seen for all the mixtures except CIR-E when the LMLC-L, LMLC-S, and PMLC-L had very similar densities and modulus values.

A master curve containing each of the CR mixture's PMFC-S specimen is in Figure 78. It can be seen that the CR mixtures with emulsion as the recycling agent were generally stiffer at higher reduced frequencies. The higher the average dry density in the PMFC-S specimen for each mixture, the higher the dynamic modulus at low pavement temperatures. These results may suggest that emulsion mixtures can achieve higher dry densities than foamed mixtures, raising the stiffness

of the base layer. It is unclear whether this is actually the case or not. Additional testing of these materials may allow better indication of what a good cracking threshold is for these mixtures.

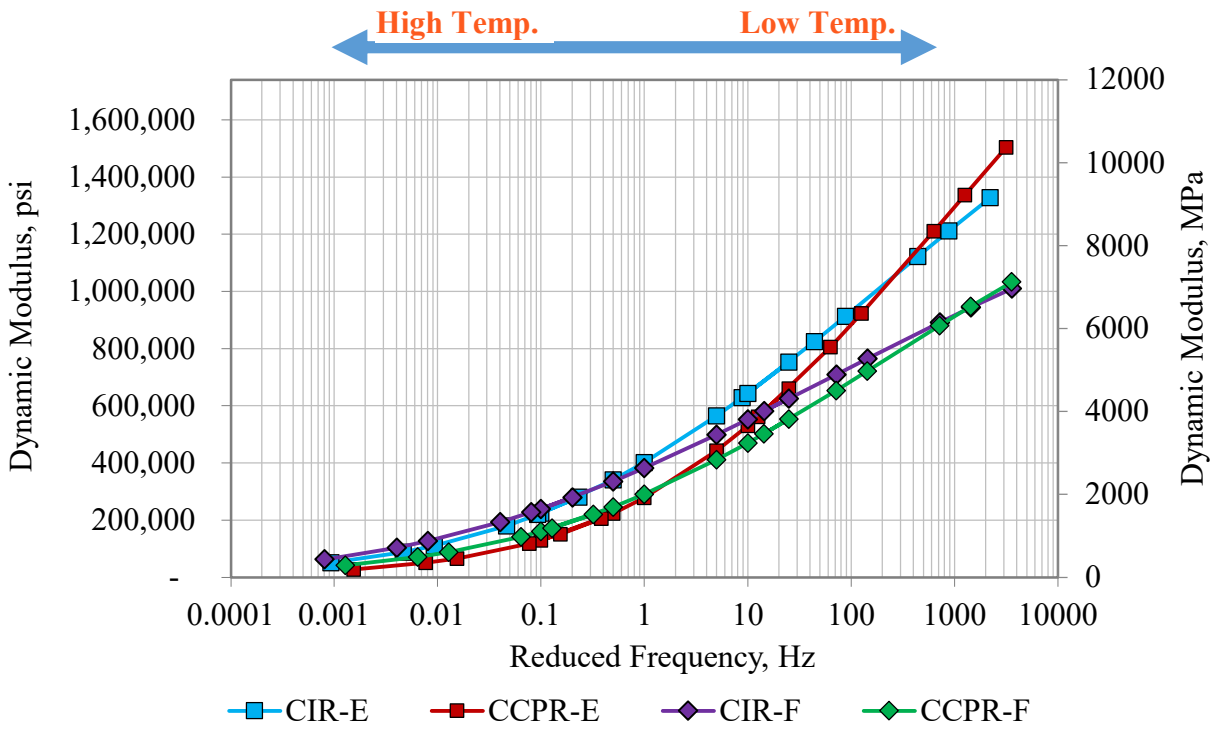

Figure 78: CR PMFC-S semi-log master curves.

4.5 Summary of the Results

The gradations of the CIR-F and CCPR-F RAP showed that there were some differences in the material size distribution, which was expected because of the method for retrieving RAP for the CIR-F and the change of the CCPR-F RAP stockpile. The CIR-F and CCPR-F ITS results showed that the changes to the RAP gradation and moisture content during construction possibly affected the acceptance test results. The CCPR-F material did not pass the minimum average dry ITS requirement. The emulsion mixtures had significant increases in the MSR values for the as-built mixtures as compared to the mixture designs.

The CCPR-F as-built material showed the best cracking resistance as compared to the other four CR and FDR mixtures tested. This section should resist cracking longer than the others, with the FDR-E section being most likely to crack based on the low CT_{Index}.

The HWT rutting test indicated that if the materials were unconfined by a surfacing, they would all fail prematurely in accordance to the 12.5 mm specified rutting failure depth.

Dynamic modulus testing showed that while the pavement temperature is high, all four dynamic modulus specimen types resulted in similar responses to repetitive non-destructive compressive loads. As the pavement temperature decreases, a correlation between the average dry density and dynamic moduli of the specimen types can be seen. This was an unexpected result of the testing, which should be further studied.

CHAPTER 5 – CONCLUSIONS AND RECOMMENDATIONS

5.1 Conclusions

The following conclusions have been made based on observations throughout this study:

- A statistical comparison of the indirect tensile strength results showed that there was a significant difference between the means of the mixture design and as-built specimen's strengths. The gradation changes for the CIR and CCPR foamed mixtures likely affected the indirect tensile strengths of the mixtures.
- The emulsified mixtures comprising of only bound materials had higher stabilities when conditioned. This is not an uncommon occurrence based on the emulsion stabilized CR and FDR.
- The IDEAL-CT resulted in the highest CT_{Index} for the CCPR-E mixture. This may be a good indicator that the test section on 70th Street will resist cracks from occurring longer as compared to the other CR and FDR sections.
- The FDR-E mixture had the lowest CT_{Index} of the five mixtures. The FDR-E test section may result in earlier cracking as compared to the other CR sections.
- The failure rutting depth of 12.5 mm as specified by Ingevity may not be indicative of the CR and FDR mixtures resistance to rutting because they are used as pavement base mixtures. The HWT test is conducted on samples that are unconfined at the surface while base pavement layers are confined by the surface lifts.

- Higher dynamic modulus values were recorded in laboratory mixed LS specimen as compared to the SS counterparts. Composition of the recycled material may impact the SS's ability to accurately represent moduli.
- The dynamic moduli of CR pavements, especially at lower temperatures, may be affected by the dry density of the material.

5.2 Recommendations

The following recommendations should be considered for future research of CR and FDR mixtures:

- Research into validating whether the characteristics of the IDEAL-CT and HWT for CR and FDR accurately represent relative field performance.
- Analyze the SS and LS dynamic modulus specimens' relationship to ensure the results correlate for all CR mixtures. A correction factor in the moduli may be required to achieve adequate representation between the two laboratory mixed specimen types.
- Investigate the impact of dry density of CR and FDR mixtures on the dynamic modulus.
- Examine the MnROAD 70th Street test sections to verify whether the results from this thesis correlate to the field performance.

REFERENCES

AASHTO. 2020. *Standard Practice for Reducing Samples of Aggregate to Testing Size*. AASHTO R76. Washington, DC: AASHTO.

AASHTO. 2017. *Standard Practice for Preparation of Cylindrical Performance Test Specimens Using the Superpave Gyratory Compactor (SGC)*. AASHTO R83. Washington, DC: AASHTO.

AASHTO. 2020. *Standard Method of Test for Materials Finer Than 75-μm (No. 200) Sieve in Mineral Aggregates by Washing*. AASHTO T11. Washington, DC: AASHTO.

AASHTO. 2020. *Standard Method of Test for Sieve Analysis of Fine and Coarse Aggregates*. AASHTO T27. Washington, DC: AASHTO.

AASHTO. 2020. *Standard Method of Test for Moisture-Density Relations of Soil Using a 4.54-kg (10-lb) Rammer and a 457-mm (18-in.) Drop*. AASHTO T180. Washington, DC: AASHTO.

AASHTO. 2018. *Standard Method of Test for Resistance of Compacted Asphalt Mixtures to Moisture0Induced Damage*. AASHTO T283. Washington, DC: AASHTO.

AASHTO. 2019. *Standard Method of Test for Hamburg Wheel-Track Testing of Compacted Asphalt Mixtures*. AASHTO T324. Washington, DC: AASHTO.

AASHTO. 2017. *Standard Method of Test for Determining the Dynamic Modulus and Flow Number for Asphalt Mixtures Using the Asphalt Mixture Performance Tester (AMPT)*. AASHTO T324. Washington, DC: AASHTO.

Asphalt Academy. (2009). *Technical Guideline: Bitumen Stabilised Materials*. Asphalt Academy, Pretoria, South Africa.

Asphalt Institute. (2014) *MS-2 Asphalt Mix Design Methods*. 7th Edition.

Asphalt Recycling & Reclaiming Association. (2015). *Basic Asphalt Recycling Manual*. Federal Highway Administration, Maryland.

Bowers, B. F., Diefenderfer, B. K., Diefenderfer, S. (2015). "Evaluation of Dynamic Modulus Paving Mixtures Utilizing Small-Scale Specimen Geometries". Asphalt Paving Technology: Association of Asphalt Paving Technologists-Proceedings of the Technical Sections. Volume 84.

Brown, E. R., Kandhal, P. S., Roberts, F. L., Kim, Y. R., Lee, D., Kennedy, T. W. (2009). *HOT MIX ASPHALT MATERIALS, MIXTURE DESIGN, AND CONSTRUCTION.* NAPA Research and Education Foundation. Lanham, Maryland.

Cross, S. A. (2003). "Determination of Superpave® Gyratory Compactor Design Compactive Effort for Cold In-Place Recycled Mixtures". *Transportation Research Record* 1819: 1, 152-160.

Csanyi, L. H. (1957). "FOAMED ASPHALT IN BITUMINOUS PAVING MIXTURES." *Highway Research Board Bulletin*, (160), 108–122.

Diefenderfer, B. K., Apeagyei, A. K. (2014). *I-81 In-Place Pavement Recycling Project* (Report No. VCTIR 15-R1). Richmond, Virginia, 23219: Virginia Department of Transportation.

Diefenderfer, B. K., Bowers, B. F., & Diefenderfer, S. D. (2015). *Asphalt Mixture Performance Characterization Using Small-Scale Cylindrical Specimens* (Report No. VCTIR-15-R26). Richmond, Virginia, 23219: Virginia Department of Transportation.

Diefenderfer, B. K., Boz, I., and Bowers, B. F. (2019). "Evaluating Cracking Tests for Performance-Based Design Concept for Cold Recycled Mixtures." ASCE TD&I Conference Proceedings.

Dong, W., & Charmot, S. (2018). Proposed Tests for Cold Recycling Balanced Mixture Design with Measured Impact of Varying Emulsion and Cement Contents. *Journal of Materials in Civil Engineering*, 31.

Hamburg Wheel Tracker [Online Image]. (2018). James Cox and Sons. https://www.jamescoxandsons.com/hamburg-wheel-tracker/

Kennedy, T. W., & Hudson, W. R. (1968). APPLICATION OF THE INDIRECT TENSILE TEST TO STABILIZED MATERIALS. *Highway Research Record*.

Kim, B., Lee. H., Park, H., & Kim, H. (2012). "Framework for Estimating Greenhouse Gas Emissions Due to Asphalt Pavement Construction. *Journal of Construction Engineering and Management.* 138(11), 1312-1321.

Ma, F., Sha, A., Lin, R., Huang, Y., & Wang, C. (2016). Greenhouse Gas Emissions from Asphalt Pavement Construction: A Case Study in China. *International journal of environmental research and public health*, *13*(3), 351.

Martinez, D. S. (2020). *Field Assessment of Cold Recycling Technologies Used for Pavement Preservation*. Auburn University, Auburn, AL.

Scherocman, J. A. (1983). "Cold in-place recycling of low-volume roads." *Transportation Research Record* 898: 308-315.

Schwartz, C. W., Diefenderfer, B. K., Bowers, B. F. (2017). *Material Properties of Cold In-Place Recycled and Full Depth Reclamation Asphalt Concrete*. Washington, DC: The National Academies Press.

Sebaaly, P. E., Castro, J. A., Hajj, E. Y., & Sebaaly, P. S. (2018). *Development of In-Place Density Method for Cold In-Place Recycling*.

Stroup-Gardiner, M. (2011). *Recycling and Reclamation of Asphalt Pavements Using In-Place Methods*. National Cooperative Highway Research Program Synthesis Program, National Academies Press, Washington, D.C.

Valentin, J., Čížková, Z., Suda, J. Batista, F., Mollenhauer, K., and Simnfske, D. (2016). Stiffness Characterization of Cold Recycled Mixtures. *Transportation Research Procedia*, (14), 758-767.

Vargas, A. (2019). *Pavement Preservation Group Study Summary of Findings 2019*. The National Center for Asphalt Technology at Auburn University. Auburn, AL.

West, R. (2015). *Best Practices for RAP and RAS Management*. National Asphalt Pavement Association, Maryland.

West, R., Timm, D., Powell, B., Heitzman, M., Tran, N., Rodezno, C., Watson, D., Leiva, F., Vargas, A., Willis, R., Vrtis, M., & Diaz, M. (2018). Phase V (2012-2014) NCAT Test Track Findings. NCAT Report 16-04. National Center for Asphalt Technology, Auburn, Ala.

West, R., Timm, D., Powell, B., Heitzman, M., Tran, N., Rodezno, C., Watson, D., Leiva, F., Vargas, A. (2019). Phase VI (2015-2017) NCAT Test Track Findings. NCAT Report 18-04. National Center for Asphalt Technology, Auburn, Ala.

Wirtgen Group. (2012). *Wirtgen Cold Recycling Manual*. Wirtgen GmbH, Germany.

Witczak, M. W., Kaloush, K., Pellinen, T., El-Basyouny, M., & Von Quintus, H. (2002). NCHRP Report 465: Simple Performance Test for Superpave Mix Design. TRB, National Research Council, Washington, D.C., 2002.

Zhou, F., Im, S., Sun, L., & Scullion, T. (2013). Development of an IDEAL Cracking Test for Asphalt Mix Design, Quality Control and Quality Assurance. *Road Materials and Pavement Design*, 18, 405-427.

APPENDIX A: DYNAMIC MODULUS RESULTS

CIR-E LMLC-L	Temp, °C	4.4	4.4	4.4	4.4	4.4	4.4	21.1	21.1	21.1	21.1	21.1	21.1	37.8	37.8	37.8	37.8	37.8	37.8
	Frequency, Hz	25	10	5	1	0.5	0.1	25	10	5	1	0.5	0.1	25	10	5	1	0.5	0.1
Specimen 1	Modulus (ksi)	1245.294	1153.920	1084.737	927.516	860.509	711.120	749.410	655.281	591.174	450.922	396.823	284.564	336.633	268.900	230.030	151.709	125.835	78.886
	Phase Angle (deg)	7.50	8.10	8.55	9.95	10.66	12.68	13.01	14.41	15.31	17.98	19.02	21.91	22.04	23.89	24.50	26.51	26.89	27.72
Specimen 2	Modulus (ksi)	1271.691	1181.913	1113.890	956.089	888.936	737.517	721.853	630.479	566.953	428.296	375.793	267.595	317.343	252.076	215.526	139.990	115.769	72.214
	Phase Angle (deg)	7.44	7.96	8.43	9.82	10.48	12.40	13.51	14.92	15.86	18.55	19.64	22.51	22.78	24.65	25.19	27.12	27.43	27.85
Specimen 3	Modulus (ksi)	1206.714	1118.821	1052.394	899.524	833.532	687.624	673.265	584.067	521.266	389.716	340.694	239.747	287.030	225.969	191.160	123.500	101.802	63.193
	Phase Angle (deg)	7.40	8.02	8.48	9.84	10.57	12.50	13.82	15.24	16.22	19.05	20.14	23.07	23.17	25.12	25.64	27.57	27.74	28.15
CIR-E LMLC-S	Temp, °C	4.4	4.4	4.4	4.4	4.4	4.4	21.1	21.1	21.1	21.1	21.1	21.1	37.8	37.8	37.8	37.8	37.8	37.8
	Frequency, Hz	25	10	5	1	0.5	0.1	25	10	5	1	0.5	0.1	25	10	5	1	0.5	0.1
Specimen 1	Modulus (ksi)	1030.493	953.043	893.578	759.563	702.998	578.701	622.357	543.311	486.457	368.831	323.144	229.305	261.358	207.839	173.030	111.810	92.911	57.333
	Phase Angle (deg)	7.84	8.41	8.95	10.35	11.02	12.96	13.28	14.46	15.50	18.03	19.15	22.09	22.67	24.35	25.49	27.52	27.74	28.71
Specimen 2	Modulus (ksi)	1136.806	1057.470	996.699	853.547	793.356	656.151	657.891	573.914	513.724	387.396	340.404	241.778	290.946	231.625	192.030	123.804	102.948	64.368
	Phase Angle (deg)	7.49	8.06	8.55	9.93	10.61	12.62	13.66	14.86	15.92	18.51	19.60	22.46	22.84	24.29	25.60	28.07	28.41	29.46
Specimen 3	Modulus (ksi)	1220.638	1138.546	1074.149	923.600	859.494	715.326	691.975	602.777	539.395	407.701	359.113	254.976	311.251	247.869	206.679	133.507	111.041	68.907
	Phase Angle (deg)	7.33	7.90	8.40	9.70	10.35	12.21	13.70	14.84	15.99	18.79	19.83	22.78	22.91	24.39	25.58	27.51	27.62	28.27
Specimen 4	Modulus (ksi)	1091.119	1020.921	965.951	825.845	766.234	632.219	613.655	531.998	472.678	352.732	308.205	216.251	273.251	217.267	180.717	117.002	97.364	60.698
	Phase Angle (deg)	7.58	8.18	8.78	10.15	10.83	12.74	14.07	15.36	16.36	18.99	20.09	23.03	23.11	24.55	25.79	27.74	27.81	28.54
CIR-E PMLC-L	Temp, °C	4.4	4.4	4.4	4.4	4.4	4.4	21.1	21.1	21.1	21.1	21.1	21.1	37.8	37.8	37.8	37.8	37.8	37.8
	Frequency, Hz	25	10	5	1	0.5	0.1	25	10	5	1	0.5	0.1	25	10	5	1	0.5	0.1
Specimen 1	Modulus (ksi)	1332.897	1237.027	1167.119	1002.066	932.158	771.891	736.502	641.357	574.494	428.151	373.037	260.053	324.304	258.022	215.526	137.728	113.579	70.735
	Phase Angle (deg)	7.57	8.15	8.57	9.93	10.60	12.59	14.17	15.59	16.64	19.53	20.65	23.59	23.89	25.23	26.00	27.51	27.47	27.54
Specimen 2	Modulus (ksi)	1345.225	1250.950	1180.317	1015.119	943.325	784.799	753.326	655.571	587.693	441.640	387.106	272.526	329.526	263.969	221.183	142.790	118.496	74.491
	Phase Angle (deg)	7.42	7.93	8.40	9.69	10.38	12.24	13.83	15.19	16.18	19.02	20.12	23.17	23.54	24.87	25.69	27.22	27.17	27.17
Specimen 3	Modulus (ksi)	1414.553	1309.401	1232.096	1055.295	977.264	806.845	775.227	671.525	599.586	446.571	389.861	271.946	335.617	267.740	224.228	143.645	118.800	74.274
	Phase Angle (deg)	7.32	8.01	8.50	9.95	10.66	12.70	14.23	15.66	16.66	19.64	20.75	23.78	24.07	25.36	26.10	27.45	27.26	27.11
CIR-E PMFC-S	Temp, °C	4.4	4.4	4.4	4.4	4.4	4.4	21.1	21.1	21.1	21.1	21.1	21.1	37.8	37.8	37.8	37.8	37.8	37.8
	Frequency, Hz	25	10	5	1	0.5	0.1	25	10	5	1	0.5	0.1	25	10	5	1	0.5	0.1
Specimen 1	Modulus (ksi)	1237.897	1129.264	1048.623	865.295	791.906	629.319	756.662	649.189	573.624	420.319	364.915	254.976	318.358	250.190	204.793	128.677	105.849	64.484
	Phase Angle (deg)	9.62	10.45	11.11	12.77	13.54	15.65	15.40	16.70	17.79	20.17	21.03	23.27	25.23	26.61	27.61	28.72	28.51	27.89
Specimen 2	Modulus (ksi)	1415.568	1295.767	1206.714	1003.226	921.135	737.662	860.799	743.463	657.601	485.006	422.495	296.022	376.953	298.053	245.259	154.320	127.024	76.710
	Phase Angle (deg)	9.22	9.98	10.63	12.35	13.12	15.27	14.95	16.27	17.39	19.89	20.81	23.16	24.85	26.18	27.20	28.63	28.42	28.77
Specimen 3	Modulus (ksi)	1259.653	1129.989	1033.829	824.249	740.563	565.212	658.471	547.662	472.098	326.190	275.572	179.122	233.221	173.465	135.755	78.451	62.511	35.592
	Phase Angle (deg)	10.87	11.91	12.75	14.80	15.65	18.02	18.56	20.08	21.18	23.59	24.43	26.21	29.82	30.79	31.64	31.93	31.23	29.97
Specimen 4	Modulus (ksi)	1315.637	1190.905	1099.241	894.448	811.776	633.960	767.250	650.204	569.998	407.701	348.671	235.686	292.686	223.068	178.396	106.994	86.109	50.111
	Phase Angle (deg)	10.11	10.96	11.67	13.58	14.44	16.73	16.71	18.23	19.43	22.12	23.07	25.33	27.77	28.89	29.81	30.54	30.31	29.81
Specimen 5	Modulus (ksi)	1361.324	1222.378	1118.676	891.112	800.608	608.433	721.418	597.555	513.289	353.457	298.053	193.915	249.320	185.938	145.038	84.702	67.718	39.247
	Phase Angle (deg)	10.89	11.87	12.69	14.86	15.77	18.18	18.78	20.42	21.69	24.36	25.14	27.00	29.21	30.22	30.99	30.87	30.23	28.29
Specimen 6	Modulus (ksi)	1466.767	1307.225	1187.569	941.730	840.349	635.845	781.463	646.433	556.365	384.205	324.449	212.045	264.404	197.686	155.190	90.562	71.895	42.061
	Phase Angle (deg)	10.50	11.80	12.72	15.07	15.99	18.60	18.42	20.13	21.38	24.14	24.92	26.76	29.31	30.33	31.16	31.14	30.38	29.65

Figure 79: CIR-E dynamic modulus and phase angle data.

CIR-F LMLC-L	Temp, °C	4.4	4.4	4.4	4.4	4.4	4.4	21.1	21.1	21.1	21.1	21.1	21.1	37.8	37.8	37.8	37.8	37.8	37.8
	Frequency, Hz	25	10	5	1	0.5	0.1	25	10	5	1	0.5	0.1	25	10	5	1	0.5	0.1
Specimen 1	Modulus (ksi)	1195.981	1108.959	1044.707	900.539	840.204	705.754	704.883	623.227	565.792	441.930	395.663	295.587	354.327	294.717	255.411	176.076	150.549	99.322
	Phase Angle (deg)	7.68	8.10	8.47	9.57	10.11	11.61	12.73	13.59	14.33	16.27	17.09	19.26	20.03	21.10	21.89	23.56	23.78	24.75
Specimen 2	Modulus (ksi)	1082.562	1001.196	942.020	811.776	756.807	637.151	638.166	565.212	512.853	403.350	362.449	272.816	307.190	254.541	219.587	151.419	129.475	85.442
	Phase Angle (deg)	7.80	8.19	8.56	9.62	10.07	11.54	12.58	13.44	14.19	16.19	16.96	19.14	20.28	21.41	22.17	23.85	24.09	24.87
Specimen 3	Modulus (ksi)	1046.012	970.448	920.990	795.677	748.685	631.929	633.815	564.632	516.624	405.380	364.915	273.541	303.709	253.816	219.442	150.259	128.547	84.659
	Phase Angle (deg)	7.85	8.27	8.64	9.67	10.17	11.59	12.79	13.55	14.39	16.28	17.09	19.26	20.41	21.46	22.20	23.70	23.81	24.57

CIR-F LMLC-S	Temp, °C	4.4	4.4	4.4	4.4	4.4	4.4	21.1	21.1	21.1	21.1	21.1	21.1	37.8	37.8	37.8	37.8	37.8	37.8
	Frequency, Hz	25	10	5	1	0.5	0.1	25	10	5	1	0.5	0.1	25	10	5	1	0.5	0.1
Specimen 1	Modulus (ksi)	853.402	789.730	743.754	638.601	598.861	504.731	538.525	473.983	428.441	333.732	298.633	222.488	234.816	191.885	161.717	109.591	93.767	61.148
	Phase Angle (deg)	8.28	8.66	9.03	10.16	10.71	12.17	12.78	13.68	14.50	16.28	17.07	19.14	20.86	21.91	22.91	24.38	24.52	25.15
Specimen 2	Modulus (ksi)	755.502	694.151	648.754	548.968	508.792	420.029	434.533	379.999	341.999	262.663	233.511	171.435	192.755	155.045	128.561	85.224	72.127	45.194
	Phase Angle (deg)	8.99	9.47	9.89	11.06	11.57	13.14	14.01	14.89	15.74	17.63	18.43	20.59	21.89	23.14	24.31	25.77	25.88	26.67
Specimen 3	Modulus (ksi)	770.440	705.173	658.181	556.075	515.609	424.670	411.617	353.602	316.617	240.182	212.480	152.580	180.862	144.487	119.236	77.465	64.658	40.262
	Phase Angle (deg)	8.40	8.99	9.50	11.04	11.65	13.44	14.95	15.19	16.40	18.31	19.02	21.17	22.19	23.35	24.57	26.11	26.34	26.92
Specimen 4	Modulus (ksi)	885.455	817.288	765.654	651.800	606.548	504.296	491.243	427.861	383.770	291.526	258.747	188.114	226.549	182.457	151.564	99.887	84.064	52.997
	Phase Angle (deg)	8.49	9.09	9.51	10.67	11.2	12.79	14.22	15.18	16.04	18.08	18.83	21.08	21.82	23.09	24.16	25.68	25.76	26.44

CIR-F PMLC-L	Temp, °C	4.4	4.4	4.4	4.4	4.4	4.4	21.1	21.1	21.1	21.1	21.1	21.1	37.8	37.8	37.8	37.8	37.8	37.8
	Frequency, Hz	25	10	5	1	0.5	0.1	25	10	5	1	0.5	0.1	25	10	5	1	0.5	0.1
Specimen 1	Modulus (ksi)	1258.492	1171.905	1105.623	958.409	895.608	757.097	744.189	659.051	599.006	467.892	418.579	311.106	352.732	291.381	251.060	170.564	145.908	94.927
	Phase Angle (deg)	7.29	7.72	8.08	9.22	9.76	11.40	12.45	13.46	14.34	16.67	17.67	20.33	21.22	22.57	23.52	25.58	25.85	26.95
Specimen 2	Modulus (ksi)	1210.340	1128.104	1066.898	925.921	867.181	733.311	736.647	653.250	593.639	463.251	414.663	307.625	345.045	285.289	246.129	166.503	142.514	91.925
	Phase Angle (deg)	7.38	7.89	8.24	9.36	9.94	11.60	12.43	13.40	14.24	16.54	17.53	20.18	20.95	22.39	23.30	25.34	25.59	26.72
Specimen 3	Modulus (ksi)	1225.424	1145.943	1087.203	950.287	892.997	763.334	744.769	663.258	605.678	479.640	432.648	327.205	360.854	302.839	264.984	183.328	158.671	104.500
	Phase Angle (deg)	7.04	7.45	7.76	8.82	9.30	10.77	12.01	12.97	13.72	15.86	16.75	19.25	20.22	21.46	22.34	24.29	24.54	25.61

CIR-F PMFC-S	Temp, °C	4.4	4.4	4.4	4.4	4.4	4.4	21.1	21.1	21.1	21.1	21.1	21.1	37.8	37.8	37.8	37.8	37.8	37.8
	Frequency, Hz	25	10	5	1	0.5	0.1	25	10	5	1	0.5	0.1	25	10	5	1	0.5	0.1
Specimen 1	Modulus (ksi)	985.096	910.257	853.547	724.899	671.525	550.853	606.838	530.983	475.434	360.999	317.633	228.725	246.709	194.786	160.267	101.875	83.861	50.676
	Phase Angle (deg)	8.29	9.01	9.49	10.87	11.53	13.60	13.72	14.90	15.84	18.09	19.03	21.35	24.11	25.46	26.57	27.73	27.68	27.20
Specimen 2	Modulus (ksi)	1035.569	954.493	895.028	756.372	699.662	569.998	628.158	549.548	493.128	374.052	328.801	235.686	264.114	207.984	170.564	106.893	87.675	52.852
	Phase Angle (deg)	8.46	8.98	9.54	11.03	11.76	13.84	13.68	14.77	15.78	18.17	19.10	21.49	23.63	25.05	26.21	27.59	27.64	27.86
Specimen 3	Modulus (ksi)	1101.272	1012.073	945.791	797.127	735.776	598.426	652.815	567.823	506.907	380.434	333.297	235.831	265.419	208.129	169.549	105.994	86.747	52.185
	Phase Angle (deg)	8.69	9.32	9.87	11.38	12.14	14.28	14.43	15.66	16.68	19.13	20.10	22.34	24.73	25.99	27.05	28.08	27.94	27.79
Specimen 4	Modulus (ksi)	953.913	883.135	831.211	709.235	662.822	552.594	616.700	542.731	490.953	378.548	337.938	248.305	319.373	259.182	217.702	143.399	119.845	74.317
	Phase Angle (deg)	8.07	8.61	9.11	10.47	11.16	13.08	12.94	13.88	14.9	17.2	18.22	20.46	21.26	22.59	23.66	25.11	25.29	26.33
Specimen 5	Modulus (ksi)	1057.615	982.776	929.402	804.669	755.792	638.456	650.784	577.685	525.037	409.877	366.945	271.076	338.663	279.198	237.862	161.427	136.742	87.574
	Phase Angle (deg)	7.39	7.88	8.30	9.53	10.14	11.73	12.50	13.44	14.34	16.60	17.45	19.74	20.31	21.59	22.66	24.32	24.46	25.46
Specimen 6	Modulus (ksi)	990.173	923.745	875.883	758.547	711.410	597.701	594.655	524.892	475.434	366.655	326.770	237.282	283.404	227.999	189.854	123.645	102.498	63.033
	Phase Angle (deg)	7.67	8.18	8.58	9.77	10.35	11.95	13.17	14.22	15.09	17.20	18.10	20.31	21.75	23.03	24.03	25.13	25.20	26.36

Figure 80: CIR-F dynamic modulus and phase angle data.

CCPR-E LMLC-L	Temp, °C	4.4	4.4	4.4	4.4	4.4	4.4	21.1	21.1	21.1	21.1	21.1	21.1	37.8	37.8	37.8	37.8	37.8	37.8
	Frequency, Hz	25	10	5	1	0.5	0.1	25	10	5	1	0.5	0.1	25	10	5	1	0.5	0.1
Specimen 1	Modulus (ksi)	1113.600	995.104	906.341	712.715	635.265	472.243	607.998	501.831	430.182	290.656	243.083	151.709	207.404	153.885	123.210	72.504	58.407	35.447
	Phase Angle (deg)	10.94	11.97	12.83	15.31	16.39	19.46	18.23	20.26	21.66	24.96	26.02	28.68	28.94	30.21	30.44	29.92	29.06	27.05
Specimen 2	Modulus (ksi)	1228.760	1101.707	1006.852	797.998	711.555	531.273	599.876	492.258	420.900	281.373	233.511	145.618	205.083	151.855	121.571	72.330	58.871	37.028
	Phase Angle (deg)	10.43	11.53	12.41	14.88	16.01	19.10	19.44	21.33	22.63	25.73	26.57	28.79	28.88	30.08	29.95	28.87	27.76	25.03
Specimen 3	Modulus (ksi)	1279.813	1140.722	1038.325	818.303	725.914	537.655	584.357	477.174	405.235	269.625	224.228	138.482	200.297	148.229	118.423	70.633	57.653	36.637
	Phase Angle (deg)	10.53	11.65	12.59	15.11	16.24	19.39	20.02	21.89	23.27	26.22	27.02	29.24	29.07	30.21	30.15	28.98	27.80	24.91

CCPR-E LMLC-S	Temp, °C	4.4	4.4	4.4	4.4	4.4	4.4	21.1	21.1	21.1	21.1	21.1	21.1	37.8	37.8	37.8	37.8	37.8	37.8
	Frequency, Hz	25	10	5	1	0.5	0.1	25	10	5	1	0.5	0.1	25	10	5	1	0.5	0.1
Specimen 1	Modulus (ksi)	941.440	843.394	770.731	610.029	546.502	410.457	424.090	344.030	290.221	189.419	156.206	94.927	180.862	135.335	105.733	62.308	50.169	30.139
	Phase Angle (deg)	10.76	11.70	12.57	14.93	16.10	19.12	20.59	22.61	24.13	27.67	28.71	31.48	29.26	30.27	31.26	31.81	31.25	30.52
Specimen 2	Modulus (ksi)	1152.470	1038.760	953.188	761.593	682.838	515.754	535.624	438.884	370.281	245.114	203.343	124.761	191.160	139.135	107.023	58.421	46.078	25.266
	Phase Angle (deg)	10.02	10.97	11.85	14.30	15.49	18.62	19.91	21.93	24.39	27.16	28.04	30.95	30.84	32.35	33.50	34.79	34.19	32.32
Specimen 3	Modulus (ksi)	1003.951	898.219	820.043	648.319	578.846	432.938	455.709	370.861	313.717	204.938	169.404	102.252	n/a	n/a	n/a	n/a	n/a	n/a
	Phase Angle (deg)	10.55	11.61	12.54	14.93	16.01	19.13	20.34	22.30	23.83	27.27	28.36	31.09	n/a	n/a	n/a	n/a	n/a	n/a
Specimen 4	Modulus (ksi)	1149.279	1035.860	950.432	757.967	679.212	512.418	533.304	436.419	370.281	244.099	202.038	123.210	194.641	141.528	109.387	60.379	47.253	25.512
	Phase Angle (deg)	10.17	11.25	12.11	14.43	15.52	18.58	19.85	21.81	23.38	26.99	28.18	30.89	30.03	31.84	32.87	33.88	33.54	33.49

CCPR-E PMLC-L	Temp, °C	4.4	4.4	4.4	4.4	4.4	4.4	21.1	21.1	21.1	21.1	21.1	21.1	37.8	37.8	37.8	37.8	37.8	37.8
	Frequency, Hz	25	10	5	1	0.5	0.1	25	10	5	1	0.5	0.1	25	10	5	1	0.5	0.1
Specimen 1	Modulus (ksi)	1489.102	1344.500	1236.302	993.073	892.852	676.891	712.715	587.983	503.281	336.197	279.488	172.450	298.053	224.518	178.396	101.164	79.133	43.105
	Phase Angle (deg)	9.93	10.90	11.71	14.03	15.16	18.26	19.34	21.27	22.69	26.12	27.16	29.77	29.87	31.21	31.93	32.85	32.38	31.71
Specimen 2	Modulus (ksi)	1285.324	1163.058	1071.974	865.150	781.028	595.815	630.769	522.861	449.617	302.404	251.931	155.335	238.297	179.267	142.964	82.309	65.354	38.188
	Phase Angle (deg)	9.99	10.87	11.64	13.79	14.78	17.60	19.06	20.87	22.26	25.61	26.63	29.18	29.89	30.87	31.27	31.18	30.36	28.27
Specimen 3	Modulus (ksi)	1303.019	1176.981	1084.737	871.677	784.509	592.914	628.739	517.495	442.365	293.846	243.663	148.954	229.160	170.564	134.798	77.044	61.061	35.723
	Phase Angle (deg)	9.94	10.87	11.68	13.93	15.03	18.03	19.37	21.25	22.71	26.18	27.26	29.84	30.29	31.26	31.64	31.37	30.57	28.26

CCPR-E PMFC-S	Temp, °C	4.4	4.4	4.4	4.4	4.4	4.4	21.1	21.1	21.1	21.1	21.1	21.1	37.8	37.8	37.8	37.8	37.8	37.8
	Frequency, Hz	25	10	5	1	0.5	0.1	25	10	5	1	0.5	0.1	25	10	5	1	0.5	0.1
Specimen 1	Modulus (ksi)	1625.293	1433.118	1289.966	985.386	866.310	622.212	696.471	558.250	468.037	298.923	244.389	147.648	232.786	166.213	125.443	69.821	54.911	30.487
	Phase Angle (deg)	12.24	13.58	14.64	17.46	18.67	21.92	22.49	24.40	25.65	27.94	28.37	29.44	32.44	32.88	33.47	32.72	31.50	29.95
Specimen 2	Modulus (ksi)	1538.125	1356.103	1221.363	931.287	818.303	586.968	660.937	526.777	438.594	275.572	224.228	132.405	214.656	153.595	115.218	63.222	49.487	28.413
	Phase Angle (deg)	12.45	13.80	14.87	17.84	19.08	22.33	23.42	25.45	26.73	29.15	29.55	30.69	33.35	33.61	34.13	32.90	31.84	29.13
Specimen 3	Modulus (ksi)	1529.713	1347.981	1212.951	919.249	806.700	573.189	666.593	527.647	437.724	273.976	222.488	131.694	214.511	153.305	115.407	64.353	50.720	29.254
	Phase Angle (deg)	12.73	14.12	15.29	18.24	19.51	22.81	23.34	25.40	26.73	29.15	29.60	30.57	33.24	33.40	33.78	32.15	31.00	28.75
Specimen 4	Modulus (ksi)	1487.217	1305.050	1170.310	881.974	772.326	543.601	627.143	494.724	408.136	252.946	204.503	119.903	196.816	139.236	104.036	56.260	43.627	23.772
	Phase Angle (deg)	12.84	14.21	15.37	18.4	19.68	23.01	23.92	25.97	27.26	29.82	30.28	31.36	34.54	34.63	35.02	33.63	32.33	29.93
Specimen 5	Modulus (ksi)	1426.881	1248.630	1118.676	838.608	730.845	511.548	n/a	n/a	n/a	n/a	n/a	n/a	n/a	n/a	n/a	n/a	n/a	n/a
	Phase Angle (deg)	13.19	14.62	15.83	18.89	20.22	23.60	n/a	n/a	n/a	n/a	n/a	n/a	n/a	n/a	n/a	n/a	n/a	n/a
Specimen 6	Modulus (ksi)	1526.377	1342.179	1207.874	913.883	800.608	568.838	659.051	521.266	431.487	270.060	219.587	130.171	207.694	148.954	112.607	62.961	49.458	27.876
	Phase Angle (deg)	12.64	13.92	15.00	17.84	19.07	22.30	23.61	25.62	26.97	29.53	29.94	30.94	33.25	33.45	33.79	32.37	31.06	29.16

Figure 81: CCPR-E dynamic modulus and phase angle data.

CCPR-F LMLC-L	Temp, °C	4.4	4.4	4.4	4.4	4.4	4.4	21.1	21.1	21.1	21.1	21.1	21.1	37.8	37.8	37.8	37.8	37.8	37.8
	Frequency, Hz	25	10	5	1	0.5	0.1	25	10	5	1	0.5	0.1	25	10	5	1	0.5	0.1
Specimen 1	Modulus (ksi)	658.471	602.922	563.472	472.533	438.739	359.404	409.151	358.388	324.885	248.595	222.778	162.587	199.572	163.603	140.426	94.202	80.554	52.591
	Phase Angle (deg)	9.65	10.33	10.85	12.32	12.91	14.67	14.37	15.39	16.08	17.97	18.57	20.49	21.59	22.58	23.18	24.21	24.04	24.21
Specimen 2	Modulus (ksi)	767.105	706.914	663.403	561.296	522.716	430.037	467.022	409.877	371.587	284.854	254.541	185.648	226.114	185.793	158.816	106.356	90.692	59.103
	Phase Angle (deg)	9.22	9.79	10.30	11.73	12.36	14.09	14.30	15.33	16.05	17.98	18.70	20.60	21.64	22.59	23.22	24.17	24.08	24.19
Specimen 3	Modulus (ksi)	719.097	660.357	618.731	523.296	486.457	399.289	434.968	378.984	343.304	261.503	233.511	169.114	208.709	170.854	145.763	96.349	81.729	52.634
	Phase Angle (deg)	9.21	9.89	10.39	11.85	12.41	14.21	14.68	15.56	16.26	18.17	18.77	20.62	21.71	22.62	23.25	24.10	23.98	24.09
Specimen 4	Modulus (ksi)	701.112	642.807	602.342	506.327	471.373	386.090	434.098	377.678	341.419	258.312	230.465	165.778	210.740	171.725	145.908	96.015	81.221	51.895
	Phase Angle (deg)	9.67	10.30	10.77	12.27	12.86	14.69	15.17	16.10	16.79	18.71	19.32	21.16	22.02	22.98	23.61	24.65	24.45	24.57

CCPR-F LMLC-S	Temp, °C	4.4	4.4	4.4	4.4	4.4	4.4	21.1	21.1	21.1	21.1	21.1	21.1	37.8	37.8	37.8	37.8	37.8	37.8
	Frequency, Hz	25	10	5	1	0.5	0.1	25	10	5	1	0.5	0.1	25	10	5	1	0.5	0.1
Specimen 1	Modulus (ksi)	467.602	418.434	383.625	310.236	283.839	223.358	270.060	225.969	197.396	143.080	125.675	86.892	141.890	108.851	87.443	56.478	47.601	30.690
	Phase Angle (deg)	11.47	12.35	13.08	14.87	15.54	17.51	17.22	18.48	19.45	21.16	21.53	23.06	22.45	23.38	24.41	24.49	24.03	24.80
Specimen 2	Modulus (ksi)	683.853	618.731	572.754	473.258	436.854	351.717	403.930	346.060	307.480	229.305	202.908	144.835	197.541	156.496	128.735	84.397	71.228	46.195
	Phase Angle (deg)	10.56	11.26	11.89	13.46	14.05	15.81	15.82	16.75	17.53	19.13	19.61	21.04	21.88	22.61	23.51	23.85	23.65	23.11
Specimen 3	Modulus (ksi)	614.525	554.479	513.724	421.915	388.411	310.381	339.678	288.915	254.976	188.549	166.503	117.568	166.503	130.635	105.762	68.501	57.536	36.404
	Phase Angle (deg)	10.84	11.61	12.21	13.81	14.45	16.33	16.33	17.42	18.29	20.00	20.55	22.01	22.44	23.47	24.45	25.04	24.57	23.15

CCPR-F PMLC-L	Temp, °C	4.4	4.4	4.4	4.4	4.4	4.4	21.1	21.1	21.1	21.1	21.1	21.1	37.8	37.8	37.8	37.8	37.8	37.8
	Frequency, Hz	25	10	5	1	0.5	0.1	25	10	5	1	0.5	0.1	25	10	5	1	0.5	0.1
Specimen 1	Modulus (ksi)	1217.447	1128.249	1062.546	913.303	852.097	713.151	740.128	652.960	592.479	460.495	411.182	304.724	387.396	322.419	278.617	193.480	165.633	112.390
	Phase Angle (deg)	7.48	7.95	8.39	9.64	10.19	11.84	12.65	13.60	14.38	16.42	17.22	19.27	19.33	20.31	20.97	22.19	22.23	22.51
Specimen 2	Modulus (ksi)	1153.485	1078.646	1021.211	882.990	825.555	694.876	686.319	608.288	553.029	431.052	385.365	285.724	350.266	291.961	252.366	173.900	149.389	100.091
	Phase Angle (deg)	7.66	8.11	8.50	9.64	10.21	11.81	12.95	13.83	14.66	16.71	17.49	19.56	19.97	20.91	21.52	22.69	22.61	22.91
Specimen 3	Modulus (ksi)	1149.714	1064.722	1002.211	860.219	802.639	669.349	663.838	584.212	528.372	404.655	359.549	261.648	330.251	270.640	231.045	155.335	131.897	86.559
	Phase Angle (deg)	7.70	8.15	8.60	9.85	10.43	12.14	13.36	14.34	15.24	17.43	18.27	20.38	20.85	21.87	22.50	23.60	23.50	23.64

CCPR-F PMFC-S	Temp, °C	4.4	4.4	4.4	4.4	4.4	4.4	21.1	21.1	21.1	21.1	21.1	21.1	37.8	37.8	37.8	37.8	37.8	37.8
	Frequency, Hz	25	10	5	1	0.5	0.1	25	10	5	1	0.5	0.1	25	10	5	1	0.5	0.1
Specimen 1	Modulus (ksi)	1166.539	1069.943	995.829	828.746	759.998	608.723	640.777	549.403	486.166	356.503	310.236	216.541	274.411	216.106	177.091	113.303	93.375	58.523
	Phase Angle (deg)	8.89	9.60	10.21	11.85	12.56	14.61	15.45	16.68	17.64	19.69	20.37	22.09	23.45	24.49	25.30	25.77	25.42	25.81
Specimen 2	Modulus (ksi)	1043.837	930.852	847.020	661.082	590.014	436.709	516.914	422.060	358.243	233.656	193.190	117.089	182.748	132.158	99.887	55.042	42.322	22.220
	Phase Angle (deg)	11.61	12.66	13.57	16.08	17.22	20.19	20.17	21.97	23.38	26.34	27.21	29.24	30.14	31.12	32.18	32.28	31.66	31.28
Specimen 3	Modulus (ksi)	885.891	791.036	723.013	569.563	509.953	379.564	432.357	348.091	294.572	191.305	158.236	96.320	152.580	108.227	80.133	43.018	32.633	17.434
	Phase Angle (deg)	11.56	12.68	13.59	15.87	16.92	19.75	21.14	22.90	24.35	27.18	27.77	29.23	30.68	32.01	33.19	33.48	33.14	31.68
Specimen 4	Modulus (ksi)	1171.470	1064.142	982.631	798.288	724.899	561.586	611.044	512.708	444.976	310.236	262.808	172.305	243.518	185.068	148.374	90.199	73.273	44.570
	Phase Angle (deg)	10.11	10.99	11.8	13.77	14.73	17.18	17.67	19.17	20.31	22.76	23.48	25.25	26.62	27.69	28.45	28.36	27.94	27.33
Specimen 5	Modulus (ksi)	1136.951	1049.783	985.676	833.387	771.891	631.639	658.616	572.174	510.678	383.770	337.648	241.923	310.526	248.160	207.259	138.134	116.364	77.015
	Phase Angle (deg)	8.39	8.98	9.58	11.06	11.75	13.55	14.47	15.60	16.56	18.57	19.30	21.00	21.61	22.61	23.29	23.70	23.36	23.32
Specimen 6	Modulus (ksi)	866.455	783.929	724.028	588.708	537.075	419.014	464.121	392.617	343.884	243.953	210.160	140.310	199.572	153.160	121.803	73.984	60.495	35.766
	Phase Angle (deg)	10.22	11.07	11.75	13.54	14.32	16.44	17.41	18.74	19.75	21.86	22.44	24.12	24.80	25.78	26.70	26.92	26.40	24.97

Figure 82: CCPR-F dynamic modulus and phase angle data.

FDR-E LMLC-L	Temp, °C	4.4	4.4	4.4	4.4	4.4	4.4	21.1	21.1	21.1	21.1	21.1	21.1	37.8	37.8	37.8	37.8	37.8	37.8
	Frequency, Hz	25	10	5	1	0.5	0.1	25	10	5	1	0.5	0.1	25	10	5	1	0.5	0.1
Specimen 1	Modulus (ksi)	831.356	767.685	720.547	615.540	573.769	477.899	473.548	413.503	372.602	287.320	257.732	192.610	282.243	235.831	204.793	146.053	127.474	88.618
	Phase Angle (deg)	8.78	9.35	9.76	11.10	11.66	13.38	14.70	15.76	16.55	18.52	19.25	21.19	20.05	21.15	21.97	23.32	23.49	24.28
Specimen 2	Modulus (ksi)	869.936	803.219	755.647	647.594	604.082	505.747	496.899	435.838	393.632	303.999	272.816	204.358	268.610	222.923	193.045	135.581	118.336	81.294
	Phase Angle (deg)	8.61	9.30	9.71	11.08	11.65	13.32	14.67	15.68	16.47	18.47	19.22	21.24	21.06	22.15	22.88	24.17	24.25	24.78
Specimen 3	Modulus (ksi)	907.501	841.364	793.066	682.258	636.716	532.579	520.976	457.449	413.067	318.793	284.999	212.045	288.335	237.427	204.358	140.672	121.150	80.989
	Phase Angle (deg)	8.25	8.78	9.25	10.53	11.16	12.87	14.38	15.46	16.29	18.41	19.18	21.37	20.80	22.00	22.73	24.05	24.14	24.85

FDR-E LMLC-S	Temp, °C	4.4	4.4	4.4	4.4	4.4	4.4	21.1	21.1	21.1	21.1	21.1	21.1	37.8	37.8	37.8	37.8	37.8	37.8
	Frequency, Hz	25	10	5	1	0.5	0.1	25	10	5	1	0.5	0.1	25	10	5	1	0.5	0.1
Specimen 1	Modulus (ksi)	903.295	835.562	786.830	674.861	630.769	529.098	472.243	410.312	366.945	281.228	251.350	185.938	259.037	208.854	176.076	121.411	105.094	70.213
	Phase Angle (deg)	8.47	9.01	9.50	10.82	11.42	13.16	14.72	15.94	16.89	19.05	19.83	22.01	21.45	22.92	23.97	25.33	25.48	26.19
Specimen 2	Modulus (ksi)	733.456	677.761	636.716	546.502	510.098	428.006	396.098	342.144	304.724	233.076	208.129	152.870	219.877	179.702	151.129	104.688	90.881	62.018
	Phase Angle (deg)	8.48	9.06	9.52	10.83	11.42	13.21	14.67	15.84	16.87	19.11	19.93	22.41	21.19	22.63	23.84	25.40	25.51	26.21
Specimen 3	Modulus (ksi)	867.906	800.898	753.761	649.914	608.288	511.693	476.304	409.587	365.495	279.053	249.755	184.778	258.167	211.320	178.541	124.109	108.256	73.244
	Phase Angle (deg)	8.18	8.88	9.41	10.74	11.38	13.05	14.46	15.76	16.74	18.93	19.74	21.90	21.27	22.49	23.57	24.81	24.82	24.98
Specimen 4	Modulus (ksi)	800.173	738.677	694.441	595.815	556.800	467.312	430.762	373.037	333.732	254.831	229.305	169.984	247.434	202.618	169.984	116.886	102.484	69.183
	Phase Angle (deg)	8.89	9.53	10.01	11.26	11.91	13.71	15.15	16.25	17.27	19.46	20.25	22.61	21.48	22.70	23.96	25.19	25.36	25.85

FDR-E PMLC-L	Temp, °C	4.4	4.4	4.4	4.4	4.4	4.4	21.1	21.1	21.1	21.1	21.1	21.1	37.8	37.8	37.8	37.8	37.8	37.8
	Frequency, Hz	25	10	5	1	0.5	0.1	25	10	5	1	0.5	0.1	25	10	5	1	0.5	0.1
Specimen 1	Modulus (ksi)	719.677	689.799	670.219	623.517	605.823	561.441	563.327	530.113	505.892	448.167	424.525	367.091	390.442	350.411	323.434	262.373	239.892	188.549
	Phase Angle (deg)	5.76	5.79	5.89	6.34	6.49	7.22	7.88	8.18	8.51	9.48	9.87	11.25	11.42	12.25	12.99	14.57	15.07	16.38

Figure 83: FDR-E Dynamic Modulus and Phase Angle Data.